Technical Report Documentation Page

1. Report No.	2. Government Accession No.	3. Recipient's Catalog No.
FHWA/TX-09/0-6069-1		

4. Title and Subtitle	5. Report Date
LONG-TERM PERFORMANCE OF GFRP REINFORCEMENT: TECHNICAL REPORT	February 2009 Published: December 2009
	6. Performing Organization Code
7. Author(s)	8. Performing Organization Report No.
David Trejo, Paolo Gardoni, Jeong Joo Kim, and Jason Zidek	Report 0-6069-1
9. Performing Organization Name and Address	10. Work Unit No. (TRAIS)
Texas Transportation Institute The Texas A&M University System College Station, Texas 77843-3135	11. Contract or Grant No. Project 0-6069
12. Sponsoring Agency Name and Address	13. Type of Report and Period Covered
Texas Department of Transportation Research and Technology Implementation Office P. O. Box 5080 Austin, Texas 78763-5080	Technical Report: September 2007 – August 2008
	14. Sponsoring Agency Code

15. Supplementary Notes

Project performed in cooperation with the Texas Department of Transportation and the Federal Highway Administration.

Project Title: Long-Term Performance of GFRP Reinforcement URL: http://tti.tamu.edu/documents/0-6069-1.pdf

16. Abstract

Significant research has been performed on glass fiber-reinforced polymer (GFRP) concrete reinforcement. This research has shown that GFRP reinforcement exhibits high strengths, is lightweight, can decrease time of construction, and is corrosion resistant. Regarding the corrosion resistance, research has shown that the chemical reactions that occur in GFRP bars do not result in expansive products—products that can damage the concrete surrounding the reinforcement. Although not classical steel corrosion, much research that has been performed shows that GFRP reinforcing bars do corrode, reducing the tensile capacity of the GFRP reinforcing bars as a function of time. The American Concrete Institute (ACI) recognized this and places a reduction factor on the allowable design strength of GFRP reinforcing bars. A drawback of the majority of the research is that GFRP reinforcing bars have typically been directly exposed to aggressive solutions, exposure conditions possibly not similar to the exposure they would encounter while embedded in concrete. Limited research has been performed evaluating the tensile capacity reduction of bars embedded in concrete; however, these bars were only exposed for relatively short durations.

This research investigated the characteristics of GFRP reinforcing bars embedded in concrete for 7 years and exposed to a mean annual temperature of 69 ^{o}F (23 ^{o}C) and an average precipitation of 39.7 inches (1008 mm), fairly evenly distributed throughout the year. Three manufacturers provided #5 and #6 bars for this research. Results indicate that GFRP reinforcing bars do exhibit reduced capacities when embedded in concrete. A model was developed to assess the tensile capacity of bars embedded in concrete. The model was based on a general diffusion model, where diffusion of water or ions penetrate the bar matrix and degrade the glass fibers. The model is dependent on time, diffusion characteristics of the matrix material, and the radius of the GFRP reinforcing bar. The model indicates that GFRP reinforcement bars with larger diameters exhibit lower rates of capacity loss. However, the times required for the tensile capacity of the GFRP bars to drop below the ACI design requirements for #3, #5, and #6 bars were less than 6 years. Further research is needed to determine how this will affect the design of GFRP-reinforced concrete structures; however, consideration of changing the ACI design requirement may be warranted.

17. Key Words	18. Distribution Statement
Glass, Fiber-Reinforcement, Glass Fiber-Reinforced Polymer, Polymer, Durability, Deterioration, Service Life, Concrete Reinforcement	No restrictions. This document is available to the public through NTIS: National Technical Information Service Springfield, Virginia 22161 http://www.ntis.gov

19. Security Classif.(of this report)	20. Security Classif.(of this page)	21. No. of Pages	22. Price
Unclassified	Unclassified	140	

Form DOT F 1700.7 (8-72) Reproduction of completed page authorized

LONG-TERM PERFORMANCE OF GFRP REINFORCEMENT: TECHNICAL REPORT

by

David Trejo, Ph.D., P.E.
Associate Research Engineer

Paolo Gardoni, Ph.D.
Assistant Research Engineer

Jeong Joo Kim
Graduate Student Researcher

Jason Zidek
Undergraduate Student Researcher

Zachry Department of Civil Engineering
Texas A&M University

Report 0-6069-1
Project 0-6069
Project Title: Long-Term Performance of GFRP Reinforcement

Performed in cooperation with the
Texas Department of Transportation
and the
Federal Highway Administration

February 2009

Published: December 2009

TEXAS TRANSPORTATION INSTITUTE
The Texas A&M University System
College Station, Texas 77843-3135

DISCLAIMER

The contents of this report reflect the views of the authors, who are responsible for the facts and accuracy of the data herein. The contents do not necessarily reflect the official view or policies of the Federal Highway Administration (FHWA) or the Texas Department of Transportation (TxDOT). This report does not constitute a standard, specification, or regulation. The researcher in charge was David Trejo, P.E. #93490.

The United States Government and the State of Texas do not endorse products or manufacturers. Trade or manufacturers' names appear herein solely because they are considered essential to the objective of this report.

ACKNOWLEDGMENTS

This project was conducted in cooperation with TxDOT and FHWA. The researchers would like to gratefully acknowledge the assistance provided by TxDOT officials, in particular, Timothy Bradberry, David Hohmann, and German Claros. The assistance on the original GFRP project (9-1520) from Doug Gremel and Sam Steere was very much appreciated. The assistance of Matt Potter of the High Bay Structural and Materials Laboratory is always very much appreciated. The authors also appreciate the help of Paul Mostella and Brad Shinpaugh, students who contributed to the project.

TABLE OF CONTENTS

Page

LIST OF FIGURES

LIST OF TABLES

1. INTRODUCTION AND RESEARCH SIGNIFICANCE

Glass fiber-reinforced polymer (GFRP) reinforcement has emerged as a potential candidate as an alternative reinforcement to conventional steel reinforcing bars for concrete structures. GFRP reinforcing bars are non-corrosive, have high tensile strength, are lightweight, and have high strength to weight ratios. Considering the significant rehabilitation costs associated with the deterioration of existing bridges, mostly a result of steel corrosion, the potential corrosion resistance of GFRP reinforcing bars could provide significant value for structures containing reinforcement. The use of GFRP reinforcing bars has increased significantly in many infrastructure applications, including bridge decks, pavements, walls, and other systems. However, there still is a reluctance to use GFRP reinforcing bars; this reluctance mostly results from the lack of long-term performance data of GFRP reinforcing bars embedded in concrete.

Although GFRP reinforcing bars do not exhibit "classical" corrosion, many publications have reported a significant reduction in the tensile capacity of GFRP reinforcement when exposed to various solutions. Classical corrosion in reinforced concrete is defined as reactions that take place between the base reinforcement material and its environment to form a product of increased volume that creates internal tensile forces that exceed the tensile capacity of the concrete, causing cracking and spalling of the concrete. Significant literature exists on the reduction in GFRP reinforcement tensile capacity when the GFRP is exposed to various solutions. Some literature is available on the reduction in the tensile capacity of GFRP reinforcement when embedded in concrete, but these data are based on short-term exposure durations. Because GFRP reinforcing bars are specifically designed for use in concrete and because the environmental exposure conditions inside concrete are likely significantly different

than direct exposure conditions, research is needed to better determine the influence of the concrete environment on the tensile capacity of GFRP reinforcement. Also, because the potential benefits of using GFRP could provide significant value to owners, managers, and users of infrastructure systems, the performance of GFRP reinforcement should be determined such that value is optimized while maintaining safety.

Over the past several decades significant research has been performed assessing the durability of GFRP reinforcing bars by measuring the reduction of mechanical properties after exposure to various environments. Research evaluating changes in the tensile strength and modulus of elasticity (MOE) has been prevalent. Based on many accelerated exposure tests, researchers have developed models to predict the long-term performance of these GFRP reinforcing bars. However, significant debate exists on the recommended models and the limits published in the design codes. This debate is a direct result of the lack of performance data from GFRP reinforcing bars embedded in concrete for longer periods. A "valid" prediction model that includes influencing parameters is needed. Once this model is defined, the actual value of using GFRP reinforcing bars in concrete can be determined.

Research Project 9-1520, performed by Trejo et al. (2005), evaluated the performance of GFRP reinforcing bars. Research on three different GFRP reinforcing bars included evaluating the solution uptake of the bars, bar tensile tests, bar shear strength, and bar creep tests. In addition, the research evaluated GFRP-reinforced concrete specimens for cracking, deflections due to cyclic loading, bond tests, and evaluation of the thermal expansion of GFRP bars embedded in concrete. In general, the GFRP reinforcing bars performed well with the exception of the tensile strength. The researchers exposed the GFRP reinforcing bars to water and alkaline solutions and reported that the capacity of the GFRP bars could be lower than the design tensile

strength within a period of 7 years. However, these results were based on exposing the GFRP bars directly to water and alkaline solutions. It has been well established that concrete not continuously exposed to water does not have saturated pores and thus exposing the GFRP reinforcing bars to solution represents a "worst" case scenario of the GFRP performance. Considering that GFRP bars are being used in applications where the concrete is not continuously exposed to wet conditions, an alternative model may be warranted.

At the conclusion of the testing program reported by Trejo et al. (2005), the researchers stored the tested GFRP-reinforced concrete samples at the Riverside campus at Texas A&M University in College Station, Texas, with the understanding that these samples could be used to assess the residual strength of the GFRP bars at a later time. These GFRP-reinforced samples were fabricated in 2000 and exposed to a mean annual temperature of 69 ^{o}F (23 ^{o}C) and average precipitation of 39.7 inches (1008 mm), fairly evenly distributed throughout the year. The minimum and maximum average daily temperatures were 40 ^{o}F (5 ^{o}C) and 96 ^{o}F (32.2 ^{o}C), respectively. In 2007, funding was provided to assess the tensile capacity and MOE of the GFRP reinforcing bars embedded in the concrete specimens.

This research consisted of extracting the GFRP reinforcing bars from the concrete specimens stored at the Riverside campus and testing these bars for residual tensile capacity and MOE. After performing a literature review, the 7-year exposure period seems to be the longest duration in which the residual properties will be reported. Using data from the original research project and data from this research project, the researchers developed models to assess the residual tensile capacity. The researchers then used this model to assess requirements for the design tensile strength of GFRP reinforcing bars embedded in concrete.

Three types of GFRP bars were extracted in this research. The bars were manufactured by Hughes Brothers, Pultrall Inc., and Marshall Industries, and are referred to as Types V1, V2, and P, respectively.

2. LITERATURE REVIEW

Many studies assessed the degree and mechanisms of degradation and characterized the parameters that impact the long-term characteristics of GFRP reinforcing bars. GFRP reinforcing bars are composed of aligned glass fibers surrounded by a polymer matrix. When GFRP reinforcement is used as an internal reinforcement in concrete, tensile strength decreases as a function of time. This is a result of "corrosion" of the glass fibers as a result of the presence of moisture and/or alkaline solution. Because this is a chemical reaction, the rate of the degradation reactions would be expected to increase at elevated temperatures, and this has been established in the literature.

In addition to being exposed to moisture and alkaline solutions, GFRP reinforcing bars placed in service are exposed to sustained loads. Moisture or alkaline solutions can diffuse into the polymer matrix, eventually reaching the depth of the glass fibers and deteriorating these fibers. However, if in-service loads crack the polymer matrix, moisture and other deleterious solutions can be transported to the glass fibers at a faster rate than the diffusion rate. Thus, the diffusion coefficient of the polymer matrix and cracking of the polymer matrix as a function of the level of the sustained load would be a useful parameter for assessing the residual strength of GFRP reinforcing bars. Several studies (Benmokrane et al. 2002 and Micelli and Nanni 2004) have assessed the diffusivity, matrix cracking, and residual strength of GFRP bars exposed to various environments for relatively short durations.

2.1. GFRP REINFORCING BAR PERFORMANCE: SOLUTION EXPOSURE

A critical parameter influencing the deterioration rate of GFRP is the rate at which solution is transported into the GFRP reinforcing bar. A significant amount of research has been

performed assessing the residual tensile strength of GFRP reinforcing bars exposed to various solutions. These studies provide valuable information on the general mechanisms of deterioration and the level of deterioration as a function of time and are essential for developing models to predict the deterioration and residual strength of GFRP reinforcing bars in concrete. Although essential for modeling the performance of GFRP reinforcing bars, challenges do exist on how to correlate the mechanical property performance from the samples exposed to solution with the mechanical property performance of samples embedded in concrete—no correlation exists.

In addition to the condition of the environment surrounding the GFRP reinforcing bars, the mechanical properties could be affected by the imposed load on the bars, bar size, diffusion characteristics of the polymer matrix material, and temperature. This section of the report will provide a literature review summarizing papers and reports on GFRP reinforcing bars exposed to solutions under various conditions. The following section will provide a review of the performance of GFRP bars embedded in concrete and subjected to various conditions. It should be noted that most publications do not provide specific information on the constituent materials used to fabricate the GFRP bars. In cases where this information was reported, the authors have provided this information in this review. The reader is cautioned when specific information was not provided, as the performance could deviate from the anticipated performance.

Katsuki and Uomoto (1995) provided an early report on the performance of GFRP reinforcing bars. The researchers conducted accelerated tests in alkaline solution (simulated concrete pore solution) to evaluate the residual tensile strength of GFRP bars as a function of exposure time. They also developed a prediction model based on diffusion of moisture into the polymer resin matrix of the GFRP bar. After exposure to the simulated concrete pore solution, the authors assessed the GFRP bars for tension capacity and degradation. Degradation was

assessed with an electron microscope analyzer (EMA). The authors reported a residual tensile strength of 28 percent after 120 days of exposure to the alkaline solution.

Tannous and Saadatmanesh (1999) studied the durability of GFRP bars made with alkali resistant (AR) glass. They subjected a total of 160 GFRP reinforcing bars to seven different exposure solutions at temperatures of 77 °F (25 °C) and 140°F (60 °C) with and without ultraviolet radiation. They evaluated two polymer matrix materials, polyester and vinyl ester. The authors reported that higher exposure temperatures led to higher reductions in tensile strength and that the ultraviolet exposure had limited effect on the tensile strength. The authors also reported a reduction in tensile capacity after a 1-year exposure to $Ca(OH)_2$ solution of 20.8 percent for GFRP bars made with polyester resin and 12.8 percent for GFRP bars made with vinyl ester resin. Similar to Katsuki and Uomoto (1995), the authors developed a model to estimate the residual tensile strength and reported that the model predicted this strength within 15 percent of the actual residual tensile strength. The authors reported that exposing the GFRP bars to a NaCl and $MgCl_2$ (2:1) solution (7 percent by weight) resulted in the highest reduction in tensile strength (26.2 percent after 1 year). The authors also noted that Fick's law is appropriate for predicting the residual strength for short-term exposures only, as the polymer matrix tended to crack after longer exposure times. The authors also investigated the residual strength of GFRP bars embedded in concrete. These results will be reported in the next section.

Tannous and Saadatmanesh (1998) conducted accelerated aging tests using different types of resin matrix at different ranges of temperature. The authors concluded that the diffusion rate of solutions increases with increasing temperatures. Moreover, they found that the degradation of tensile strength is dependent on the combination of the bars' constituent materials and that vinyl ester resin has higher resistance to alkaline attack than the polyester resin matrix.

This was believed to be due to the lower diffusivity and absorption of the vinyl ester resin material evaluated.

Mukherjee and Arwikar (2005) later reported that although vinyl ester resin could protect the glass fibers from the alkaline solution, the tensile strength can be reduced due to the synergetic effects of other environmental factors.

Abbasi and Hogg (2005) evaluated the effect of alkaline solution and water not only on the strength and stiffness of GFRP reinforcing bars, but also on the bond strength between concrete and the bars at different temperature ranges. The researchers evaluated three types of GFRP reinforcing bars, subjecting these to an alkaline solution at 140 °F (60 °C) for 30, 120, and 240 days. Tension tests were performed to characterize the material properties of the exposed GFRP rebar. The authors reported a reduction in the MOE and tensile strength and linked these reductions to reductions in the glass fiber strength when exposed to the alkaline solution—higher temperatures exhibited larger decreases in properties.

Uomoto (1996) reported that when loaded, the resin matrix transfers the stress from the resin matrix to the glass fibers. As the resin matrix is exposed to the solution, the resin is damaged. This damage results in non-uniform stress transfer from the resin to the glass fibers. This non-uniform stress transfer increases the rate of failure of the glass fibers, thereby reducing the capacity of the GFRP bar.

Nishizaki and Meiarashi (2002) also evaluated the deterioration of GFRP specimens exposed to water and moist environments at different temperatures (140 °F [60 °C] and 104 °F [40 °C]). The authors reported higher reductions in bending strength for the samples exposed to the higher temperatures and reported that this was a result of the dissolution of the resin matrix

and separation between the glass fibers and resin. The researchers reported that water absorption is the critical factor in determining the long-term behavior of GFRP.

Sen et al. (2002) performed accelerated tests to evaluate the performance of E-glass/vinyl ester reinforcement subjected to sustained loads for a 9-month period. They evaluated 36 specimens. One-third of the samples were unstressed, one-third were stressed to 10 percent of ultimate, and one-third were stressed to 15 percent of the ultimate strength or higher. All specimens were exposed to simulated pore solution with a pH in the range of 13.35 to 13.5 for 1-, 3-, 6-, and 9-month durations. After exposure, tension tests were performed to evaluate the residual tensile strength of each bar. The researchers reported that specimens stressed to 25 and 15 percent of their ultimate strength failed at 25 and 180 days of exposure, respectively. In the case of the unstressed samples, the residual tensile strength was 70 percent of the initial strength after 9 months of exposure. Of the samples subjected to the 10 percent load that did not fail, the residual strength was 63 percent of the original unexposed ultimate strength. The authors concluded that higher stress levels result in resin cracking and accelerate the degradation process. Vijay and GangaRao (1999) and Porter and Barnes (1998) reported similar findings.

Sen et al. (2002) performed further testing on GFRP, Aramid-fiber reinforced polymer (AFRP), and carbon-fiber-reinforced polymer (CFRP) to investigate the relationship between exposure and residual properties in a marine environment. The researcher exposed GFRP specimens to simulated tidal and thermal cycles for a 20-month period and assessed the residual strength. The test results indicated that the GFRP specimens containing epoxy resin were not resistant to the marine exposure environment. The author used scanning electron microscopy (SEM) to identify evidence of degradation of the glass fiber's surface.

Karbhari et al. (2002, 2007) also evaluated the performance of GFRP specimens, exposing the samples to elevated temperatures to accelerate deterioration. Moisture uptake tests were conducted in de-ionized water and alkaline solutions at different temperatures. Results indicated that immersion in the alkaline solution resulted in higher weight gains and higher diffusivities than samples immersed in de-ionized water. The researchers assessed the residual strength of wet and dry samples exposed for 75 weeks of exposure. The dry samples that were immersed in water and exposed to lower temperatures exhibited limited deterioration. However, the samples exposed to water and elevated temperature exhibited irreversible degradation of the interface and glass fibers. For the samples immersed in alkaline solution the degradation was irreversible—degradation caused by exposure to high alkali solutions was reported to be more harmful than exposure to de-ionized water. The authors also reported that the accelerated aging test is appropriate for predicting the long-term behavior of GFRP samples.

The changes in tensile strength, ultimate elongation, and MOE of GFRP reinforcing bars were also evaluated by Debaiky et al. (2006). The researchers used accelerated aging tests and found that the maximum reduction of tensile strength was 11 percent below the guaranteed ultimate tensile strength (GUTS) when exposed to a temperature of 140 °F (60 °C) and a sustained load of 29 percent of the GUTS. The ultimate strain was 43 percent higher than that recommended in the ACI 440.1R-03 (ACI 2003) design guidelines. No significant reduction in the elastic modulus was detected.

Similar tests were performed by Micelli and Nanni (2004) to evaluate the reduction of tensile strength. In this study the tensile strength of the GFRP specimens decreased by up to 59 and 70 percent after 21 and 42 days of immersion in alkaline solution, respectively. Electron microscopy was used to identify the deterioration of the fiber, resin, and interfacial areas. This

research demonstrated the importance of the resin in resisting the transport of elements or compounds toward the glass fibers and recommended the use of thermoplastic resins. Earlier accelerated testing was performed by Micelli et al. (2001); this research concluded that after exposure to alkaline solution the reduction in tensile strength as a function of time was dependent on resin type, specifically the absorption characteristics.

Although much research has been performed using accelerated aging tests with elevated temperatures, Kajorncheappunngam et al. (2002) reported that the degradation mechanisms are different at different temperatures and using elevated temperatures as an accelerating factor may not always be appropriate. The researchers immersed glass-reinforced epoxy samples in four different aqueous media (distilled water, a saturated salt solution [30 g/100 cc NaCl], 5-molar NaOH solution, and a 1-molar hydrochloric acid solution) at two different temperatures for up to 5 months. Accelerated aging was performed by exposing the specimens at room temperature and at 140 °F (60 °C). After 5 months the residual tensile strengths of the specimens were assessed. The tensile strengths of the specimens immersed in hydrochloric acid at room temperature were higher than specimens subjected to the 140 °F (60 °C) environment. As such, the authors advised caution when using accelerated tests. However, it should be noted that the mechanisms of degradation are different for acidic and alkaline exposure and that these exposure conditions likely have a more significant impact on residual strength than temperature. Exposing GFRP specimens to elevated temperatures and the environment in which they are to be exposed can provide an indication of deterioration.

Benmokrane et al. (2002) categorized the degradation mechanisms of GFRP into three types: stress dominated, crack propagation dominated, and diffusion dominated. In this study, GFRP reinforcing bars composed of different constituent materials were exposed to simulated

alkaline solution combined with sustained loads at various temperatures for specific periods. Tension tests and assessment of the microstructure were performed to estimate the changes in the mechanical properties of the specimens. The authors concluded that the degradation mechanism changed depending on stress level. The diffusion rate of the alkaline solution dominates the degradation at low stress level, while the crack propagation on the surface of the resin matrix influences the rate of degradation at higher stress levels. Clearly, the transport of solution increases with the cracking of the resin matrix. Bank et al. (1998), Bakis et al. (1998), and Tannous and Saadatmanesh (1999) also made similar findings.

2.2. GFRP REINFORCING BAR PERFORMANCE: BARS EMBEDDED IN CONCRETE

A number of studies have evaluated the influence of the concrete pore solution on the tensile capacity of GFRP reinforcement. Almusallam et al. (2002) reported up to a 10.3 percent reduction in tensile capacity for unstressed GFRP bars and up to 27.9 percent reduction in tensile capacity for stressed bars after only 120 days of embedment in concrete. Giernacky et al. (2002) reported almost a 20 percent reduction in tensile capacity of GFRP bars for beams subjected to a service load after only 180 days of embedment in concrete. Svecova et al. (2002) also reported significant reductions in GFRP tensile capacity; 36 to 53 percent reduction in tensile capacity for GFRP bars embedded in concrete beams immersed in a 140 ^{o}F (60 ^{o}C) water bath. Mukherjee and Arwikar (2005) reported GFRP reinforcing bars embedded in concrete beams and conditioned outdoors for 18 and 30 months exhibited residual strengths of approximately 61 percent of the unexposed GFRP bars.

Bakis et al. (2005) proposed that the residual tensile strength of GFRP depends on the environmental conditions and duration of loading. In this study, GFRP specimens with E-glass and vinyl ester resin were embedded in concrete beams. Beams were pre-cracked and subjected to a sustained load. After loading, specimens were placed in four separate environmental conditions (outdoor, indoor, $Ca(OH)_2$ solution, and freeze-thaw). After exposure the beams were unloaded and evaluated for capacity. The mean tensile strength of the bars was determined to be a function of conditioning times from each environmental condition. The authors reported that the residual tensile strength of the GFRP reinforcement embedded in concrete beams was only 2.5 percent lower than the control samples (samples not embedded in concrete nor loaded). The influence of the indoor and outdoor exposure conditions were reported to have no significant affect on the rebar capacity. However, the rebar immersed in $Ca(OH)_2$ exhibited a 25 percent reduction in capacity after 1 year of exposure. Moreover, the specimens subjected to freeze-thaw cycles exhibited a 15 percent loss in capacity after 6 months. It was reported that the MOE of the GFRP bars was not significantly affected by the different exposure conditions.

Salts and alkaline solutions can influence the performance of GFRP bars. Vijay and GangaRao (1999) evaluated the performance of GFRP bars embedded in concrete specimens exposed to salt with and without sustained load conditioning at various temperatures. The authors reported that all specimens exhibited linear stress-strain relationships. For the samples without loads the maximum reductions of strength were as high as 32.2 percent after 15 months of exposure. The specimens that were subjected to freeze-thaw conditions exhibited a reduction in capacity of up to 37.5 percent. The authors concluded that the alkaline environment had a more significant affect than the salt exposure on the strength of the GFRP specimens.

A field study conducted by Laoubi et al. (2006) investigated the damage to GFRP reinforcing bars embedded in concrete beams exposed to freeze-thaw cycles and sustained bending. The GFRP reinforcing bar used in the study was sand-coated, second-generation GFRP bar made with 75.9 percent E-glass and vinyl ester resin. A total of 21 concrete beams were exposed to a sustained load for 50, 100, and 150 days at room temperature while undergoing freeze-thaw cycles. The authors concluded that exposure to freeze-thaw cycles and sustained stress were not critical environmental factors affecting the performance of GFRP reinforcement.

Dejke (2001) evaluated the performance of GFRP bars from different manufacturers. These GFRP bars were embedded in concrete for up to approximately 600 days. Dejke reported that the residual tensile strength decreases with both time and temperature. For one manufacturer, he reported a loss in tensile strength of almost 50 percent at 176^{o}F (80 ^{o}C) after less than 250 days of embedment in concrete. The same GFRP bars embedded in concrete and exposed to 60 ^{o}C and 20 ^{o}C exhibited approximately 42 and 25 percent loss in tensile capacity after 520 days. He also reported that another manufacturer's GFRP bars tested lost approximately 15 and 56 percent of their strength after 528 days of embedment in concrete when exposed to 20 ^{o}C and 60 ^{o}C, respectively. It should be noted that Dejke maintained the humidity of the exposure environments at 100 percent relative humidity and he concluded that the deterioration in "real" concrete would likely be lower, as the relative humidity of the concrete pores is typically lower (80 to 85 percent relative humidity).

Although much research has reported significant loss in the tensile capacity of GFRP bars, a field study conducted by Mufti et al. (2007a, 2007b) concluded that the GFRP reinforcement is durable when embedded in concrete. Concrete cores reinforced with GFRP were removed from five structures located in North America. The GFRP bars were made with

E-glass embedded in a vinyl ester resin, and embedment ages were from 5 to 8 years. The structures were exposed to a wide range of environmental conditions. SEM and energy dispersive X-ray analyses (EDX) were performed to detect possible degradation of the matrix and glass fibers. Fourier transform infrared spectroscopy (FTIR) was also used to estimate the changes in the glass transition temperature (T_g) of the resin. Based on these tests the authors reported no evidence of deterioration due to alkaline ingress and/or moisture absorption. The authors concluded that GFRP reinforcement is appropriate for use as reinforcement in concrete structures. It should be noted that no data on mechanical test results of the GFRP bars after embedment in the concrete environment were reported.

2.3. PREDICTION MODELS FOR LONG-TERM PERFORMANCE

Significant work has assessed the performance and deterioration of GFRP reinforcement for concrete. A wide range of results reports that clearly bar constituent materials and exposure conditions play a significant role in the performance of these systems. Researchers have used these results to generate deterioration models. These models can be used to predict the residual strengths at different times, thereby providing the designer with possible estimates of bar capacity at later ages. These residual strengths, or factored residual strengths, could then be used in the design of GFRP reinforced concrete elements. The following sections provide a review of proposed models for assessing the residual strength of GFRP bars embedded in concrete. It should be noted that only limited longer-term data are available on the performance of GFRP bars embedded in concrete and all data on the residual strength of these bars are for exposure periods of less than 3 years.

2.3.1. Models from the Literature

Research has been performed to correlate the mechanical degradation of GFRP reinforcing bars and the diffusion rate of alkaline solution into the GFRP matrix. As noted in the earlier sections, the rate of transport, or the rate of diffusion of elements or compounds, has a significant impact on the bars' residual strength. The apparent diffusion coefficient is a common parameter used to predict the reduction of mechanical properties of GFRP, as this coefficient is directly related to the rate of transport of the aggressive compound. Fick's law and the Arrhenius model have been used to predict the residual strength of GFRP bars embedded in concrete. Shen and Springer (1976) recommended that the diffusion coefficient (required in Fick's law) be obtained using the following equation:

$$D = \frac{\pi r^2}{16}\left(\frac{M_2 - M_1}{M_m}\right)^2\left(\frac{1}{\sqrt{t_2} - \sqrt{t_1}}\right)^2 \tag{2.1}$$

where, M_1, M_2, and M_m are the moisture contents of the bar (in percent) at time t_1, t_2, and at saturation, respectively.

Katsuki and Uomoto (1995) proposed a prediction model based on Fick's first law. The authors assumed that the tensile strength of GFRP bar can be determined quantitatively by the amount of alkali penetration area into the bars and recommended that the depth of penetration be calculated using the following:

$$X = \sqrt{2 \cdot D \cdot C \cdot t} \tag{2.2}$$

Where, X is the depth of penetration from the surface, C is the alkaline concentration (percent), t is the curing time, and D is the diffusion coefficient. It should be noted that various units can be used in this equation and the units of the square root of the product should result in a length unit.

The authors assumed that as glass fibers were exposed to the diffusing solution these fibers exhibited complete failure and no longer contributed to the bars' capacity. Using this assumption the authors proposed the following equation for estimating the residual strength:

$$\sigma_t = \left(1 - \frac{\sqrt{2 \cdot D \cdot C \cdot t}}{R_0}\right)^2 \cdot \sigma_0 \tag{2.3}$$

where, σ_0 and σ_t are the tensile strengths before and after exposure (stress units), respectively, and R_0 is the radius of GFRP bar.

A similar approach was proposed by Tannous and Saadatmanesh (1998). Using results from moisture absorption and tensile strength tests the authors recommended that Fick's law be used to predict the residual strength. The authors recommended that moisture absorption be used to estimate the diffusion coefficient.

Trejo et al. (2005) reported that the assumption of complete loss of glass fiber capacity likely overestimated the loss of capacity and proposed an exposure factor, λ, to account for this time-dependent deterioration of the bond between the glass and resin. The proposed modified formula, modified with the exposure factor, is as follows:

$$\sigma_t = \left(1 - \frac{\sqrt{2 \cdot D \cdot \lambda \cdot t}}{R_0}\right)^2 \cdot \sigma_0 \tag{2.4}$$

where, the definition of the variables has already been reported and λ is the reduction factor less than unity.

The Arrhenius equation has been widely used to establish relationships between degradation data from laboratory accelerated aging tests and service-life of field structures. Proctor et al. (1982) suggested that the time-temperature relationship can be obtained using the deterioration data of material after exposure in concrete at different temperatures. If the shape of the residual strength curves is a function of the logarithm of time and is similar for different temperatures, the Arrhenius equation could be applicable. Katsuki and Uomoto (1995) reported that the Arrhenius equation offers a good correlation between the temperature and the rate of diffusivity and chemical reaction. The Arrhenius equation is shown as follows:

$$k = A\exp\left(-\frac{E_a}{RT}\right) \tag{2.5}$$

where, k = the rate constant,

A = the frequency factor,

E_a = activation energy (KJ),

R = the universal gas constant, and

T = the absolute temperature (Kelvin).

Equation 2.5 can also be used to determine the influence of temperature on the apparent diffusion coefficient, D_{at}, at some temperature, T, by substituting k and A with and D_{at} and D_{a0} as follows:

$$D_{at} = D_{a0}e^{-E_a/RT} \tag{2.6}$$

This approach was used by Dejke (2001) to generate a relative time shift factor (*TSF*). Dejke (2001) proposed using the *TSF* to transform the time in the accelerated test to actual service lives for GFRP reinforcement. Because the time for a certain reaction to take place must be proportional to the inverse of the rate of reaction, Dejke (2001) proposed determining the *TSF* as follows:

$$TSF = \frac{t_1}{t_2} = \frac{c/k_1}{c/k_2} = \frac{A \cdot e^{\frac{-E_a}{RT_2}}}{A \cdot e^{\frac{-E_a}{RT_1}}} = e^{\frac{E_a}{R}\left(\frac{1}{T_1} - \frac{1}{T_2}\right)} \tag{2.7}$$

where, T_1 and T_2 are the exposure temperatures (in Kelvin) and t_1 and t_2 are the times required for a certain decrease in some mechanical property at temperatures T_1 and T_2, respectively. The *TSF* is sensitive to the activation energy, and a good estimate of this is needed to generate a reasonable *TSF*.

Vijay and GangaRao (1999) also developed a formula to associate the time between an accelerated aging test in an alkaline solution with in-service field performance as follows:

$$\frac{N}{C} = 0.098 \cdot e^{0.0558 \cdot T} \tag{2.8}$$

where, N is the in-service field performance in days and C is the accelerated exposure age (in days) in the laboratory exposed to temperature, T.

This correlation model was based on climate conditions of the Northeastern United States, with the assumption that the average annual temperature was 53 ^{o}F (11.7 ^{o}C). Based on this equation, if 104 days of laboratory exposure at 140 ^{o}F (60 ^{o}C) resulted in a 10 percent loss in

tensile capacity the same reduction in tensile capacity would occur at 69 years of in-service conditions in a standard concrete environment exposed to a temperature of 53 ^{o}F (11.7 ^{o}C).

2.4. TENSILE STRENGTH DESIGN REQUIREMENTS

The American Concrete Institute's (ACI) Committee 440 and the American Association of State Highway and Transportation Officials Load and Resistance Factor Design (AASHTO LRFD) Specifications 2008 require using an environmental reduction factor as a design parameter when considering the reduction in tensile strength of GFRP in actual structures. This reduction factor, C_E, is dependent on the exposure conditions of the GFRP-reinforced concrete; for concrete not exposed to earth and weather the reduction factor is 0.8 and for concrete exposed to earth and weather the reduction factor is 0.7. The design tensile strength, f_{fu}, of FRP reinforcing bar considering these required reductions can then be determined as follows:

$$f_{fu} = C_E f_{fu}^* \tag{2.9}$$

where, f_{fu}^* is the GUTS of a FRP bar. The GUTS is defined as the mean tensile strength of a set of test specimens minus three standard deviations ($f_{fu}^* = f_{u,ave} - 3\sigma$).

3. MATERIALS

Project 9-1520 reported on the performance of GFRP bars with diameters of 0.625 and 0.75 inch (16 and 19 mm) provided by three different manufacturers. The bars contained approximately 70 percent of unidirectional glass fibers by volume—the remaining volume being resin and air voids. Three different bar types representing each manufacturer were evaluated. The bars were identified in that report as P, V1, and V2 and were manufactured by Marshall Industries, Hughes Brothers, and Pultrall Inc., respectively. Type P bars are no longer being produced.

Schaefer (2002) reported that bar Type P bar was made with a polyethylene terephthalate (PET) polyester matrix and E-glass fibers. Bar Type V1 contained E-glass fibers embedded in a vinyl ester resin. This bar was made with external helical fiber wrapping and the surface of the bar was coated with fine sand. Bar Type V2 was composed of E-glass fibers embedded in a vinyl ester resin and had a circular cross section coated with coarser sand. Figures 3.1 and 3.2 show the surface and cross section of this bar type (Trejo et al., 2005). Trejo et al. (2005) also reported a range of diffusion coefficients for the different GFRP bars from 4.47×10^{-10} in^2/sec (2.88×10^{-13} m^2/sec) to 2.39×10^{-9} in^2/sec (1.54×10^{-12} m^2/sec), with a mean value of 1.38×10^{-9} in^2/sec (8.9×10^{-13} m^2/sec). The mean value was used for the modeling.

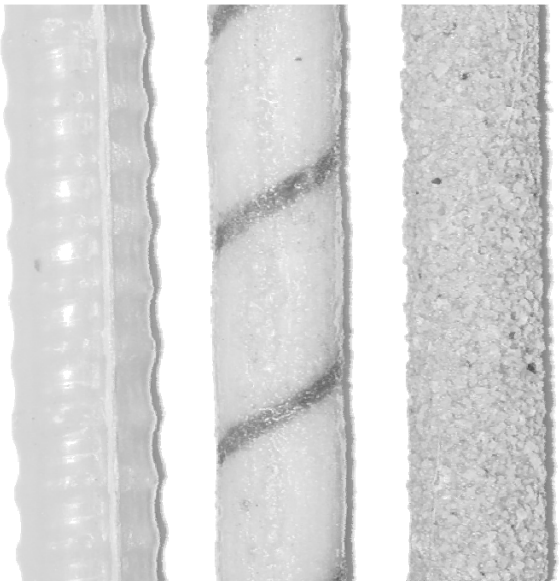

Figure 3-1. Surface of GFRP Bar Types P, V1, and V2.

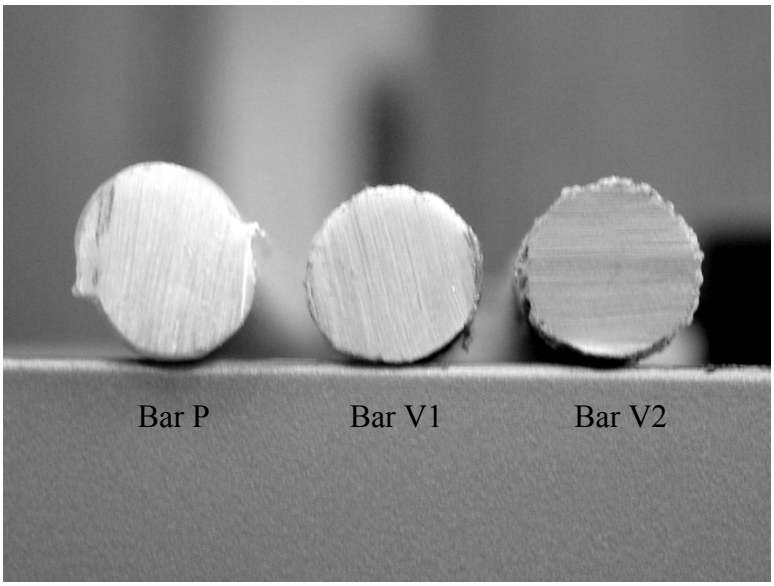

Figure 3-2. Cross-section Views of GFRP Bar Types P, V1, and V2.

Schaefer (2002) conducted an examination of the bars under SEM and found that the thickness of the resin around the circumference of all three bar types was non-uniform. A layer of resin needed to protect the fibers was present on most of the surface of the bars and was more prevalent on one side of the bar (likely a result of gravity during the production process). This resulted in portions of the glass fibers having no protective resin. None of the bar types exhibited a uniform resin matrix cover over the glass fibers.

It should be noted that bars not used in research Project 9-1520 served as control specimens for this research project. In addition, bars that were embedded in concrete and tested were also used in this research project—these bars, embedded in concrete for 7 years, were characterized to assess the change in properties as a function of time. These beams were embedded in concrete and exposed to the outside environment in College Station, Texas, for approximately 7 years.

3.1. CONCRETE USED IN TXDOT PROJECT 9-1520

The GFRP-reinforced concrete specimens were fabricated with Texas Department of Transportation (TxDOT) class "S" concrete. The 28-day design compressive strength was 4000 psi (28 MPa) and the target water-cement ratio was 0.35. The concrete mixture contained the following proportions: 1895 lb/cy (1224 kg/m^3) of limestone (maximum size aggregate [MSA] = 1 inch [25 mm]), 1180 lb/cy (762 kg/m^3) of sand, 488 lb/cy (315 kg/m^3) of TxDOT type-1-3 aggregate, 116 lb/cy (75 kg/m^3) of Type C fly ash, 210 lb/cy (136 kg/m^3) of water, 4 fl. oz. (118 mL) of air entraining (Type AE90), 24 fl. oz. (710 mL) of superplasticizer, and 603 lb/cy (390 kg/m^3) of cement. The 28-day compressive strengths ranged from approximately 4200 to 6000 psi (29 to 41 MPa).

3.2. GFRP CHARACTERIZATION – POST-EXTRACTION

Sufficient samples were available from research Project 9-1520 such that a statistically valid number of samples could be extracted and tested for the current research project. The following sections provide a description of the GFRP bar characteristics.

3.2.1. GFRP Characterization – Post-Exposure

The research team extracted and tested each of the three different reinforcement types, with each bar type having two different diameters (0.625 inch [#5] and 0.75 inch [#6]). This resulted in six bar type/size combinations. The researchers extracted the bars from the concrete, taking care not to damage the bar surface. In some cases the bars had residual concrete bound to their surfaces; this had no influence on the property characterization of the bars. Several characterization tests were performed on the post-extracted bars: SEM, EDX, and thermogravimetric analysis (TGA) tests.

3.2.1.1. Scanning Electron Microscopy and Energy Dispersive X-ray Analyses

SEM analysis identified potential damage to the glass-matrix interface. However, no micrographs were collected during the initial research and the researchers had no micrographs for comparison. As such, the researchers could not determine if the glass fiber-resin interface was damaged. EDX tests validated the glass type used in the different bars: E-glass or AR-glass. According to Mufti et al. (2007a, 2007b), the absence of zirconium (Zr) is used to determine if the glass fibers are E-glass. Zirconium was not identified in any of the bar types and researchers determined that each bar type contained E-glass.

3.2.1.2. Thermogravimetric Analyses

Thermogravimetric analysis provides the mass fraction of the fibers in the composite. For this test the bars were ground into a powder. The sample was then heated to a temperature of approximately 620 °F (327 °C), effectively burning away the polymer resin and leaving behind the glass fibers. The mass of the specimen before and after the test was documented, and the mass volumes of the fibers were determined. The testing indicated that the approximate fiber content of the Type V1 and P bars was 79 and 71 percent, respectively. Bar V2 was not evaluated. These values meet the 70 percent minimum glass fiber content required by ASTM D2584, *Standard Test Method for Ignition Loss of Cured Reinforced Resins* (ASTM, 2008).

3.3. CONCRETE CHARACTERIZATION – POST-EXTRACTION

One objective of this research is to determine how the environment influences the properties of GFRP bars; more specifically, how the embedment of GFRP bars in concrete influences the residual tensile capacity and MOE of the GFRP bars. Because the concrete environment may have a significant influence on the GFRP properties, the research team evaluated the concrete in which the GFRP bars were embedded. The following sections describe the tests and characteristics of the concrete.

3.3.1. Alkalinity of Concrete Pore Solution

It has been reported that GFRP bars embedded in concrete are susceptible to the high pH pore solution typical of concrete, which could lead to a reduction in tensile strength and MOE (Ceroni et al., 2006). The issue of how the alkalinity (pH level) of the concrete pore solution

affects the degradation and long-term performance of GFRP bars needs to be addressed. As presented earlier, significant research on the deterioration of GFRP specimens exposed to high pH solutions has been performed and models have been developed from these solution studies. However, the concrete pore solution differs from many of the simpler solutions and is more complex. The objective of this work is not to assess the constituents of the concrete pore solution but simply to assess the pH and to determine if the deterioration, if any, is a function of the pH of the concrete pore solution.

Researchers collected two to three small concrete samples from each of the 36 beams that contained GFRP bars. In cases where large deviations in the pH were observed, a third sample was collected and evaluated. The mean value of the pH results from each beam is reported. Statistical analyses determined if a correlation exists between concrete pore solution pH values and GFRP bar tensile capacity.

The researchers used Environmental Protection Agency (EPA) Method 9045D, Soil and Waste pH, to obtain pH values of the pore solution from the concrete beams. Specimens were collected from as close to the GFRP as possible. A 1:1 weight ratio of concrete to water was used. A Denver Instrument model 250 pH meter with a Denver Instrument pH electrode was used to evaluate the pH.

The pH values of the pore solution ranged from 12.25 to 13.05 for all tests, which is typical of field concrete. These values are also representative of the values used in many accelerated aging tests identified in the literature. The results of the pH tests are shown in Figure 3.3, with the data separated according to the type of bar that was embedded in each beam. Although the concrete containing the GFRP Type P bars indicates that the pore solution pH may be higher, based on a statistical t-test of equality, at a 0.05 level of significance (which is the

probability of erroneously rejecting the hypothesis), the hypothesis that the mean pore solution pH of the concrete containing the GFRP Type P bars is the same as the mean pore solution pH of the concrete containing the GFRP Types V1 and V2 bars cannot be rejected.

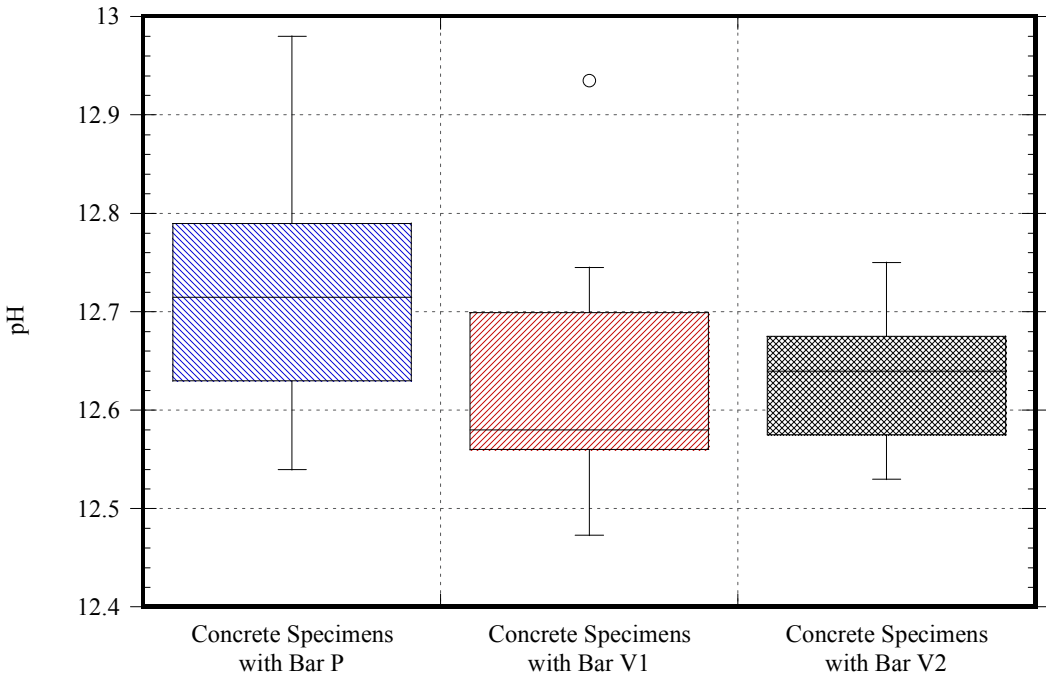

Figure 3-3. pH Results from Concrete Beams.

3.3.2. Permeable Voids in Concrete

Because the exposure of GFRP to moisture influences the rate of deterioration, it is important to know if the concrete has sufficient moisture to cause deterioration. The literature has shown that moisture uptake by GFRP bars can result in changes in properties of the bars. Therefore, the research team assessed the amount of voids in the concrete. As with the pH test, the data collected from these tests will be correlated with the tensile capacity of the GFRP bars.

The standard test procedure (ASTM C642 [1997], Standard Test Method for Density, Absorption, and Voids in Hardened Concrete) used to determine the quantity of permeable voids of the concrete requires that a 21 in^3 (350 cm^3) or 1.75 lb (800 g) specimen be used for the test. The research team used two 4-inch (101.6 mm) diameter cores from each beam to assess these characteristics (a total of 72 tests). Mean values of the permeable voids from each beam were used to determine if a correlation exists between permeable voids and the GFRP tensile capacity data.

The volume of permeable voids as determined by the ASTM standard ranges from approximately 11 to 17 percent and the average for all beams was 13.9 percent. These data will be used in an attempt to correlate any reduction in capacity with void density. The results of the void density tests are shown in Figure 3.4. Based on a statistical t-test of equality, at a 0.05 level of significance, the hypotheses that the means of the volumes of permeable voids of the concretes containing the GFRP Types P, V1, and V2 bars are the same cannot be rejected.

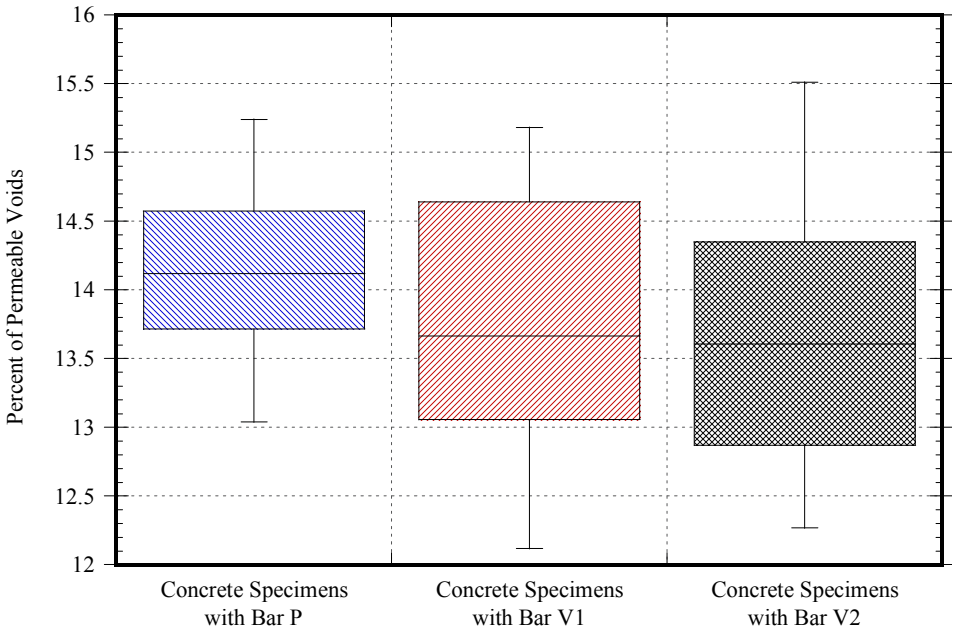

Figure 3-4. Volume of Permeable Voids for Concrete with All Bar Types.

3.4. SUMMARY

The investigation on the existing samples from Project 9-1520 consisted of assessing the concrete and GFRP bars from the project. The pH values of the concrete pore solution varied from 12.25 to 13.05, and no significant differences were identified between beams with different bar types. The permeable voids in the concrete from the beams ranged from 11 to 17 percent, and no significant differences were identified between beams with different bar types. All GFRP bar types had E-glass fibers and bar Types V1 and P had more than 70 percent fibers, as required by the ASTM D2584 standard.

4. EXPERIMENTAL PROGRAM AND PROCEDURES

The primary objective of this research is to generate long-term data on the residual strength of GFRP reinforcing bars that have been embedded in concrete for 7 years. If possible, correlations will be made with material characteristics. Samples from a previous research project (9-1520, Fiber-Reinforced Polymer Bars for Reinforcement in Bridge Decks) were stored in the outside environment in College Station, Texas. Most samples had been tested in the previous research project. The researchers identified undamaged GFRP samples to use in this research program. Using these data from this research project, a probabilistic model will be developed to estimate the residual strength of GFRP bars embedded in concrete.

4.1. ANALYSIS OF LOAD CONDITIONS FROM PREVIOUS TESTING

The beams that contained the GFRP bars were previously tested in a four-point beam bending test as part of research Project 9-1520. Because GFRP bars can be damaged when loaded, the research team needed to establish if these tests resulted in reduced capacities for the bars embedded in the concrete samples and subjected to the test loads. The research team subjected untested bars to the stresses imposed on the GFRP bars embedded in concrete and subjected to the four-point bending tests. In most cases, GFRP bars were removed from locations that exhibited limited damage and lower stresses (i.e., the beam ends).

The bar layout and test setup used in research Project 9-1520 are shown in Figure 4.1. During this test program the center 32 inches (0.813 m) of the beam was subjected to a constant maximum moment, calculated to be approximately 15 kips (66.72 N). The researchers were concerned that the test may have damaged the GFRP reinforcement and reductions in strength after 7 years of exposure could be a result of this loading instead of the deterioration of the bars.

To assess the influence of load on residual strength the researchers evaluated the tensile capacity of unexposed, unstressed bars that remained from the original test program (Project 9-1520). However, to determine if these bars were damaged during the original testing, the unexposed, unstressed bars had to be subjected to similar stresses. Unexposed, unstressed GFRP specimens were loaded to 15 kips (66.72 N), the load was removed, and the specimens were then loaded to failure. The team then compared the ultimate tensile strength of these unexposed, unstressed bars subjected to 15 kips (66.72 N) with the reported values of the new GFRP bars to determine if the bars experienced significant damage during the initial test program.

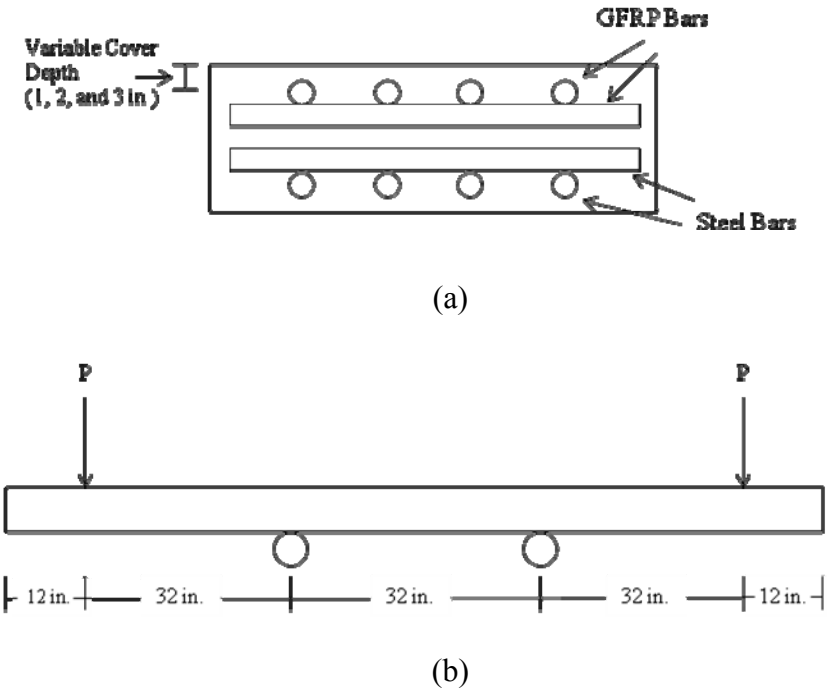

Figure 4-1. (a) Bar Layout; (b) Beam Loading (after Trejo et al., 2005). Not to scale.

The research team performed 60 tension tests with unexposed, unstressed bars (control). The stresses in the embedded GFRP bars were calculated by Trejo et al. (2005). For each bar type (V1, V2, and P) and bar diameter (0.625 inches and 0.750 inches) two sets of five specimens each were cast. For each set of two, one set was preloaded to 15 kips, unloaded, and loaded again until failure to simulate stress caused by the bending and releasing during the beam testing. The second set of bars was loaded directly to failure.

Analysis of the results from the preliminary tension test showed that the beam bending test had no effect on the ultimate tensile properties of the GFRP bars. Based on the statistical t-test of equality, at a 0.05 level of significance (which is the probability of erroneously rejecting the hypothesis), the hypothesis that the mean tensile stress for the preloaded bars is the same as

the mean tensile stress for the non-preloaded bars cannot be rejected. Hence, the research team was able to conclude that the bending test did not affect the tensile properties of the embedded bars, and bar sections could be used from any part of the concrete beam. The t-test results are provided in Appendix A.

4.2. GFRP BAR EXTRACTION

Before tests could be performed, the GFRP bars had to be extracted from the concrete beams. The research team used the following method to extract the bars, as this method proved to eliminate damage to the bar surface:

- A diamond blade saw was used to make cuts parallel to the bars over the full length of the beam.
- Small pneumatic chipping hammers were used to break the concrete from around the bars.
- The bars were removed from the concrete and stored in the laboratory until tested.
- After each bar was extracted, details such as bar type, bar size, number of bars, cover, and any exposed surfaces or concrete damage were noted on beam documentation cards. Figure 4.2 shows three extracted bars and Figure 4.3 shows an example of the information recorded on the beam cards. Beam cards for each beam are provided in Appendix B.

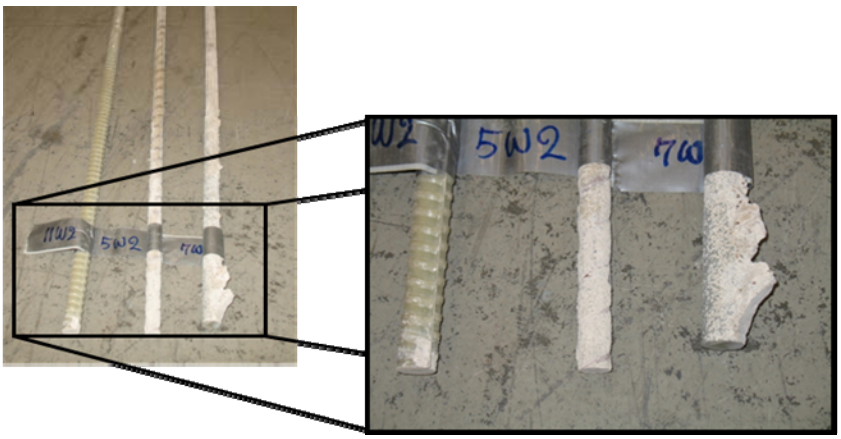

Figure 4-2. Extracted Bars.

4.2.1. GFRP Bar Inspection

Although bars were removed from all of the beams, not all parts of all the GFRP bars could be used. The bending test damaged some small portions of the beams, which in turn damaged or exposed parts of the GFRP bars. Because the objective of the program is to assess the reduction in GFRP properties for bars embedded in concrete, the research team avoided using bars that were exposed to larger cracks or delaminations. Also, prior to testing the GFRP bars the research team closely examined each individual bar for any signs of physical damage to the surface. Damaged areas were identified on the GFRP bars and documented on the beam cards. A section of bar was only tested if it was clear that there was no damage in the test area (i.e., the center section of the bar). After extraction and inspection, 160 GFRP bars were deemed usable for testing. A summary of the tested bars with nominal cover depths is shown in Table 4-1. The nominal cover was reported by Trejo et al. (2005). During the extraction of the bars, the actual measured cover was not always consistent with that provided in the report. Both covers were noted and analyzed in this report.

Table 4-1. Available Test Specimens with Nominal Cover Depths.

Bar Type	Bar Size	1 inch (25 mm) cover	2 inch (50 mm) cover	3 inch (75 mm) cover	Number of Bars Available for Testing
V1	#5	10	14	11	35
	#6	9	10	10	29
V2	#5	10	10	10	30
	#6	8	5	5	18
P	#5	5	5	5	15
	#6	11	11	11	33
TOTAL		53	55	52	160

Several factors possibly influence the capacity of the GFRP bars embedded in concrete: cover depth, concrete pH, concrete porosity, and beam position within the exposure stack. Statistical analyses were performed to determine if any of these factors influenced the capacity and/or stiffness of the GFRP bars. The data attained from the tests were normalized to evaluate the influence of the conditions.

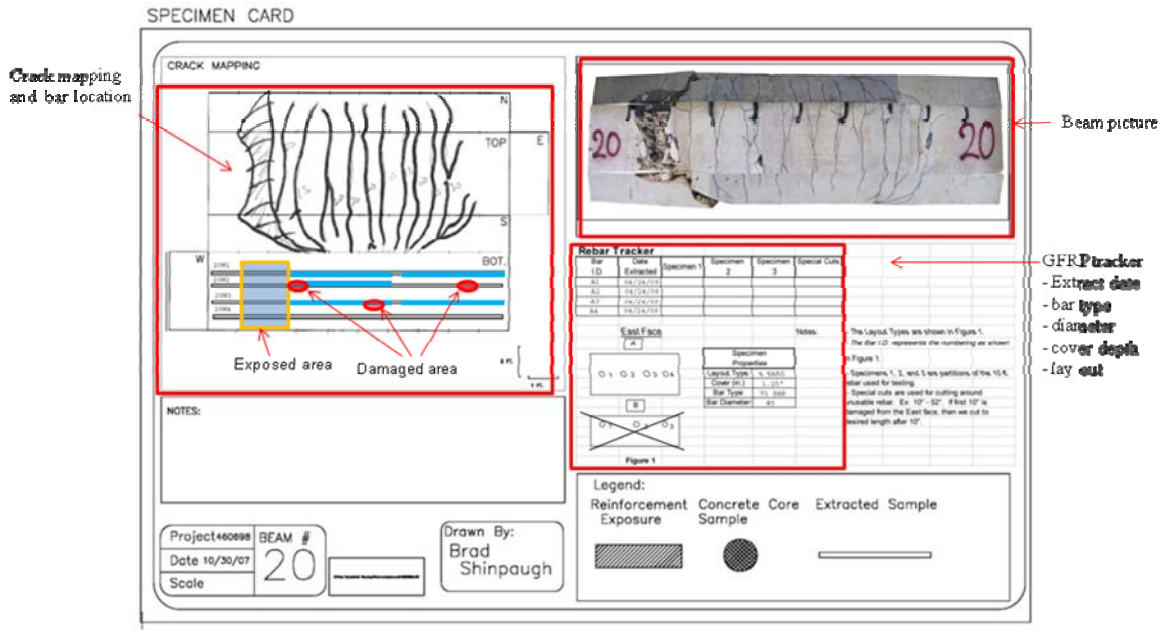

Figure 4-3. Example of Information Collected on Beam Cards.

4.3. TEST PROCEDURES

GFRP bars were assessed for tensile capacity and MOE. The following sections describe the procedures used to assess these bars.

4.3.1. Tensile Tests

GFRP bars were embedded in concrete and exposed to a natural environment for approximately 7 years. The research team extracted the GFRP bars and evaluated the tensile capacity of these exposed GFRP bars. To evaluate this capacity loss, the tensile capacities of unexposed GFRP bars also had to be assessed. The research team had data from unexposed GFRP bars from the earlier research (Project 9-1520) but also performed additional tests on GFRP bars that were not exposed to the concrete environment. These were used by the research

team to evaluate the degradation of the bars and for developing a time-variant model for predicting residual capacity as a function of time.

Tension tests were performed on 160 extracted specimens. A 110 kip (489.3 kN) load frame with 0.5 percent load accuracy (within the range tested) was used. Data were documented automatically with a data acquisition system. The tensile tests were performed with the same procedure as reported by Trejo et al. (2005). All efforts were made to be consistent with the previous sample test preparation and test methods; however, some modifications had to be implemented. The GFRP bars were prepared and tested in the following manner:

- The GFRP bars were cut into 41-inch (1041 mm) lengths, ensuring that the bar sample was taken from an area that exhibited no physical damage on the bar surface.
- Steel pipe sections (1.5-inch [38 mm] diameter) were cut into 12-inch (300 mm) sections for the grips. The grips are necessary when testing GFRP bars to prevent damage to the GFRP bar.
- A high-performance expansive grout was cast in the void between the pipe and GFRP bar and allowed to cure for a minimum of 24 hours before testing.
- The specimens were then placed in the testing apparatus. A small preload was applied prior to testing to prevent slippage during the test.
- A linear variable differential transducer (LVDT) was mounted to the GFRP specimen, the data acquisition was started, and the bar was loaded to failure at a load rate of 0.11 inch/minute (2.8 mm/minute).

4.3.2. Modulus of Elasticity Tests

The MOE of the GFRP reinforcement has a direct impact on the performance of reinforced concrete systems. The MOE can affect crack widths, deflections, and other

performance indicators (Nkurunziza et al., 2005a, 2005b). The research team assessed the modulus of elasticity of GFRP bars embedded in concrete for 7 years.

The MOE was determined for each of the 160 GFRP samples extracted. The researchers fabricated a tensiometer for determining the strain in the GFRP bars with LVDTs spaced 120 degrees apart, as shown in Figure 4.4. The gage length of the tensiometer was 2.64 inches (67 mm) and the load rate for the testing was 0.11 inch/min (2.8 mm/min). Strain data were collected until the GFRP samples were loaded to approximately 50 percent of their ultimate strength. The tensiometer was then removed and the samples were tested to failure.

Figure 4-4. (a) LVDT Being Attached to GFRP Bar before Testing; (b) Close-up of LVDT Device.

5. RESULTS AND DISCUSSION

To develop a model for predicting the change in tensile capacity and MOE of GFRP reinforcing bars embedded in concrete, the research team had to generate sufficient data on the bars embedded in the concrete for 7 years, as limited data are available in the literature. The following sections present the data from the test program.

5.1. TENSION TEST RESULTS

The researchers evaluated the tension capacity of 60 unloaded and unexposed GFRP bars and used these data as the control data. The research team used statistical analyses to assess the potential influence of concrete cover, alkalinity of the concrete pore solution, concrete porosity, and beam storage position on the time-variant changes in tensile capacity and MOE. Figure 5.1 shows the tensile capacities for the extracted GFRP bars with and without exposure as a function of bar type and size. Tables 5-1, 5-2, and 5-3 show the tensile strength results for the three different bar types. In all cases the mean bar capacity decreased as a function of time, indicating that the tensile capacity of GFRP bars is reduced when embedded in concrete. Of more importance is the rate at which the capacity of these bars decreases and how this rate correlates with design parameters. These issues will be addressed in Chapter 6 on modeling. The following sections attempt to identify other variables that influenced the reduction in capacities of the GFRP bars.

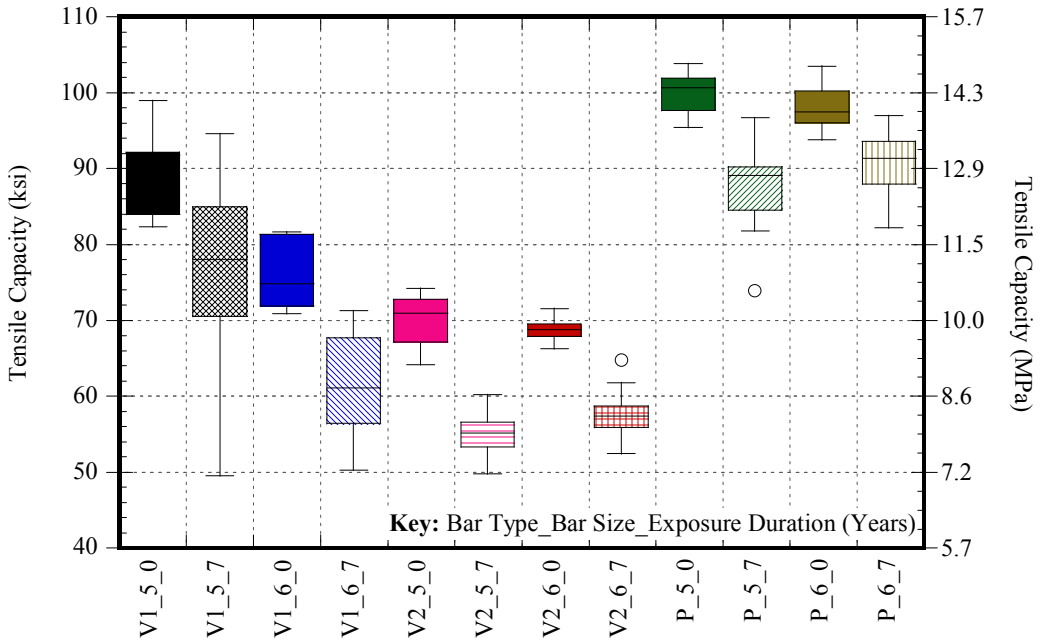

Figure 5-1. Tensile Capacities of GFRP Bars with and without Exposure in Concrete.

Table 5-1. Tensile Strength Data for Type V1 GFRP Reinforcing Bars.

V1 #5		V1 #6	
Tensile Strength - No Exposure ksi (MPa)	Tensile Strength - After Exposure ksi (MPa)	Tensile Strength - No Exposure ksi (MPa)	Tensile Strength - After Exposure ksi (MPa)
76.39 (526.71)	70.31 (484.78)	83.28 (574.19)	69.19 (477.05)
93.26 (642.99)	76.87 (530.03)	73.79 (508.74)	63.18 (435.63)
96.78 (667.26)	69.35 (478.14)	73.32 (505.54)	68.13 (469.75)
90.77 (625.81)	92.23 (635.90)	83.18 (573.51)	52.89 (364.68)
85.34 (588.39)	51.90 (357.86)	77.17 (532.04)	56.44 (389.12)
	74.45 (513.34)	82.95 (571.93)	68.28 (470.78)
	49.51 (341.37)	72.31 (498.56)	56.44 (389.12)
	70.79 (488.06)	73.32 (505.54)	56.30 (388.14)
	72.89 (502.54)	79.03 (544.90)	54.91 (378.62)
	84.97 (585.88)	75.44 (520.13)	65.03 (448.39)
	84.51 (582.66)		71.29 (491.51)
	88.98 (613.50)		63.67 (438.98)
	69.15 (476.80)		64.00 (441.24)
	74.24 (511.86)		65.48 (451.48)
	65.91 (454.41)		67.93 (468.36)
	66.32 (457.29)		67.65 (466.40)
	72.32 (498.66)		58.50 (403.37)
	67.06 (462.38)		56.80 (391.64)
	93.59 (645.28)		61.10 (421.28)
	94.65 (652.59)		50.24 (346.36)
	77.90 (537.07)		51.19 (352.95)
	89.55 (617.39)		69.16 (476.85)
	92.88 (640.39)		55.91 (385.47)
	88.88 (612.83)		58.98 (406.67)
	88.40 (609.48)		67.83 (467.69)
	69.80 (481.22)		56.19 (387.42)
	84.95 (585.68)		58.61 (404.09)
	84.11 (579.91)		58.99 (406.72)
	83.36 (578.17)		62.57 (431.42)
	80.54 (555.31)		
	83.75 (577.43)		
	79.92 (551.02)		
	72.01 (496.51)		
	82.55 (569.19)		
	77.96 (537.54)		
Mean ***Standard Deviation***	***Mean*** ***Standard Deviation***	***Mean*** ***Standard Deviation***	***Mean*** ***Standard Deviation***
88.51 (610.23)	77.92 (537.21)	77.38 (533.51)	61.27 (422.46)
7.95 (54.82)	10.91 (75.23)	4.44 (30.62)	5.99 (41.31)

Table 5-2. Tensile Strength Data for Type V2 GFRP Reinforcing Bars.

V2 #5		V2 #6	
Tensile Strength - No Exposure ksi (MPa)	Tensile Strength - After Exposure ksi (MPa)	Tensile Strength - No Exposure ksi (MPa)	Tensile Strength - After Exposure ksi (MPa)
76.67 (528.62)	58.06(400.31)	75.87 (523.12)	56.53 (389.76)
77.10 (531.56)	56.42(388.98)	72.29 (498.42)	58.71 (404.82)
75.10 (517.79)	60.25 (415.40)	73.70 (508.15)	55.90 (385.43)
71.67 (494.17)	57.85 (398.87)	73.00 (503.31)	57.38 (395.64)
71.82 (495.15)	56.65 (390.61)	70.22 (484.15)	52.45 (361.61)
	54.85 (378.18)	73.94 (509.79)	58.26 (401.67)
	50.04 (344.99)	72.72 (501.41)	57.34 (395.36)
	52.83 (364.26)	73.32 (505.55)	57.23 (394.60)
	55.31 (381.37)	71.97 (496.22)	60.67 (418.28)
	52.94 (365.04)	71.46 (492.68)	52.90 (364.76)
	56.55 (389.89)		55.89 (385.33)
	56.62 (390.41)		53.30 (367.49)
	53.80 (370.96)		59.37 (409.34)
	54.93 (378.70)		57.47 (396.25)
	49.82 (343.50)		56.58 (390.09)
	54.73 (377.34)		61.80 (426.10)
	56.39 (388.79)		64.80 (446.76)
	54.46 (375.51)		
	54.78 (377.73)		
	55.95 (385.73)		
	52.87 (364.52)		
	56.76 (391.33)		
	53.32 (367.64)		
	53.03 (365.62)		
	51.97 (358.33)		
	55.90 (385.40)		
	56.34 (388.46)		
	54.18 (373.56)		
	55.38 (381.83)		
	56.95 (392.63)		
Mean ***Standard Deviation***	***Mean*** ***Standard Deviation***	***Mean*** ***Standard Deviation***	***Mean*** ***Standard Deviation***
74.47 (513.46)	55.00 (379.20)	72.85 (502.28)	57.45 (396.08)
2.60 (17.91)	2.28 (15.72)	1.54 (10.59)	3.15 (21.71)

Table 5-3. Tensile Strength Data for Type *P* GFRP Reinforcing Bars.

P #5		P #6	
Tensile Strength - No Exposure ksi (MPa)	Tensile Strength - After Exposure ksi (MPa)	Tensile Strength - No Exposure ksi (MPa)	Tensile Strength - After Exposure ksi (MPa)
98.93 (682.07)	96.71 (666.78)	103.47 (713.41)	93.00 (641.20)
95.42 (657.86)	92.25 (636.06)	97.34 (671.17)	92.60 (638.48)
101.32 (698.60)	90.48 (623.83)	97.59 (672.83)	82.81 (570.95)
103.81 (715.71)	82.65 (569.89)	93.82 (646.88)	82.23 (566.93)
99.98 (689.36)	90.41 (623.38)	94.41 (650.90)	92.75 (639.49)
103.84 (715.97)	88.34 (609.06)	101.12 (697.21)	94.78 (653.47)
101.98 (703.15)	89.16 (614.72)	96.31 (664.03)	93.22 (642.71)
97.66 (673.35)	85.52 (589.67)	99.94 (689.07)	90.41 (623.35)
101.42 (699.25)	86.72 (597.93)	100.29 (691.48)	93.60 (645.37)
97.26 (670.55)	83.50 (575.74)	96.02 (662.02)	96.48 (665.18)
	73.91 (509.56)		85.82 (591.72)
	90.01 (620.58)		86.06 (593.33)
	89.28 (615.57)		87.52 (603.44)
	89.40 (616.41)		93.78 (646.58)
	81.78 (563.83)		86.71 (597.85)
			94.04 (648.39)
			96.62 (666.19)
			96.97 (668.55)
			92.61 (638.53)
			94.68 (652.76)
			87.95 (606.40)
			91.34 (629.73)
			87.46 (602.98)
			92.39 (636.97)
			88.08 (607.31)
			88.59 (610.78)
			92.08 (634.86)
			89.88 (619.73)
			90.17 (621.69)
			89.80 (619.17)
			91,09 (628.02)
			93.68 (645.87)
Mean ***Standard Deviation***	***Mean*** ***Standard Deviation***	***Mean*** ***Standard Deviation***	***Mean*** ***Standard Deviation***
100.16 (690.59)	87.34 (602.20)	98.03 (675.90)	90.91 (626.81)
2.83 (19.48)	5.36 (36.96)	3.10 (21.37)	3.77 (26.03)

5.1.1. Potential Influence of Beam Storage Position on GFRP Bar Tensile Capacity

Figure 5.2 shows how the GFRP-reinforced beams were stored for the 7-year exposure period. The researchers hypothesized that the beams at the tops of the stacks were exposed to higher temperatures and likely higher moisture conditions. To assess if the beam storage position influenced the beam capacity, the researchers compared the bar capacities of the top beams with the bar capacities from the beams below the top position. Figure 5.3 shows a box plot of the bar capacities from the top beams and the beams below the top. Note that none of the top beams contained Type P bars, so these were not assessed. Although the Type V1 bars embedded in the top beams seem to have lower tensile capacities, statistical t-tests of equality conducted for Types V1 #5, V1 #6, V2 #5, and V2 #6 bars at a 0.05 level of significance indicated that the hypothesis that the mean tensile stress for the bars embedded in the top beams is the same as the mean tensile stress for the bars embedded in the beams below the top cannot be rejected. That is, there is no statistically significant evidence to conclude that beam storage position results in a different mean tensile stress.

Figure 5-2. Storage Positions of GFRP-Reinforced Beams.

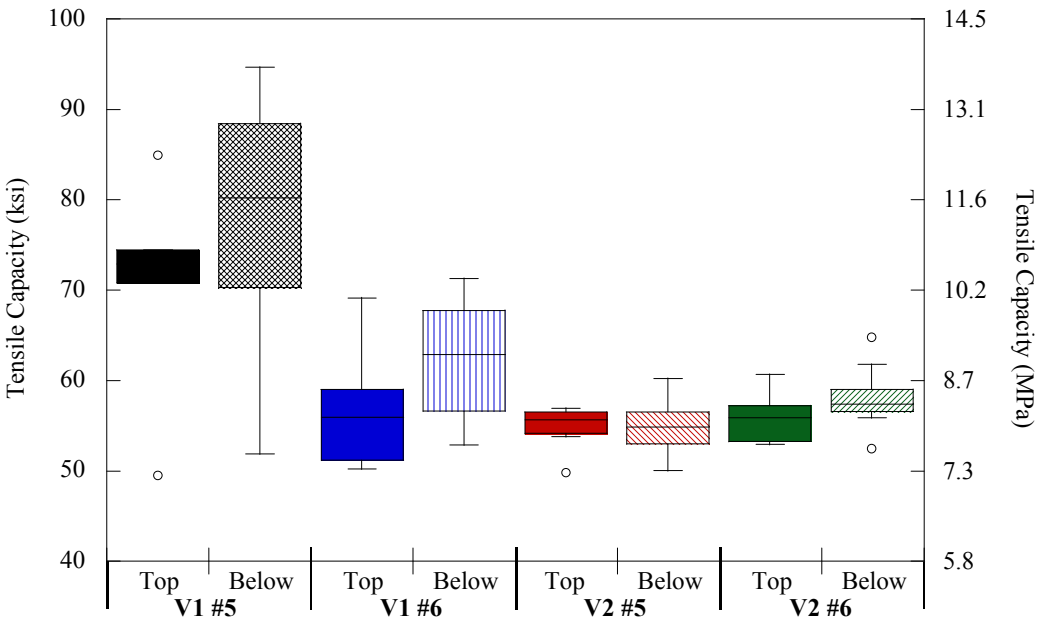

Figure 5-3. Comparison of Capacities of Bars Stored at Different Locations.

5.1.2. Potential Influence of Depth of Cover on GFRP Bar Tensile Capacity

It has been well documented that exposure conditions can influence the tensile capacity of GFRP reinforcement. Project 9-1520 evaluated the load-carrying capacity of GFRP-reinforced beams. GFRP bars were embedded in concrete beams with different depths of cover. Because the moisture in the concrete could vary as a function of depth and because the amount of moisture could influence the GFRP bar capacity, the researchers assessed if the depth of bar placement influenced the change, as a function of time, in the tensile capacity of the bars.

To compare the influence of concrete cover depth, the capacities of all GFRP bars were normalized to the capacity at time zero. These normalized capacities were then plotted as a function of depth of cover, as shown in Figure 5.4. The figure indicates that the depth of cover

had no influence on the residual bar capacity. This observation was confirmed by conducting a set of statistical t-tests of equality at a 0.05 level of significance.

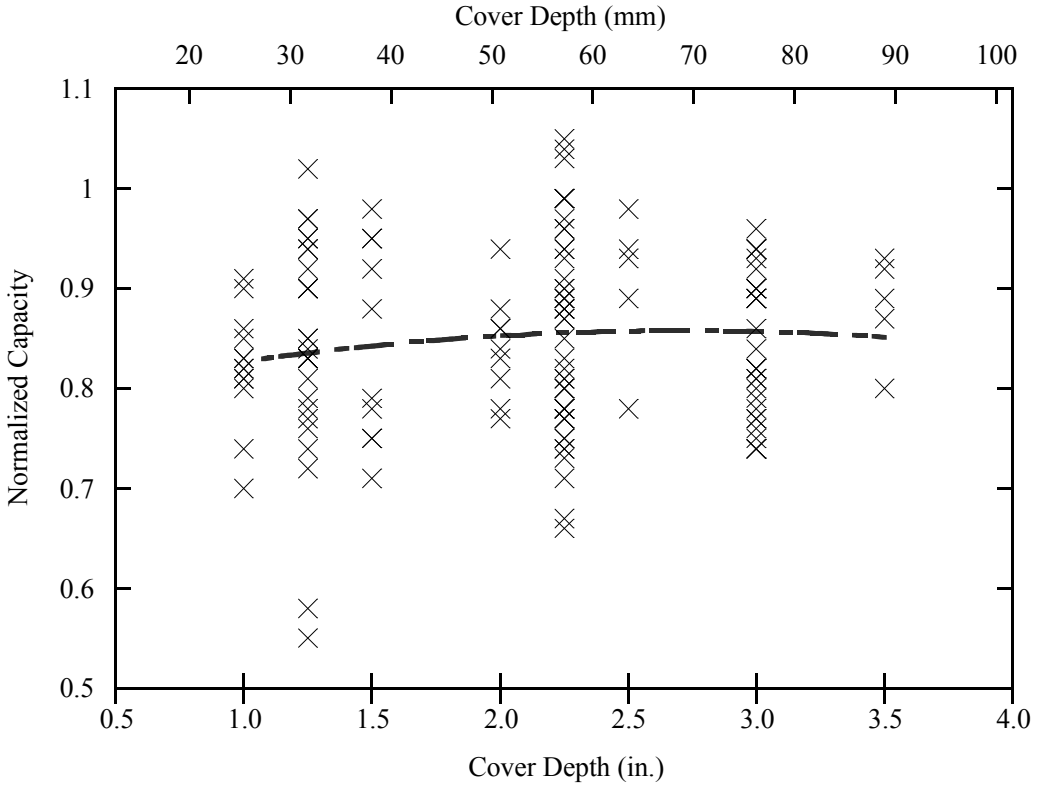

Figure 5-4. Influence of Cover Depth on Bar Capacity.

5.1.3. Potential Influence of Concrete Alkalinity on GFRP Bar Tensile Capacity

The alkalinity of the concrete pore solution of the beams was assessed using the method described in section 3.3.1. The literature reports that high alkalinity of concrete pore solution accelerates the degradation and resulting capacity loss in GFRP bars. As with the cover depth, the tensile capacities of the GFRP bars were normalized and plotted as a function of the concrete

pore solution pH (Figure 5.5). The figure indicates that there is no significant influence of concrete pore solution pH on the tensile capacity of GFRP bars. However, it should be noted that the range of the pore solution pH values only ranged from approximately 12.5 to 13—relatively high values. This indicates that variation in the alkalinity of the concrete pore solution, in the range of 12.5 to 13 pH for the specimens evaluated in this study had no influence on the tensile capacity of the GFRP bars. However, if the range of this pore solution pH had been larger, some influence may have been identified.

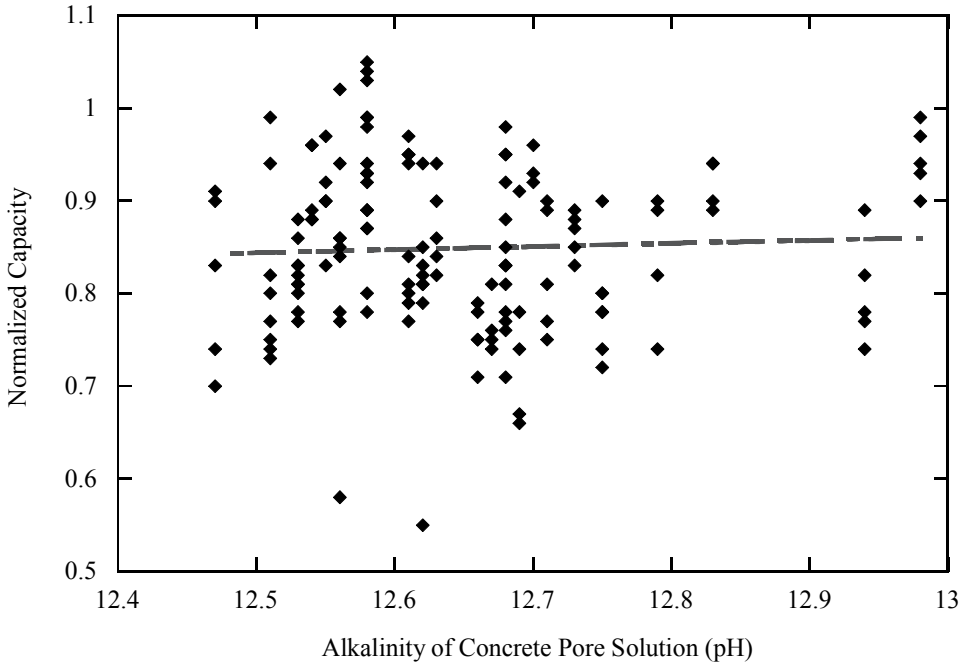

Figure 5-5. GFRP Bar Capacity as a Function of Concrete Pore Solution Alkalinity.

5.1.4. Potential Influence of Concrete Porosity on GFRP Bar Tensile Capacity

Moisture and concrete pore solution can influence the residual capacity of GFRP bars. A concrete having high porosity could have more pore solution; therefore, more pore solution can be transported into the GFRP bar to degrade the bar. As noted in section 3.3.2, the amounts of permeable voids were assessed for the different beams. Figure 5.6 shows the normalized capacities of the GFRP bars as a function of concrete porosity. Although the "best fit" line has an increasing slope, this slope is small and insignificant when compared to the scatter of the data. As such, for the porosity ranges observed in this research, no influence on GFRP bar capacity was observed.

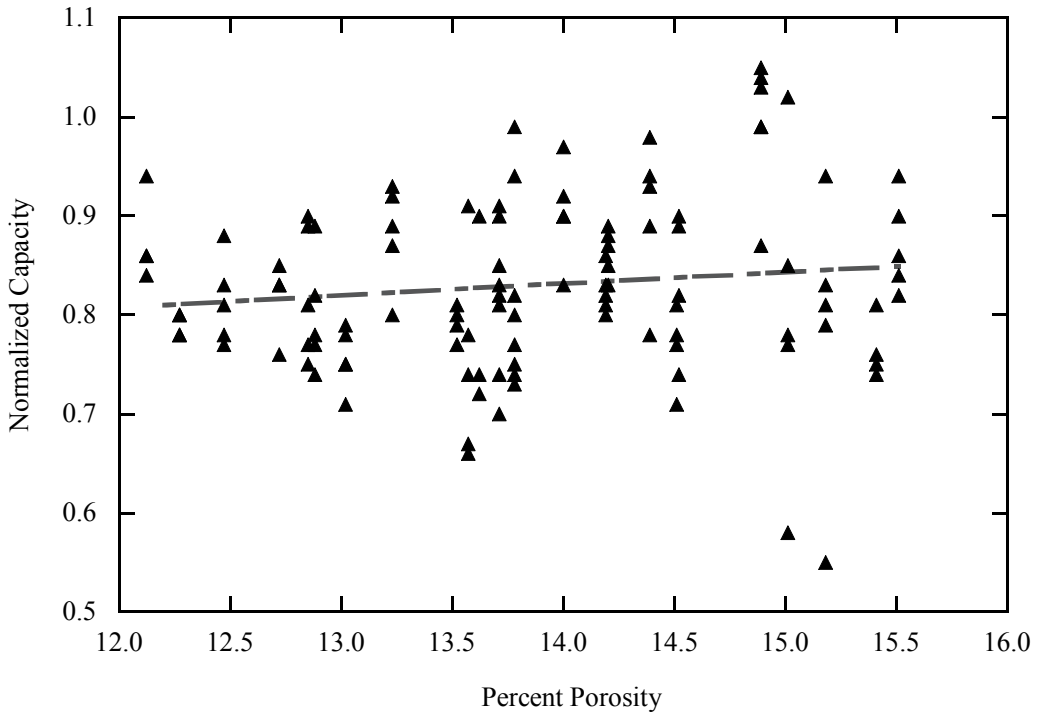

Figure 5-6. Tensile Capacity as a Function of Concrete Porosity.

5.2. MODULUS OF ELASTICITY TEST RESULTS

The MOE was assessed for all bars and these are plotted in Figure 5.7 as a function of concrete cover depth. Appendix C includes the test data from the MOE testing. Note that no significant change is observed between the unexposed GFRP samples and GFRP samples embedded in concrete for 7 years. Statistical t-tests of equality at a 0.05 level of significance indicated that the hypothesis that the mean MOE for the bars embedded in concrete is the same as the mean MOE for the unexposed bars cannot be rejected. That is, there is no statistically significant evidence to conclude that embedding the bars results in a mean MOE that differs from the mean MOE of unexposed bars. Because no significant changes in the MOE could be observed, no further analysis of the MOE is necessary, as it seems that no factors from this study impacted this GFRP characteristic. This research indicates that the MOE of GFRP is not reduced as a function of time (up to 7 years).

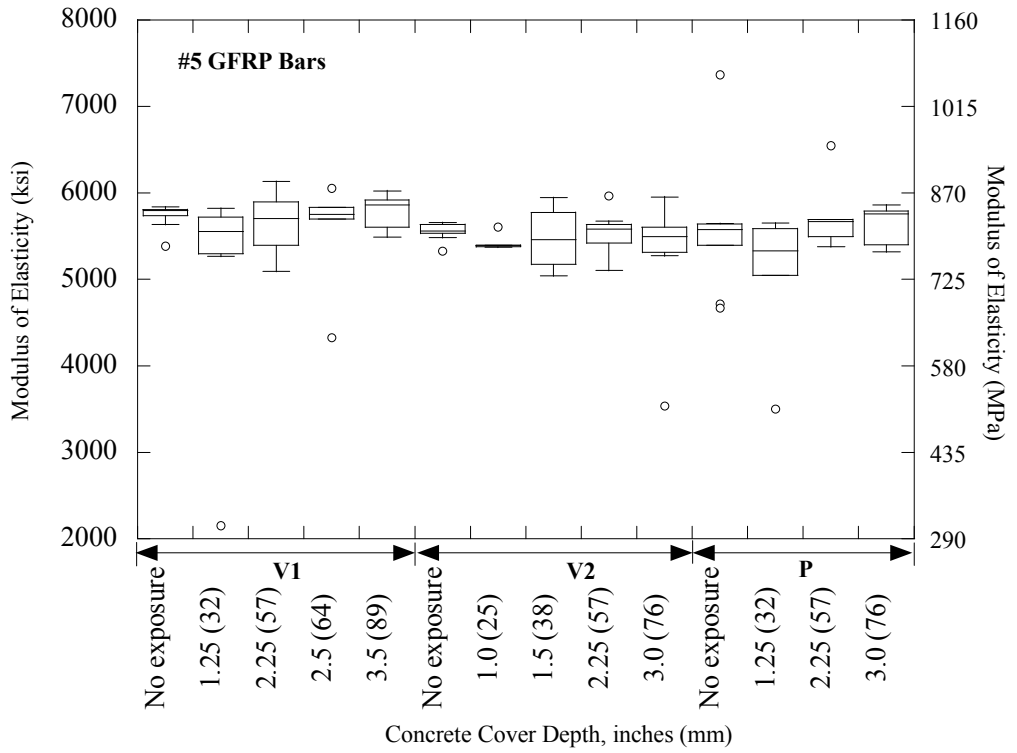

Figure 5-7. MOE as a Function of Time and Cover Depth (Note: All samples except the "no exposure" samples were embedded in concrete for 7 years).

5.3. SUMMARY

The test results indicate that none of the parameters evaluated, with the exception of embedment time, had a significant influence on the tensile capacity or MOE of the GFRP reinforcing bars. The tensile capacity of the GFRP bars exhibited a significant reduction, in some cases more than 20 percent, after 7 years of being embedded in concrete. The following chapter will develop a model to assess the time-dependent tensile capacity of GFRP bars.

6. TIME-VARIANT CAPACITY MODEL FOR GFRP BARS EMBEDDED IN CONCRETE

The data from the experimental program of this project and the additional data available from the literature were used by the research team to better understand the long-term performance of GFRP reinforcing bars embedded in concrete. In particular, the data were used to construct a probabilistic model that captures the dependency of the tensile strength on time and other influencing variables. The developed model is probabilistic to properly account for the relevant sources of uncertainties, including the statistical uncertainty in the estimation of the unknown model parameters and the model error associated to the inexact model form. This is a state-of-the-art model to predict the actual performance of GFRP bars embedded in concrete. The developed time-variant model provides the required information to assess the safety and performance of GFRP reinforcing bars embedded in decks, pavements, and other infrastructure elements reinforced with these materials.

6.1 FORMULATION OF THE PROBABILISTIC PREDICTION MODEL

The model in Eq. (2.3) was first modified to provide more flexibility to fit the experimental data as follows:

$$\sigma_t = \left[1 - \lambda\left(\frac{D \cdot t}{R_0^2}\right)^{\alpha}\right] \cdot \sigma_0 \tag{6.1}$$

where, each term has the same definition as in Eq. (2.3). To account for the uncertainty in σ_0 and σ_t, Eq. (6.1) was then modified as follows:

$$\sigma_t(\mathbf{x},\boldsymbol{\Theta}) = \left[(1 + s_0 \cdot \varepsilon_0) - \lambda \left(\frac{D \cdot t}{R_0^2} \right)^{\alpha} (1 + s \cdot \varepsilon) \right] \cdot \mu_{\sigma_0} \tag{6.2}$$

where, $\mathbf{x} = (D, R_0)$ is a vector of basic variables (i.e., diffusion coefficient and radius at $t = 0$), $s_0 \cdot \varepsilon_0$ is an error term that captures the variability of σ_0 around its mean μ_{σ_0}, $s \cdot \varepsilon$ is an error term that captures the variability in the reduction term $\lambda(D \cdot t / R_0^2)^{\alpha}$, ε_0 and ε are statistically independent identically distributed random variables with zero mean and unit variance, s_0 and s are the standard deviation of the two error terms, and $\boldsymbol{\Theta} = (\lambda, \alpha, s_0, s)$ is a vector of unknown empirical model parameters introduced to fit the data. Two assumptions were made in formulating the model: (a) s_0 and s are independent of $\mathbf{x}$ (homoskedasticity assumption), and (b) ε_0 and ε have a normal distribution (normality assumption). Diagnostic plots of the data and the residuals against model predictions (Rao and Toutenburg, 1997) were used to verify the validity of these assumptions.

Based on the normality assumption, Eq. (6.2) was rewritten as:

$$\frac{\sigma_t(\mathbf{x},\boldsymbol{\Theta})}{\mu_{\sigma_0}} = \left[1 - \lambda \left(\frac{D \cdot t}{R_0^2} \right)^{\alpha} \right] + \sqrt{s_0^2 + \lambda^2 \left(\frac{D \cdot t}{R_0^2} \right)^{2\alpha} s^2} \cdot \varepsilon \tag{6.3}$$

6.2 BAYESIAN PARAMETER ESTIMATION

The unknown model parameters $\boldsymbol{\Theta}$ (i.e., λ, α, s_0, and s) are empirical and therefore they have no direct physical meaning. These parameters were used to fit the experimental data. The parameters were estimated using the Bayesian updating rule (Box and Tiao, 1992):

$$f(\boldsymbol{\Theta}) = \gamma L(\boldsymbol{\Theta})\, p(\boldsymbol{\Theta}) \tag{6.4}$$

where, $p(\boldsymbol{\Theta})$ is the prior distribution of $\boldsymbol{\Theta}$ based on the knowledge about $\boldsymbol{\Theta}$ before observing the set of data $\mathbf{D}$ of size n (i.e., tensile strength data from n number of GFRP reinforcing samples); $L(\boldsymbol{\Theta})$ is the likelihood function that represents the information on the model parameters $\boldsymbol{\Theta}$ from the tensile strength data $\mathbf{D}$ and is proportional to the conditional probability, $p(\mathbf{D}\,|\,\boldsymbol{\Theta})$, of observing $\mathbf{D}$ (i.e., tensile strength corresponding to the parameters in the model) for given values of $\boldsymbol{\Theta}$; γ is a normalizing factor; and $f(\boldsymbol{\Theta})$ is the posterior distribution of $\boldsymbol{\Theta}$ determined using the Bayesian rule in Equation (6.4), which captures both the information in $p(\boldsymbol{\Theta})$ and in $\mathbf{D}$. The vector of posterior mean values of $\boldsymbol{\Theta}$ were obtained once $f(\boldsymbol{\Theta})$ was determined using the Equation (6.4). In the analysis presented in this report, a non-informative prior distribution provided in Box and Tiao (1992) was assumed to reflect that there is no or little information available about the model parameters before collecting the experimental data.

For i^{th} data point among the tensile strength data, the residual, $r_i(\lambda,\alpha)$, was calculated by subtracting the mean strength predicted using the proposed model in Equation (6.3) from the actual strength measured in the laboratory. This is expressed as follows:

$$r_i(\lambda,\alpha) = \underbrace{\left[\frac{\sigma_{ti}}{\mu_{\sigma_0 i}}\right]}_{\substack{\text{actual}\\ \text{strength}\\ \text{measured}}} - \underbrace{\left[1-\lambda\left(\frac{D\,t_i}{R_{0i}^2}\right)^{\alpha}\right]}_{\substack{\text{strength predicted}\\ \text{using the model}}};\ i=1,\ldots,n \tag{6.5}$$

The likelihood function, $L(\boldsymbol{\Theta})$, was written as the product of the probability of observing each residual, $r_i(\lambda,\alpha)$:

$$L(\boldsymbol{\Theta}) = P\left[\sqrt{s_0^2 + \lambda^2\left(\frac{D\cdot t_1}{R_{01}^2}\right)^{2\alpha} s^2}\cdot\varepsilon_1 = r_1(\lambda,\alpha)\right]\times\ldots$$
$$\times P\left[\sqrt{s_0^2 + \lambda^2\left(\frac{D\cdot t_n}{R_{0n}^2}\right)^{2\alpha} s^2}\cdot\varepsilon_n = r_n(\lambda,\alpha)\right] \tag{6.6}$$
$$= \prod_{i=1}^{n} P\left[\sqrt{s_0^2 + \lambda^2\left(\frac{D\cdot t_i}{R_{0i}^2}\right)^{2\alpha} s^2}\cdot\varepsilon_i = r_i(\lambda,\alpha)\right]$$

Since ε has the standard normal distribution, $L(\boldsymbol{\Theta})$ was rewritten as:

$$L(\boldsymbol{\Theta}) = \prod_{i=1}^{n} \frac{1}{\sqrt{s_0^2 + \lambda^2\left(\frac{D\cdot t_i}{R_{0i}^2}\right)^{2\alpha} s^2}}\varphi\left[\frac{r_i(\lambda,\alpha)}{\sqrt{s_0^2 + \lambda^2\left(\frac{D\cdot t_i}{R_{0i}^2}\right)^{2\alpha} s^2}}\right] \tag{6.7}$$

where, $\varphi(\cdot)$ denotes the standard normal probability density function (PDF). Table 6-1 lists the means, standard deviations, and the correlation coefficients of the empirical parameters $\boldsymbol{\Theta}$ obtained using the data from the experimental program of this project and the additional data available from the literature.

Table 6-1. Posterior Statistics of Unknown Parameter $\boldsymbol{\Theta} = (\lambda, \alpha, s_0, s)$.

Parameter	Mean	Standard Deviation	Correlation Coefficient			
			λ	α	s_0	s
λ	0.135	0.011	1			
α	0.207	0.082	–0.84	1		
s_0	0.039	0.003	–0.04	0.04	1	
s	0.557	0.043	–0.28	–0.02	–0.25	1

Figure 6.1 shows a comparison between the predicted and measured normalized stress capacity, $\sigma_t / \mu_{\sigma_0}$, over time. The experimental data are shown as unfilled circles (○) for all bar types. The mean prediction ($\varepsilon_0 = \varepsilon = 0$) is shown as a solid curve (in the left plot for the #3 bars, in the center plot for the #5 bars, and in the right plot for the #6 bars). The dashed curves delimit the region within 1 standard deviation of the mean. In addition, the horizontal solid line (at normalized stress equal to 0.6) represents the ACI 440 minimum capacity requirement, $\sigma_{\text{ACI440}} / \mu_{\sigma_0}$, discussed in the last paragraph in Section 2 (i.e., $\sigma_{\text{ACI440}} = C_E f_{fu}^* = C_E(f_{u,ave} - 3\sigma)$). An analysis of the data from the experimental program and the additional data available from the literature showed that σ / μ_{σ_0} varies between 0.02 and 0.09. For the purpose of the analysis conducted in this section, the ACI requirement was computed using $\sigma / \mu_{\sigma_0} = 0.05$. Note that the developed model is unbiased and properly accounts for the scatter in the experimental data. It can also be observed that the decrease in the mean normalized stress capacity, $E[\sigma_t / \mu_{\sigma_0}]$, is rapid over the first few years and gradually slows down as time increases. Furthermore, this reduction in $E[\sigma_t / \mu_{\sigma_0}]$ is more pronounced for smaller bars than for larger bars. Note that there is no physical relationship between C_E and the "normalized stress." This is explained in Section 2 of the report. The term C_E is the reduction factor representing the detrimental effect of environmental parameters. The "normalized stress" is the tensile stress capacity at time, *t*, divided by the mean capacity at time, *t*=0.

Figure 6.2 shows the relationship between t and $\hat{R}_0$ for which the predicted mean of the normalized stress capacity reaches the corresponding ACI 440 minimum requirement, $E[\sigma_t / \mu_{\sigma_0}] = C_E(f_{u,ave} - k\sigma) / \mu_{\sigma_0}$ for $k = 3, \ldots, 6$ (for example, $k = 3$ indicates the 3-standard deviation and is the value specified by ACI 440). It can be seen that for small GFRP bar sizes,

$E[\sigma_t / \mu_{\sigma_0}] = \sigma_{\text{ACI440}} / \mu_{\sigma_0}$ at a time less than the typical service life of a structure. For small GFRP bar sizes a larger value of k may be required so that $E[\sigma_t / \mu_{\sigma_0}] > C_E(f_{u,ave} - k\sigma) / \mu_{\sigma_0}$ during service time.

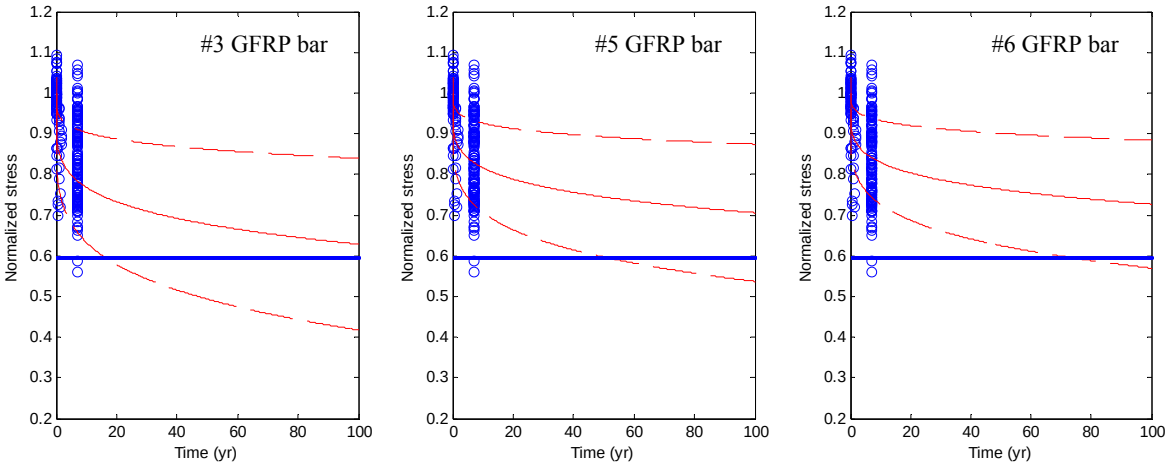

Figure 6-1. Comparison between the Predicted and Measured Normalized Stress $\sigma_t / \mu_{\sigma_0}$ over Time.

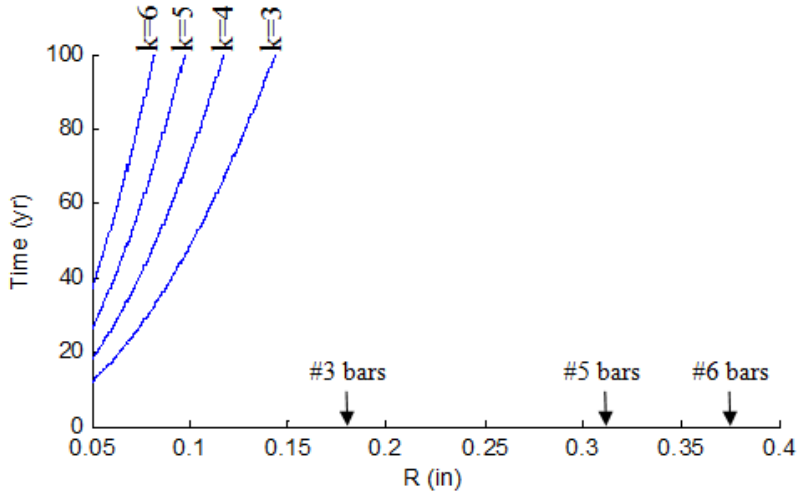

Figure 6-2. Values of t and $\hat{R}_0$ for which $E[\sigma_t / \mu_{\sigma_0}] = C_E(f_{u,ave} - k\sigma) / \mu_{\sigma_0}$ for $k = 3,\ldots,6$.

6.3 PROBABILITY OF NOT MEETING DESIGN SPECIFICATIONS OVER TIME

Following the conventional notation in reliability theory (Ditlevsen and Madsen, 1996), a limit state function $g(\cdot)$ was introduced such that the event $\{g(\cdot) \le 0\}$ denotes not meeting a specified capacity requirement. In particular, the ACI 440 minimum capacity requirement, σ_{ACI440}, was considered.

Using the probabilistic model described in Eq. (6.2), a limit state function was written as:

$$g\left(\sigma_{\text{ACI440}}, \mathbf{x}, \boldsymbol{\Theta}\right) = \sigma_t\left(\mathbf{x}, \boldsymbol{\Theta}\right) - \sigma_{\text{ACI440}} \tag{6.8}$$

Therefore, the probability of not meeting the design specifications at any time t was written as:

$$P\left[g\left(\sigma_{\text{ACI440}}, \mathbf{x}, \boldsymbol{\Theta}\right) \le 0\right] \tag{6.9}$$

The uncertainty in Eq. (6.9) arises from the inexact nature of the model $\sigma_t(\mathbf{x}, \boldsymbol{\Theta})$ captured in ε_0 and ε, the inherent randomness (or aleatory uncertainty) in $\mathbf{x}$, and the statistical uncertainty in $\boldsymbol{\Theta}$. Because the uncertainty in ε_0 and ε typically prevails over the other sources, a point estimate of Eq. (6.9) was obtained using point estimates (e.g., the nominal values or the means) $\hat{\mathbf{x}}$ and $\hat{\boldsymbol{\Theta}}$ in place of $\mathbf{x}$ and $\boldsymbol{\Theta}$ as follows:

$$P\left[g\left(\sigma_{\text{ACI440}}, \hat{\mathbf{x}}, \hat{\boldsymbol{\Theta}}\right) \le 0\right] = \Phi\left[\frac{\dfrac{\sigma_{\text{ACI440}}}{\mu_{\sigma_0}} - \left[1 - \hat{\lambda}\left(\dfrac{\hat{D}\cdot t}{\hat{R}_0^2}\right)^{\hat{\alpha}}\right]}{\sqrt{\hat{s}_0^2 + \hat{\lambda}^2\left(\dfrac{\hat{D}\cdot t}{\hat{R}_0^2}\right)^{2\hat{\alpha}}\hat{s}^2}}\right] \tag{6.10}$$

where, $\Phi(\cdot)$ denotes the standard normal cumulative distribution function. Furthermore, the reliability index (Ditlevsen and Madsen, 1996) corresponding to the probability in Eq. (6.10) was obtained as

$$\beta\left(\sigma_{\text{ACI440}}, \hat{\mathbf{x}}, \hat{\boldsymbol{\Theta}}\right) = \Phi^{-1}\left\{1 - P\left[g\left(\sigma_{\text{ACI440}}, \hat{\mathbf{x}}, \hat{\boldsymbol{\Theta}}\right) \le 0\right]\right\} \tag{6.11}$$

where, $\Phi^{-1}(\cdot)$ denotes the inverse of the standard normal cumulative distribution function. The probability of not meeting the ACI 440 design specifications and the corresponding reliability index are functions of the initial radius of a GFRP bar, R_0, and time, t. Figure 6.3 shows a conceptual three-dimensional plot of the probability of not meeting the ACI 440 Code as a function of the nominal radius, $\hat{R}_0$, and t. Consistent with the observations made for Figure 6.1, it can be seen that for a specified bar size, the probability increases with t. Conversely, at the same time, t, the probability decreases as the bar size increases.

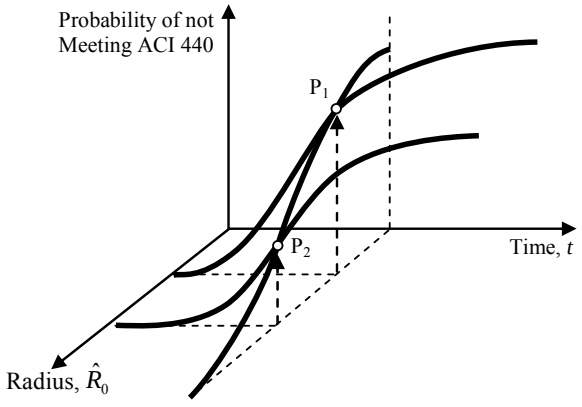

Figure 6-3. Conceptual Plot of the Probability of Not Meeting ACI 440 Specification as a Function of Time and Bar Size.

Figure 6.4 shows the $P[g(\sigma_{ACI440}, \mathbf{x}, \boldsymbol{\Theta}) \leq 0]$ as a function of time. The dotted line shows the probability for the #3 bars, the dashed line shows the probability for #5 bars, and the solid line shows the probability for #6 bars. Consistent with the observations made from Figure 6.1, in 100 years #3 bars reach a 0.44 probability of not meeting the ACI 440 requirement, #5 bars reach a 0.25 probability, and #6 bars reach a 0.2 probability. Figure 6.5 shows the $P[g(\sigma_{ACI440}, \mathbf{x}, \boldsymbol{\Theta}) \leq 0]$ as a function of $\hat{R}_0$. The solid line shows the probability for $t = 25$ years, the dashed line shows the probability for $t = 50$ years, the dashed-dotted line shows the probability for $t = 75$ years, and the dotted line shows the probability for $t = 100$ years. It can be seen that $P[g(\sigma_{ACI440}, \mathbf{x}, \boldsymbol{\Theta}) \leq 0]$ decreases as $\hat{R}_0$ increases and that the effect of $\hat{R}_0$ is more pronounced shortly after the bars are embedded in concrete than later times. Finally, Figure 6.6 shows a contour plot of the iso-probability lines for $P[g(\sigma_{ACI440}, \mathbf{x}, \boldsymbol{\Theta}) \leq 0]$ as a function of t and $\hat{R}_0$. The iso-probability lines connect pairs of values of t and $\hat{R}_0$ that correspond to the same $P[g(\sigma_{ACI440}, \mathbf{x}, \boldsymbol{\Theta}) \leq 0]$. Consistent with what was observed in Figures 6.4 and 6.5, Figure 6.6 shows that $P[g(\sigma_{ACI440}, \mathbf{x}, \boldsymbol{\Theta}) \leq 0]$ increases as t increases and that bars with larger $\hat{R}_0$ are less prone to deteriorate than bars with smaller $\hat{R}_0$.

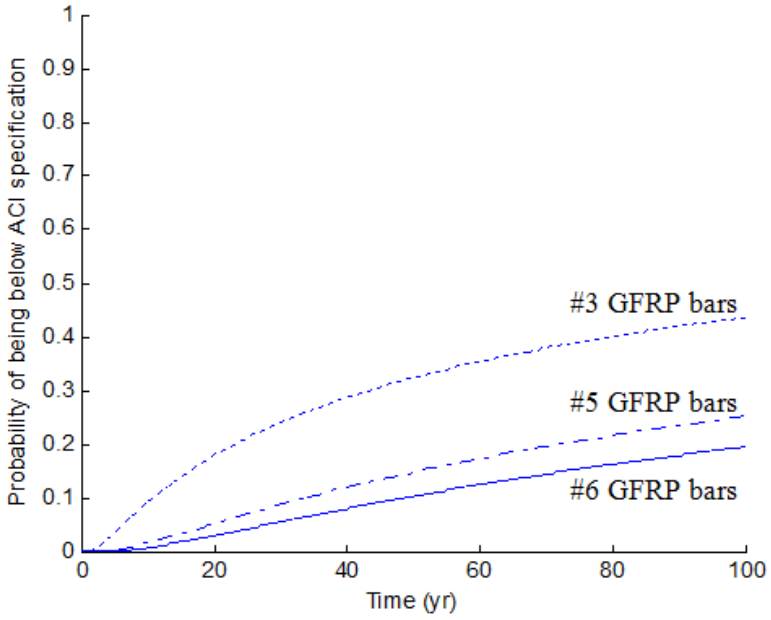

Figure 6-4. Probability of Not Meeting ACI 440 Specifications as a Function of t for #6 Bars (solid line), #5 Bars (dashed line), and #3 Bars (dotted line).

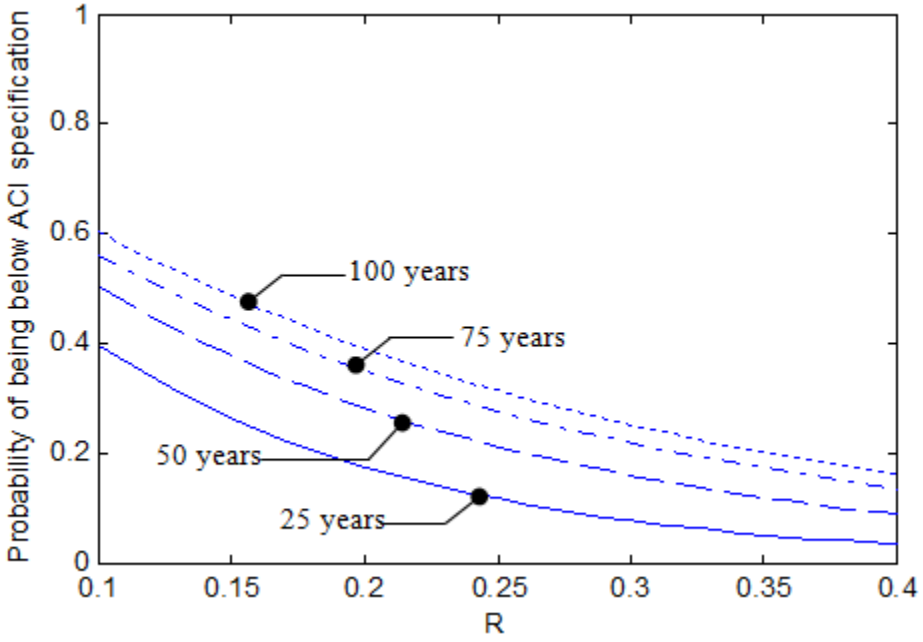

Figure 6-5. Probability of Not Meeting ACI 440 Specification as a Function of $\hat{R}_0$ for $t = 25$ years (solid line), $t = 50$ years (dashed line), $t = 75$ years (dashed-dotted line), and $t = 100$ years (dotted line).

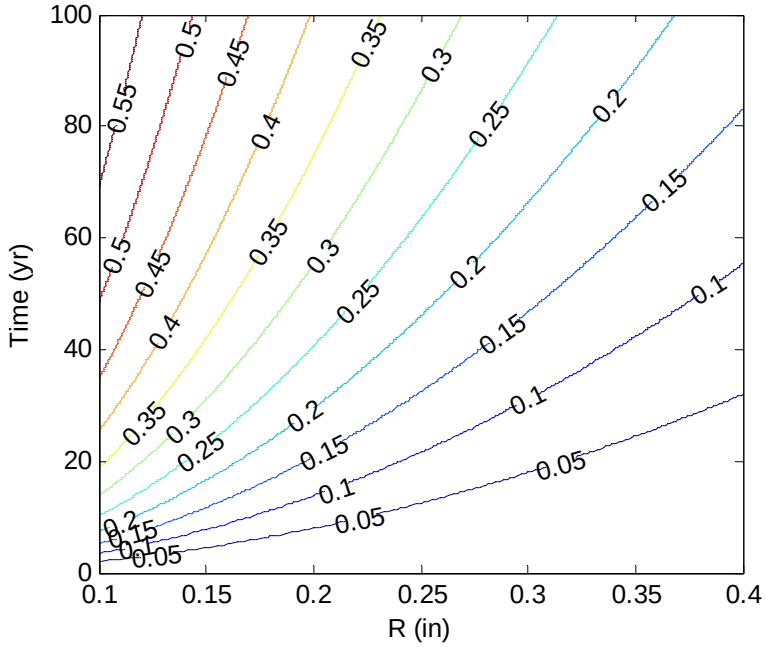

Figure 6-6. Contour Lines for the Probability of Not Meeting ACI 440 as a Function of t and the $\hat{R}_0$.

7. SUMMARY AND CONCLUSIONS

GFRP reinforcing bars can provide many advantages to the owners and constructors of infrastructure systems. These advantages have been widely reported. Although the advantages are many, the acceptance of using GFRP bars has been hampered by longer-term data on residual strengths when embedded in concrete. This research evaluated the residual capacity and modulus of elasticity of GFRP embedded in concrete for 7 years. The authors found no information in the literature that provides results from GFRP-reinforced beams beyond 3 years. These data can provide valuable information to the GFRP engineering community.

A state-of-the-art model to predict the actual performance of GFRP bars embedded in concrete was developed. The data from the experimental program of this project and the additional data available from the literature were used to construct the probabilistic model capturing the dependency of the tensile strength on time and the initial bar size. The developed probabilistic model is unbiased and properly accounts for the relevant sources of uncertainties, including the statistical uncertainty in the estimation of the unknown model parameters and the model error associated to the inexact model form. The developed time-variant model can provide required information to assess the safety and performance of GFRP reinforcing bars embedded in decks, pavements, and other infrastructure elements over time.

The model indicates that the decay of the mean stress capacity is rapid over the first few years and gradually slows as time increases. Furthermore, the decay is more pronounced for smaller bars than for larger bars. The developed probabilistic model was also used to assess the probability that the actual stress capacity of GFRP bars does not meet the ACI 440 minimum capacity requirement over time. The model predicted that for a specified bar size, the probability of not meeting the ACI 440 requirement increases with time. Conversely, at the same time, the

probability decreases as the bar size increases. In particular, in 100 years #3 bars reach a 0.44 probability of not meeting the ACI 440 requirement, #5 bars reach a 0.25 probability, and #6 bars reach a 0.2 probability.

While the developed model provides valuable information on the long-term performance of GFRP bars embedded in concrete, additional research is needed to assess the time-variant structural reliability of whole structures. A reliability analysis would answer the fundamental question on the actual safety of structures with GFRP bars. The developed probabilistic model should be used in assessing the structural capacity over time needed for a time-variant structural reliability analysis. It should also be noted that the GFRP reinforcing bars assessed in this research were embedded in concrete that was not subjected to loads other than the self-weight of the beam. The literature indicates that the residual capacity of GFRP subjected to load is less than GFRP bars subjected to no load.

REFERENCES

Abbasi, A., and Hogg, P. J. (2005). "Temperature and Environmental Effects on Glass Fiber Rebar: Modulus, Strength and Interfacial Bond Strength with Concrete." Composites Part B-Engineering, 36(5), pp. 394-404.

ACI Committee 440 (2003). "Guide for the Design and Construction of Concrete Reinforced with FRP Bars." Farmington Hills, MI, American Concrete Institute.

Almusallam, T. H., Al-Salloum, Y. A., Alsayed, S. H., and Alhozaimy, A. M. (2002). "Tensile Strength of GFRP Bars in Concrete Beams Under Sustained Loads at Different Environments," Second International Conference on Durability of Fiber Reinforced Polymer (FRP) Composites for Construction, Sherbooke, Quebec, Canada, May 29-31, 2002, pp. 523-533.

American Association of State Highway and Transportation Officials Load and Resistance Factor Design (AASHTO LRFD), Bridge Design Guide Specifications for GFRP Reinforced Concrete Decks and Traffic Railings, American Association of State Highway and Transportation Officials, Washington, D. C., 2008.

ASTM C642 (1997). "Standard Test Method for Density, Absorption, and Voids in Hardened Concrete," Annual Book of ASTM Standards, ASTM.

ASTM D2584 (2008). "Standard Test Method for Ignition Loss of Cured Reinforced Resins," Annual Book of ASTM Standards, ASTM.

Bakis, C., Freimanis, A., Gremel, D., and Nanni, A., (1998). "Effect of Material on Bond and Tensile Properties of Unconditioned and Conditioned FRP Reinforcement Rods, Proceedings of the First International Conference (CDCC'98) on Durability of Fiber Reinforced Polymer (FRP) Composites for Construction," 1998, pp. 525-535.

Bakis, C. E., Boothby, T. E., Schaut, R. A., and Pantano, C. G. (2005). "Tensile Strength of GFRP Bars Under Sustained Loading in Concrete Beams." Preceedings of the 7th International Symposium. Fiber Reinforced Polymer Reinforcement for Concrete Structures, FRPRCS-7, American Concrete Institute, pp. 1429-1446.

Bank, L. C., Puterman, M. and Katz, A. (1998). "The Effect of Material Degradation on Bond Properties of FRP Reinforcing Bars in Concrete." ACI Material Journal, 95(3), pp. 232-243.

Benmokrane, B., Wang, P., Ton-That, T. M., Rahman, H., and Robert, J. F. (2002). "Durability of Glass Fiber-Reinforced Polymer Reinforcing Bars in Concrete Environment." Journal of Composites for Construction, 6(3), pp. 143-153.

Box, G. E. P., and Tiao, G. C. (1992). Bayesian Inference in Statistical Analysis, Addison–Wesley, Reading, Mass.

Ceroni, F., Cosenza, E., Gaetano, M., and Pecce, M. (2006). "Durability Issues of FRP Rebars in Reinforced Concrete Members." Cement & Concrete Composites, 28(10), pp. 857-868.

Debaiky, A. S., Nkurunziza, G., Benmokrane, B., and Cousin, P. (2006). "Residual Tensile Properties of GFRP Reinforcing Bars After Loading in Severe Environments." Journal of Composites for Construction, 10(5), pp. 370-380.

Dejke, V. (2001). Durability of FRP Reinforcement in Concrete. Thesis, Department of Building Materials, Chalmers University of Technology, Sweden.

Ditlevsen, O., and Madsen, H. O. (1996). Structural Reliability Methods, Wiley, New York.

Environmental Protection Agency, Test Method 9045D "Soil and Waste pH." No Date Provided, Washington, D.C.

Giernacky, R. G., Bakis, C. E., Mostoller, J. D., Boothby, T. E., and Mukherjee, A. (2002). "Evaluation of Concrete Beams Reinforced with Internal GFRP Bars: A Long-Term Durability Study," Second International Conference on Durability of Fiber Reinforced Polymer (FRP) Composites for Construction (CDCC 02), Montreal, Quebec, Canada, May, pp. 39-45.

Kajorncheappunngam, S., Gupta, R. K., and GangaRao, H. V. S. (2002). "Effect of Aging Environment on Degradation of Glass-Reinforced Epoxy." Journal of Composite for Construction, 6(1), pp. 61-69.

Karbhari, V. M., Murphy, K., and Zhang, S. (2002). "Effect of Concrete Based Alkali Solutions on Short-Term Durability of E-Glass/Vinyl Ester Composites." Journal of Composite Materials, 36(17), pp. 2101-2121.

Karbhari, V. M., Stachowski, C., and Wu, L. (2007). "Durability of Pultruded E-glass/Vinyl Ester Under Combined Hygrothermal Exposure and Sustained Bending." Journal of Materials in Civil Engineering, 19(8), pp. 665-673.

Katsuki, F., and Uomoto, T. (1995). "Prediction of Deterioration of FRP Rods due to Alkali Attack." Proceedings of the Second International RILEM Symposium (FRPRCS-2), Non-Metallic (FRP) Reinforcement for Concrete Structures, L. Taerwe, ed., E&FN Spon, London, pp. 83-89.

Laoubi, K., EI-Salakawy, E., and Benmokrane, B. (2006). "Creep and Durability of Sand-Coated Glass FRP Bars in Concrete Elements Under Freeze/Thaw Cycling and Sustained Loads." Cement & Concrete Composites, 28(10), pp. 869-878.

Micelli, F., and Nanni, A. (2004). "Durability of FRP Rods for Concrete Structures." Construction and Building Materials, 18(7), pp. 491-503.

Micelli, F., Nanni, A., and Tegola, A. L. (2001). "Effects of Conditioning Environment On GFRP Bars." 22nd SAMPE Europe International Conference CNIT Paris, pp. 1-13.

Mufti, A., Banthia, N., Benmokrane, B., Boulfiza, M., and Newhook, J. (2007a). "Durability of GFRP Composite Rods." Concrete International, American Concrete Institute, pp. 37-42.

Mufti, A. A., Onofrei, M., Benmokrane, B., Banthia, N., Boulfiza, M., Newhook, J. P., Bakht, B., Tadros, G. S., and Brett, P. (2007b). "Field Study of Glass-Fibre-Reinforced Polymer Durability in Concrete." Canadian Journal of Civil Engineering, 34(3), pp. 355-366.

Mukherjee, A. and Arwikar, S. J. (2005). "Performance of Glass Fiber-Reinforced Polymer Reinforcing Bars in Tropical Environments - part I: Structural scale tests." ACI Structural Journal, 102(5), pp. 745-753.

Nishizaki, I., and Meiarashi, S. (2002). "Long-Term Deterioration of GFRP in Water and Moist Environment." Journal of Composites for Construction, 6(1), pp. 21-27.

Nkurunziza, G., Benmokrane, B., Debaiky, A. S., and Masmoudi, R. (2005). "Effect of Sustained Load and Environment on Long-Term Tensile Properties of Glass Fiber-Reinforced Polymer Reinforcing Bars." ACI Structural Journal, 102(4), pp. 615-621.

Nkurunziza, G., Debaiky, A., Cousin, P., and Benmokrane, B. (2005). "Durability of GFRP bars: A Critical Review of the Literature." Progress in Structural Engineering and Materials, 7(4), pp. 194-209.

Porter, M. L., and Barnes, B. A. (1998). "Accelerated Aging Degradation of Glass Fiber Composites." 2nd International Conference on Composites in Infrastructure, University of Arizona, Tucson, pp. 446-459.

Proctor, B. A., Oakley, D. R., and Litherland, K. L. (1982). "Developments in the Assessment and Performance of GRC over 10 years." Composites, 13, pp. 173-179.

Rao, C. R., and Toutenburg, H. (1997). Linear Models, Least Squares and Alternatives, Springer, New York, NY.

Schaefer, B. (2002). "Thermal and Environmental Effects on Fiber Reinforced Polymer Reinforcing Bars and Reinforced Concrete," M.S. Thesis, Texas A&M University, College Station, TX, May 2002.

Sen, R., Mullins, G., and Salem, T. (2002). "Durability of E-glass/Vinyl Ester Reinforcement in Alkaline Solution." ACI Structural Journal, 99(3), pp. 369-375.

Shen, C. H., and Springer, G. S. (1976). "Moisture Absorption and Desorption of Composite Materials." Journal of Composite Materials, Vol. 10, pp. 2-20.

Svecova, D., Rizkalla, S., Vogel, H., and Jawara, A. (2002). "Durability of GFRP in Low-Heat High Performance Concrete," 2nd International Conference on Durability of Fiber Reinforced Polymer (FRP) Composites for Construction, Sherbooke, Quebec, Canada, May 29-31, pp. 75-86.

Tannous, F. E., and Saadatmanesh, H. (1998). "Environmental Effects on the Mechanical Properties of E-glass FRP Rebars." ACI Materials Journal, 95(2), pp. 87-100.

Tannous, F. E., and Saadatmanesh, H. (1999). "Durability of AR Glass Fiber Reinforced Plastic Bars." Journal of Composites for Construction, 3(1), pp. 12-19.

Trejo, D., Aguiniga, F., Yuan, R., James, R. W., and Keating, P. B. (2005). Characterization of Design Parameters for Fiber Reinforced Polymer Composite Reinforced Concrete Systems, Texas Transportation Institute Research Report 9-1520-3, June 2005.

Uomoto, T. (1996). "Durability of FRP Reinforcement as Concrete Reinforcement." FRP Composites in Civil Engineering, 1, pp. 85-96.

Vijay and GangaRao,(1999)."Accelerated and Natural Weathering of Glass Fiber Reinforced Plastic Bars," SP 188-53, pp. 605-614, American Concrete Institute, Farmington Hills, MI.

APPENDIX A – T-TEST RESULTS FOR MODULUS OF ELASTICITY(MOE)

Table A-1 The t-test results for Modulus of elasticity of V1 #5 bars

BAR	V1					
	#5(1.25"-2.25")		#5(2.25"-2.5")		#5(2.5"-3.5")	
	Beam 20/1.25"	A+B	Beam 5/2.25"	A+B	Beam 8/2.5"	A+B
	Beam 19/1.25"		Beam 31/2.25"		Beam 29/3.5"	
	Beam 5/2.25"		Beam 8/2.5"			
	Beam 31/2.25"					
1	5616.67	5840.88	5695.93	5840.88	5829.48	5840.88
2	5688.72	5736.80	5505.01	5736.80	5698.19	5736.80
3	5488.62	5789.00	5397.25	5789.00	5727.73	5789.00
4	5758.70	5738.12	5855.19	5738.12	4325.29	5738.12
5	2150.77	5807.65	6132.69	5807.65	6056.01	5807.65
6	5823.07	5384.50	5977.75	5384.50	5780.36	5384.50
7	5270.64	5827.72	5830.41	5827.72	5919.23	5827.72
8	5326.62	5806.35	5894.28	5806.35	5859.67	5806.35
9	5695.93	5807.60	5345.61	5807.60	5486.71	5807.60
10	5505.01	5637.36	5319.06	5637.36	6026.31	5637.36
11	5397.25		5913.39		5605.20	
12	5855.19		5414.58			
13	6132.69		5717.65			
14	5977.75		5091.94			
15	5830.41		5829.48			
16	5894.28		5698.19			
17	5345.61		5727.73			
18	5319.06		4325.29			
19	5913.39		6056.01			
20	5414.58		5780.36			
21	5717.65					
22	5091.94					
n	22	10	20	10	11	10
x(mean)	5464.30	5737.60	5625.39	5737.60	5664.93	5737.60
S	787.09	137.72	408.46	137.72	475.56	137.72
SP^2	439342.41		119306.73		128013.17	
SP	662.83		345.41		357.79	
to	-1.08		-0.84		-0.46	
n1+n2-2	30		28		19	
t0.025, n1+n2-2	2.042		2.048		2.093	
reject or not (assume σ1=σ2)	not rejected		not rejected		not rejected	
T0*	-1.58		-1.11		-0.48	
v	24		26		12	
t0.025, v	2.07		2.06		2.20	
reject or not (assume σ1≠σ2)	not rejected		not rejected		not rejected	

Table A-2 The t-test results for Modulus of elasticity of V2 #5 bars

BAR	V2					
	#5(1"-1.5")		#5(1.5"-2.25")		#5(2.25"-3")	
	Beam 23/1"	A+B	Beam 14/1.5"	A+B	Beam 13/2.25"	A+B
	Beam 14/1.5"		Beam 13/2.25"		Beam 30/2.25"	
			Beam 30/2.25"		Beam 2/3"	
					Beam 32/3"	
1	5393.72	5637.46	5039.75	5637.46	5510.66	5637.46
2	5394.14	5625.96	5308.68	5625.96	5627.79	5625.96
3	5381.73	5635.50	5946.71	5635.50	5563.81	5635.50
4	5375.92	5532.84	5606.58	5532.84	5418.80	5532.84
5	5604.16	5482.28	5510.66	5482.28	5602.45	5482.28
6	5039.75	5558.43	5627.79	5558.43	5103.36	5558.43
7	5308.68	5659.64	5563.81	5659.64	5679.22	5659.64
8	5946.71	5327.22	5418.80	5327.22	5633.96	5327.22
9	5606.58	5546.25	5602.45	5546.25	5964.18	5546.25
10			5103.36		5309.70	
11			5679.22		5495.00	
12			5633.96		5418.45	
13			5964.18		5604.78	
14			5309.70		5952.53	
15					5495.98	
16					5316.11	
17					5276.02	
18					3539.92	
19					5551.02	
20					5626.41	
Average	5450.15	5556.18	5522.55	5556.18	5434.51	5556.18
Standard Deviation	249.93	104.29	270.17	104.29	490.85	104.29
Coefficients of Variation	0.05	0.02	0.05	0.02	0.09	0.02
n	9	9	14	9	20	9
x(mean)	5450.15	5556.18	5522.55	5556.18	5434.51	5556.18
S	249.93	104.29	270.17	104.29	490.85	104.29
SP^2	36670.27		49328.99		172770.82	
SP	191.49		222.10		415.66	
to	-1.17		-0.35		-0.73	
n1+n2-2	16		21		27	
t0.025, n1+n2-2	2.120		2.080		2.052	
reject or not	not rejected		not rejected		not rejected	
T0*	-1.17		-0.42		-1.06	
ν	11		18		22	
t0.025, ν	2.23		2.10		2.07	
reject or not	not rejected		not rejected		not rejected	

Table A-3 The t-test results for Modulus of elasticity of P #5 bars

BAR	P					
	#5(1.25"-1.5")		#5(1.5"-2.25")		#5(2.25"-3")	
	Beam 22/1.25" Beam 25/1.5"	A+B	Beam 25/1.5" Beam 3/2.25" Beam 10/2.25"	A+B	Beam 3/2.25" Beam 10/2.25" Beam 6/3" Beam 27/3"	A+B
1	3500.89	5647.66	5379.32	5647.66	5379.32	5647.66
2	5050.61	5572.83	6546.79	5572.83	6546.79	5572.83
3	5335.64	5539.47	5693.19	5539.47	5693.19	5539.47
4	5591.08	4670.91	5671.06	4670.91	5671.06	4670.91
5	5653.92	5580.77	5497.83	5580.77	5497.83	5580.77
6		5635.37		5635.37	5861.20	5635.37
7		7364.90		7364.90	5322.72	7364.90
8		5396.92		5396.92	5757.13	5396.92
9		4713.67		4713.67	5404.21	4713.67
10		5639.40		5639.40	5788.80	5639.40
Average	5026.43	5576.19	5757.64	5576.19	5692.23	5576.19
Standard Deviation	885.44	730.99	459.63	730.99	354.02	730.99
Coefficients of Variation	0.18	0.13	0.08	0.13	0.06	0.13
n	5	10	5	10	10	10
x(mean)	5026.43	5576.19	5757.64	5576.19	5692.23	5576.19
S	885.44	730.99	459.63	730.99	354.02	730.99
SP^2	611163.46		434932.60		329838.71	
SP	781.77		659.49		574.32	
to	-1.28		0.50		0.45	
n1+n2-2	13		13		18	
t0.025, n1+n2-2	2.160		2.160		2.101	
reject or not	not rejected		not rejected		not rejected	
T0*	-1.20		0.59		0.45	
v	7		12		13	
t0.025, v	2.45		2.20		2.16	
reject or not	not rejected		not rejected		not rejected	

Table A-4 The t-test results for Modulus of elasticity of V1 #6 bars

BAR	V1									
	#6(1"-1.25")		#6(1.25"-2")		#6(2"-2.25")		#6(2.25"-2.5")		#6(2.5"-3")	
	Beam 15/1" Beam 21/1.25"	A+B	Beam 21/1.25" Beam 9/2"	A+B	Beam 9/2" Beam 4/2.25"	A+B	Beam 4/2.25" Beam 1/2.5"	A+B	Beam 1/2.5" Beam 28/3"	A+B
1	4289.85	6255.60	6012.01	6255.60	6276.71	6255.60	6116.05	6255.60	5963.91	6255.60
2	5915.13	6031.66	5990.28	6031.66	6461.15	6031.66	6666.26	6031.66	5838.12	6031.66
3	5865.57	6441.40	5392.63	6441.40	5840.45	6441.40	5535.70	6441.40	6025.85	6441.40
4	5819.50	6557.23	6450.36	6557.23	6418.52	6557.23	5974.52	6557.23	5829.82	6557.23
5	6745.94	6264.67	6276.71	6264.67	6206.84	6264.67	5944.82	6264.67	6379.49	6264.67
6	6012.01	6304.24	6461.15	6304.24	6116.05	6304.24	5963.91	6304.24	6279.60	6304.24
7	5990.28	6413.70	5840.45	6413.70	6666.26	6413.70	5838.12	6413.70	5469.75	6413.70
8	5392.63	6525.39	6418.52	6525.39	5535.70	6525.39	6025.85	6525.39	6683.71	6525.39
9	6450.36	6939.83	6206.84	6939.83	5974.52	6939.83	5829.82	6939.83	5134.17	6939.83
10					5944.82		6379.49		6439.16	
Average	5831.25	6414.86	6116.55	6414.86	6144.10	6414.86	6027.45	6414.86	6004.36	6414.86
Standard Deviation	694.13	253.92	350.42	253.92	333.60	253.92	310.96	253.92	467.89	253.92
Coefficients of Variation	0.12	0.04	0.06	0.04	0.05	0.04	0.05	0.04	0.08	0.04
n	9	9	9	9	10	9	10	9	10	9
x(mean)	5831.25	6414.86	6116.55	6414.86	6144.10	6414.86	6027.45	6414.86	6004.36	6414.86
S	694.13	253.92	350.42	253.92	333.60	253.92	310.96	253.92	467.89	253.92
SP^2	273148.18		93632.90		89258.66		81531.67		146239.63	
SP	522.64		305.99		298.76		285.54		382.41	
to	-2.37		-2.07		-1.97		-2.95		-2.34	
n1+n2-2	16		16		17		17		17	
t0.025, n1+n2-2	2.120		2.120		2.110		2.110		2.110	
reject or not	rejected		not rejected		not rejected		rejected		rejected	
T0*	-2.37		-2.07		-2.00		-2.99		-2.41	
ν	10		15		17		17		14	
t0.025, ν	2.23		2.14		2.12		2.12		2.14	
reject or not	rejected		not rejected		not rejected		rejected		rejected	

Table A-5 The t-test results for Modulus of elasticity of V2 #6 bars

BAR	V2					
	#6(1"-1.5")		#6(1.5"-2.25")		#6(2.25"-3")	
	Beam 18/1"	A+B	Beam 16/1.25"	A+B	Beam 7/2"	A+B
	Beam 16/1.25"		Beam 7/2"		Beam 36/2"	
			Beam 36/2"		Beam 12/3"	
					Beam 26/3"	
1	5865.81	5511.40	5621.59	5511.40	5977.32	5511.40
2	5763.73	5609.25	6050.58	5609.25	5909.22	5609.25
3	3814.28	5742.67	6031.56	5742.67	5604.56	5742.67
4	5621.59	5730.33	5779.07	5730.33	5939.71	5730.33
5	6050.58	5532.02	5977.32	5532.02	5541.90	5532.02
6	6031.56	5810.13	5909.22	5810.13	5751.97	5810.13
7	5779.07	5723.58	5604.56	5723.58	6087.03	5723.58
8		5826.71	5939.71	5826.71	5900.86	5826.71
9		5849.82	5541.90	5849.82	5749.47	5849.82
10		5674.41		5674.41	5836.87	5674.41
Average	5560.94	5701.03	5828.39	5701.03	5829.89	5701.03
Standard Deviation	785.00	118.60	196.57	118.60	169.16	118.60
Coefficients of Variation	0.14	0.02	0.03	0.02	0.03	0.02
n	7	10	9	10	10	10
x(mean)	5560.94	5701.03	5828.39	5701.03	5829.89	5701.03
S	785.00	118.60	196.57	118.60	169.16	118.60
SP^2	254931.40		25630.98		21341.21	
SP	504.91		160.10		146.09	
to	-0.56		1.73		1.97	
n1+n2-2	15		17		18	
t0.025, n1+n2-2	2.131		2.110		2.101	
reject or not	not rejected		not rejected		not rejected	
T0*	-0.47		1.69		1.97	
v	6		13		16	
t0.025, v	2.45		2.18		2.12	
reject or not	not rejected		not rejected		not rejected	

Table A-6 The t-test results for Modulus of elasticity of P #6 bars

BAR	P					
	#6(1.25"-1.5")		#6(1.5"-2.25")		#6(2.25"-3")	
	Beam 24/1.25"	A+B (Preload)	Beam 17/1.5"	A+B (Preload)	Beam 11/2.25"	A+B (Preload)
	Beam 17/1.5"		Beam 11/2.25"		Beam 35/2.25"	
			Beam 35/2.25"		Beam 33/3"	
					Beam 34/3"	
1	4666.17	5657.14	5601.14	5657.14	5819.79	5657.14
2	5580.15	5750.12	5571.56	5750.12	5891.78	5750.12
3	5416.25	5851.85	5662.49	5851.85	5492.02	5851.85
4	5954.70	6557.23	5426.72	6557.23	5885.03	6557.23
5	5709.37	6264.67	5573.55	6264.67	5666.00	6264.67
6	5336.61	5892.61	5819.79	5892.61	5737.41	5892.61
7	5601.14	5685.78	5891.78	5685.78	5807.27	5685.78
8	5571.56	6085.75	5492.02	6085.75	5650.81	6085.75
9	5662.49	6525.39	5885.03	6525.39	5757.43	6525.39
10	5426.72	6939.83	5666.00	6939.83	5553.48	6939.83
11	5573.55		5416.93		5596.13	
12			5443.96		5912.71	
13			5400.16		5607.05	
14			5453.79		5819.24	
15			5515.06		5759.62	
16			5316.04			
Average	5499.88	6121.04	5571.00	6121.04	5730.38	6121.04
Standard Deviation	322.26	436.26	175.06	436.26	130.51	436.26
Coefficients of Variation	0.06	0.07	0.03	0.07	0.02	0.07
n	11	10	16	10	15	10
x(mean)	5499.88	6121.04	5571.00	6121.04	5730.38	6121.04
S	322.26	436.26	175.06	436.26	130.51	436.26
SP^2	144814.21		90526.85		84843.47	
SP	380.54		300.88		291.28	
to	-3.74		-4.53		-3.29	
n1+n2-2	19		24		23	
t0.025, n1+n2-2	2.093		2.064		2.069	
reject or not	rejected		rejected		rejected	
T0*	-3.68		-3.80		-2.75	
v	16		11		10	
t0.025, v	2.12		2.23		2.23	
reject or not	rejected		rejected		rejected	

APPENDIX B – BEAM CARDS

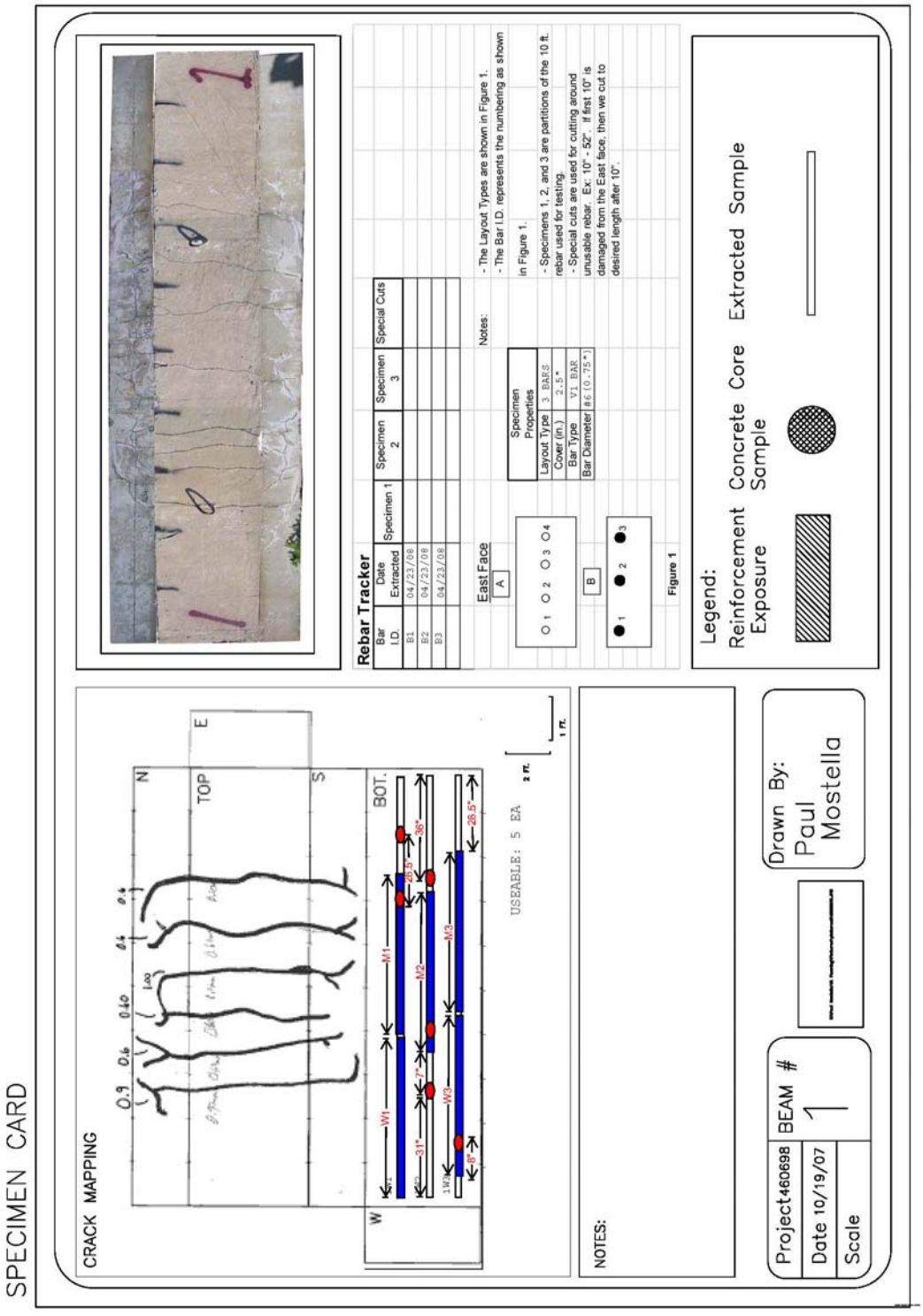

Figure B-1 Beam Card #1

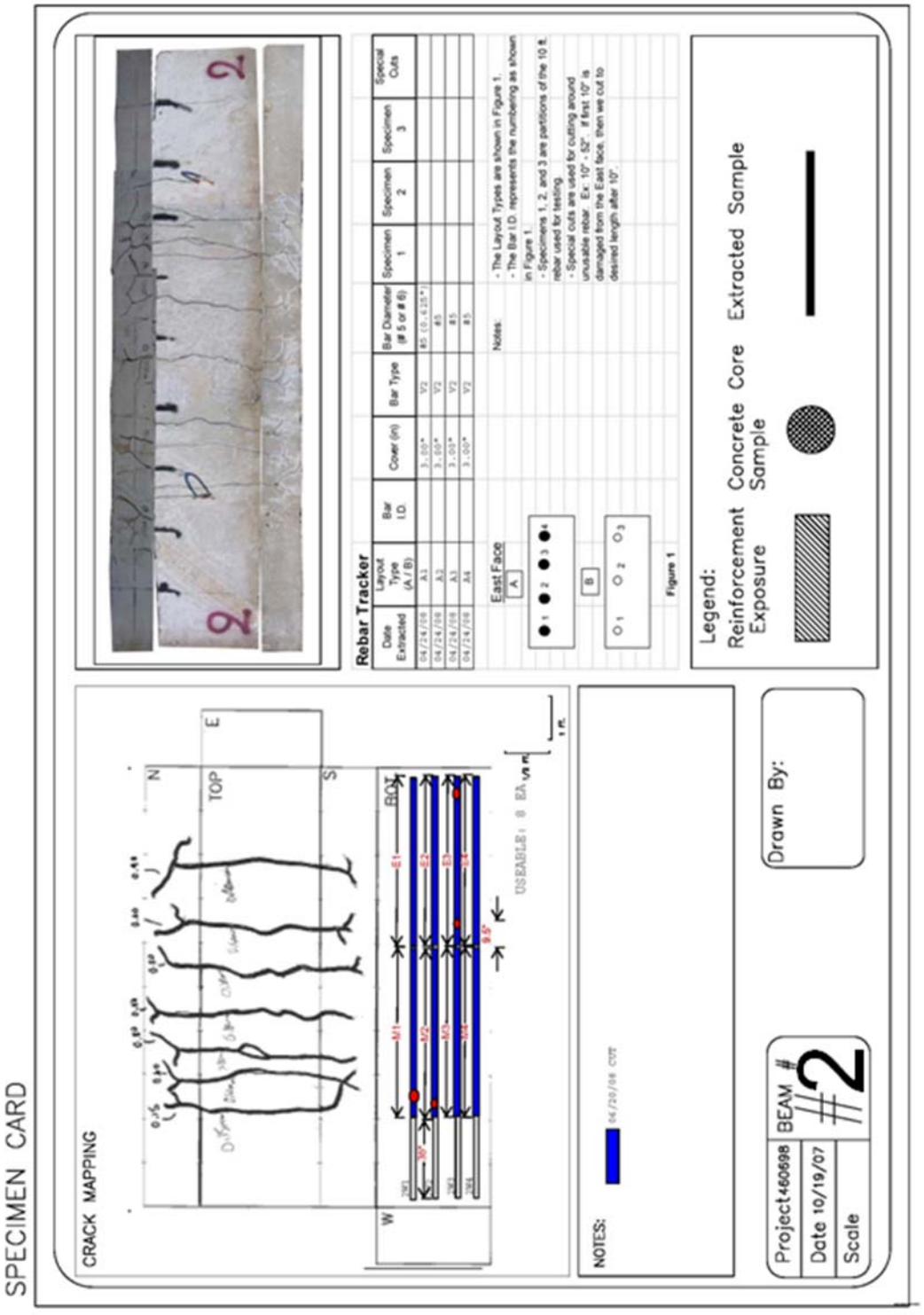

Figure B-2 Beam Card #2

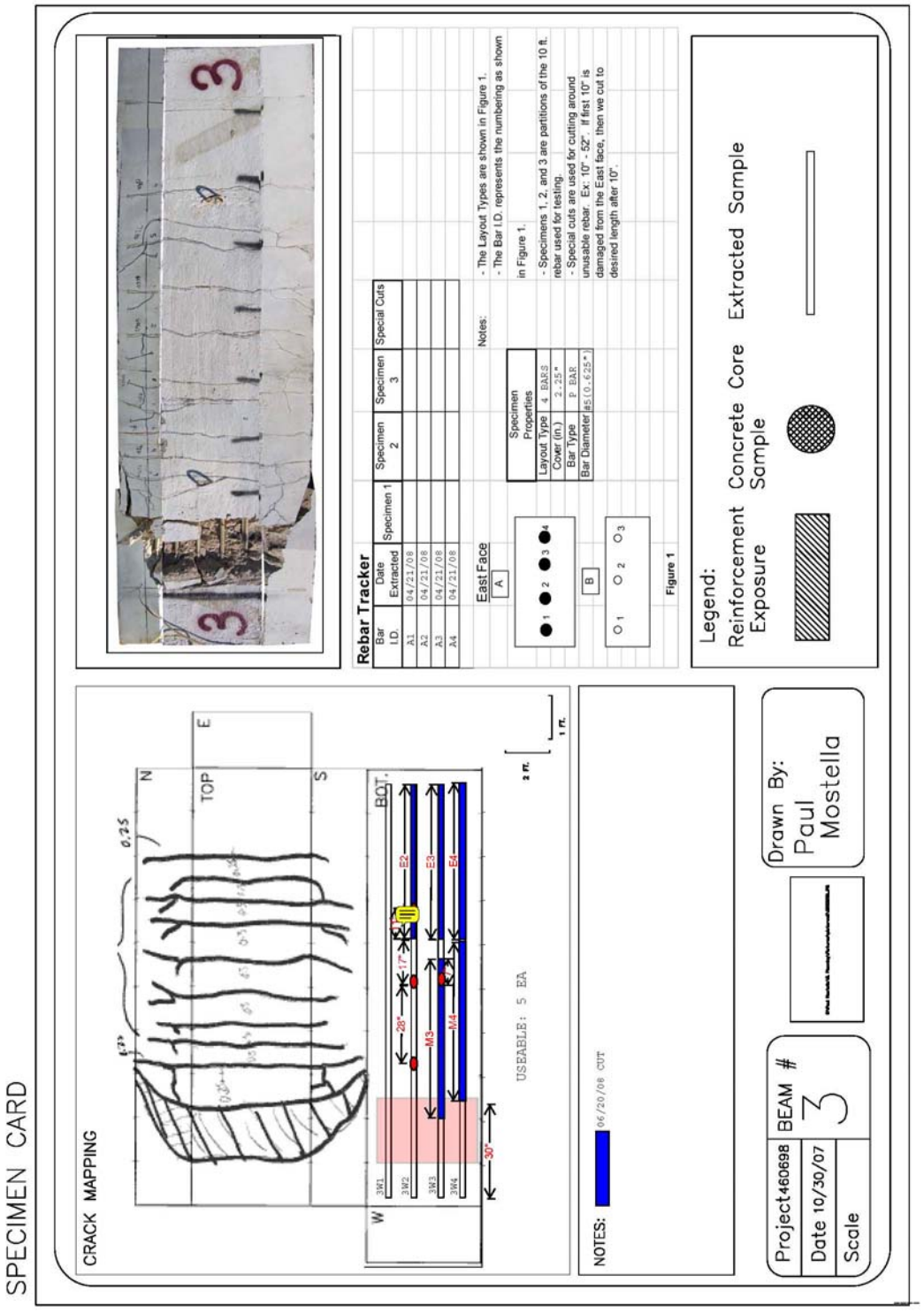

Figure B-3 Beam Card #3

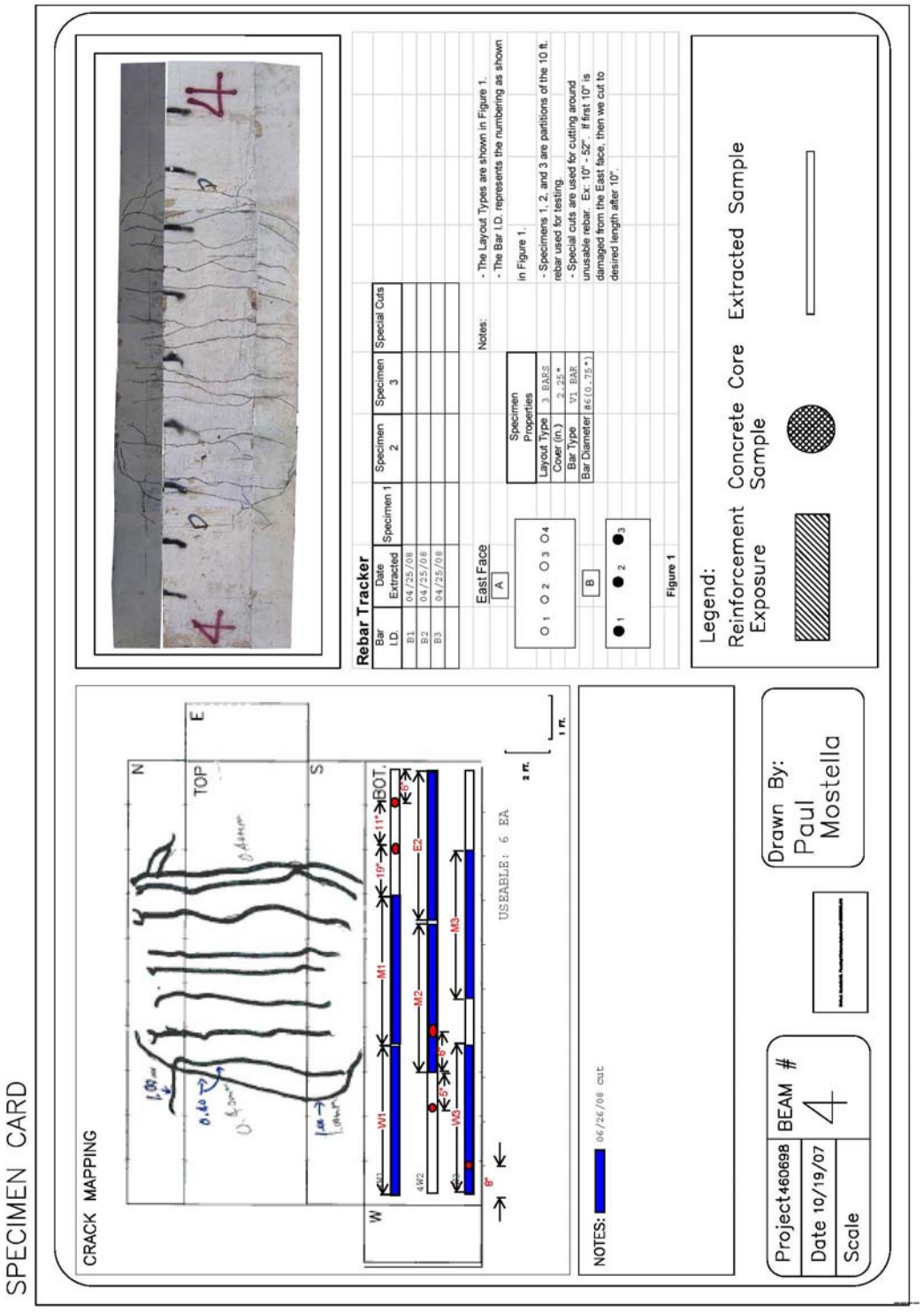

Figure B-4 Beam Card #4

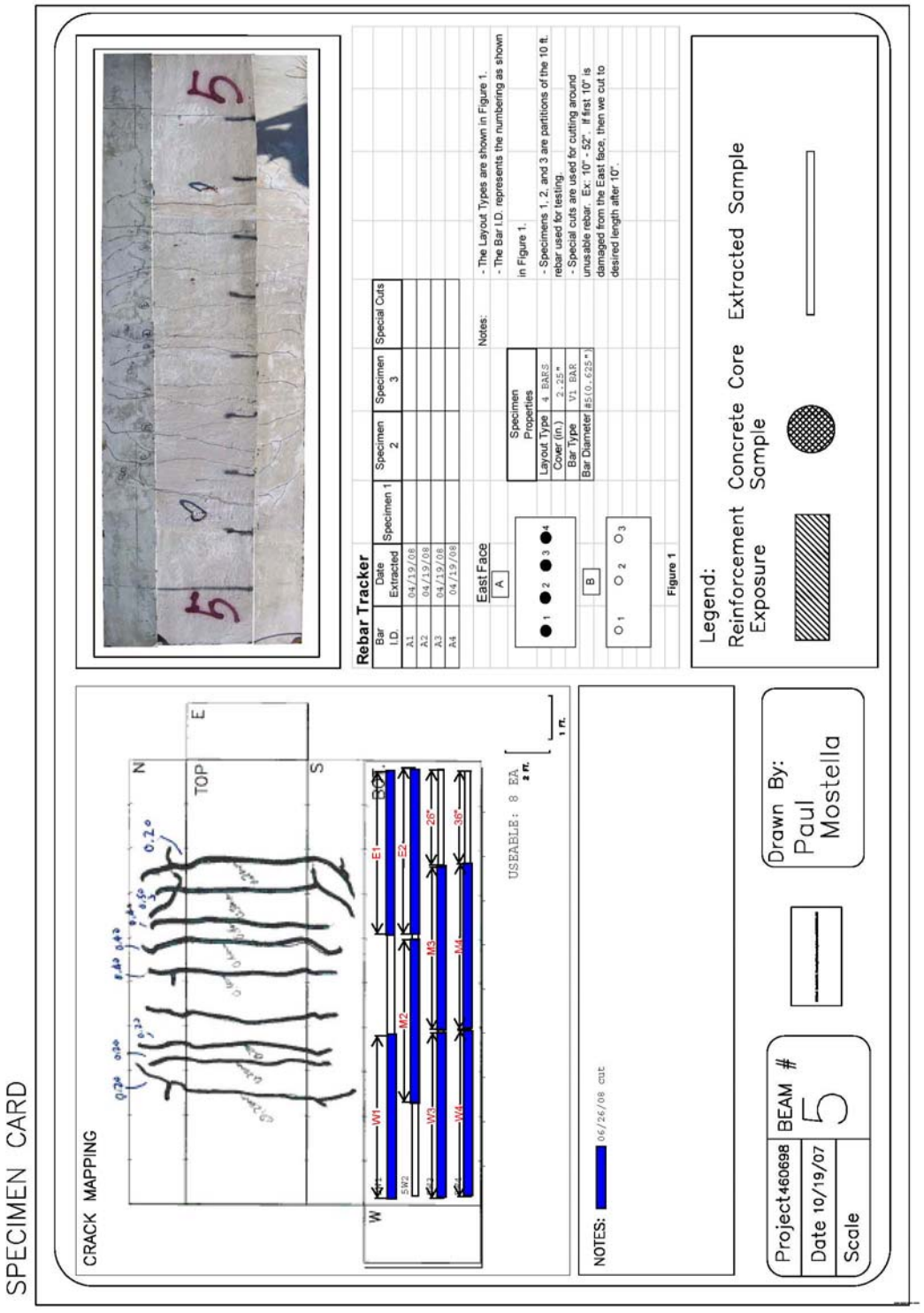

Figure B-5 Beam Card #5

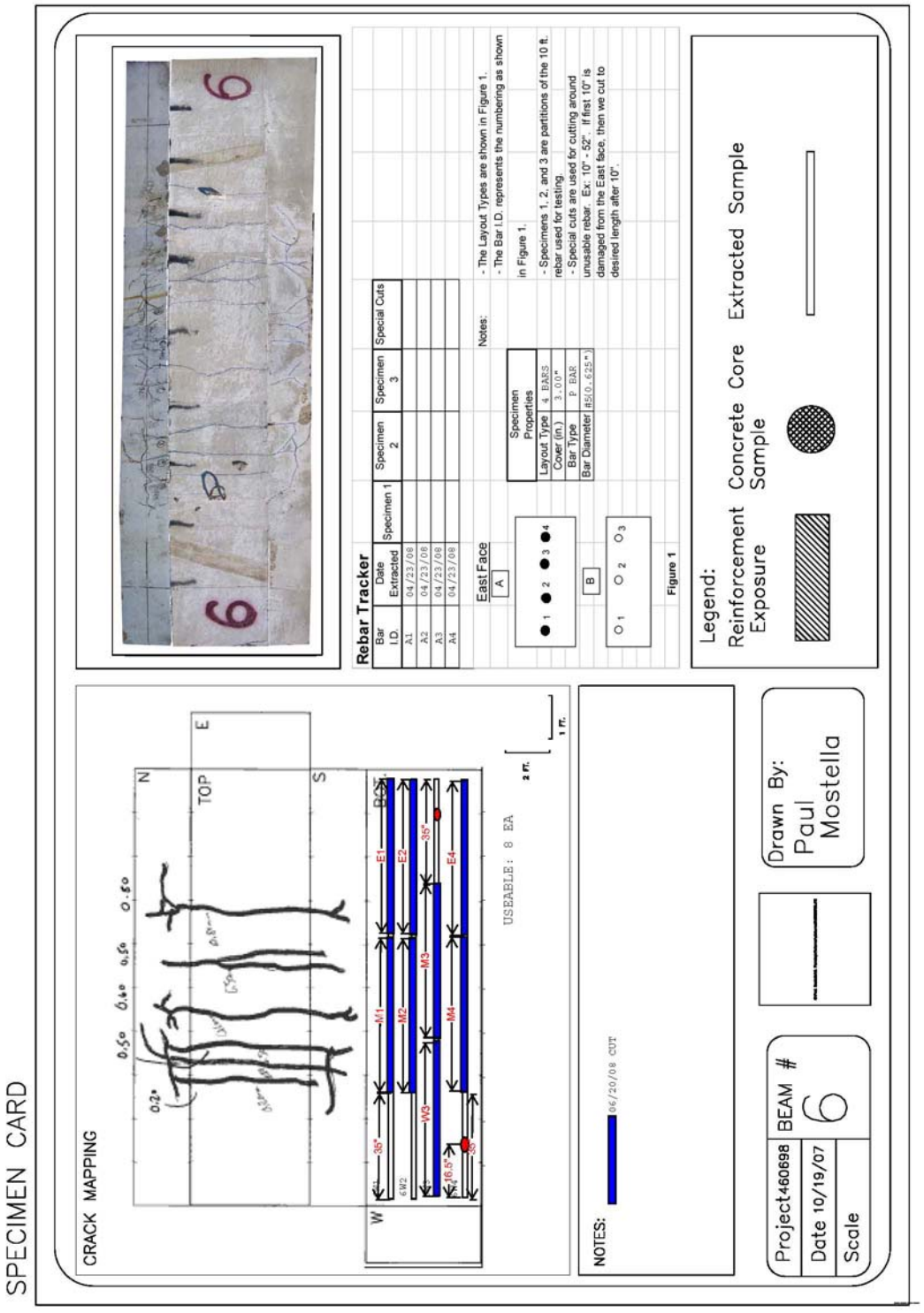

Figure B-6 Beam Card #6

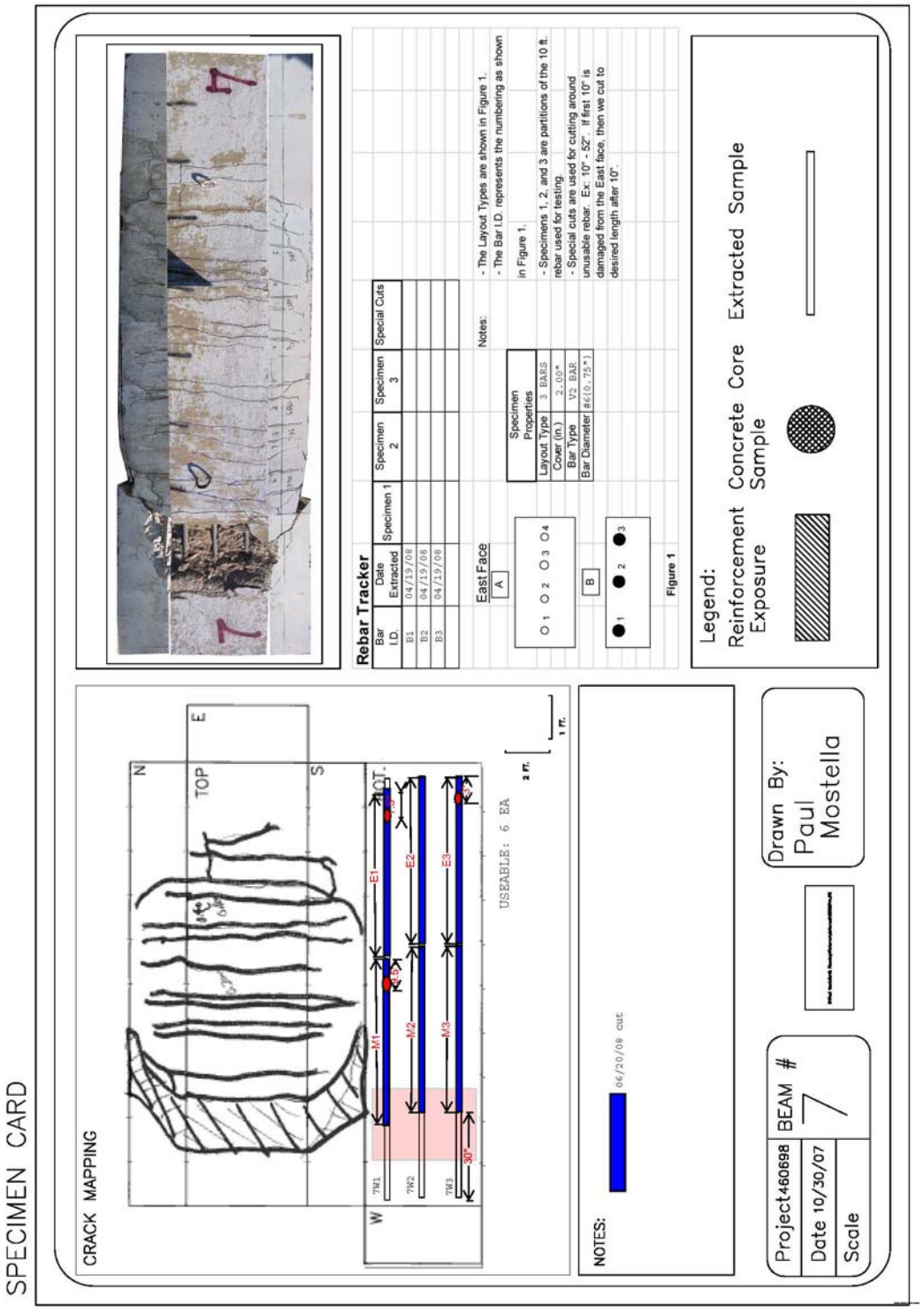

Figure B-7 Beam Card #7

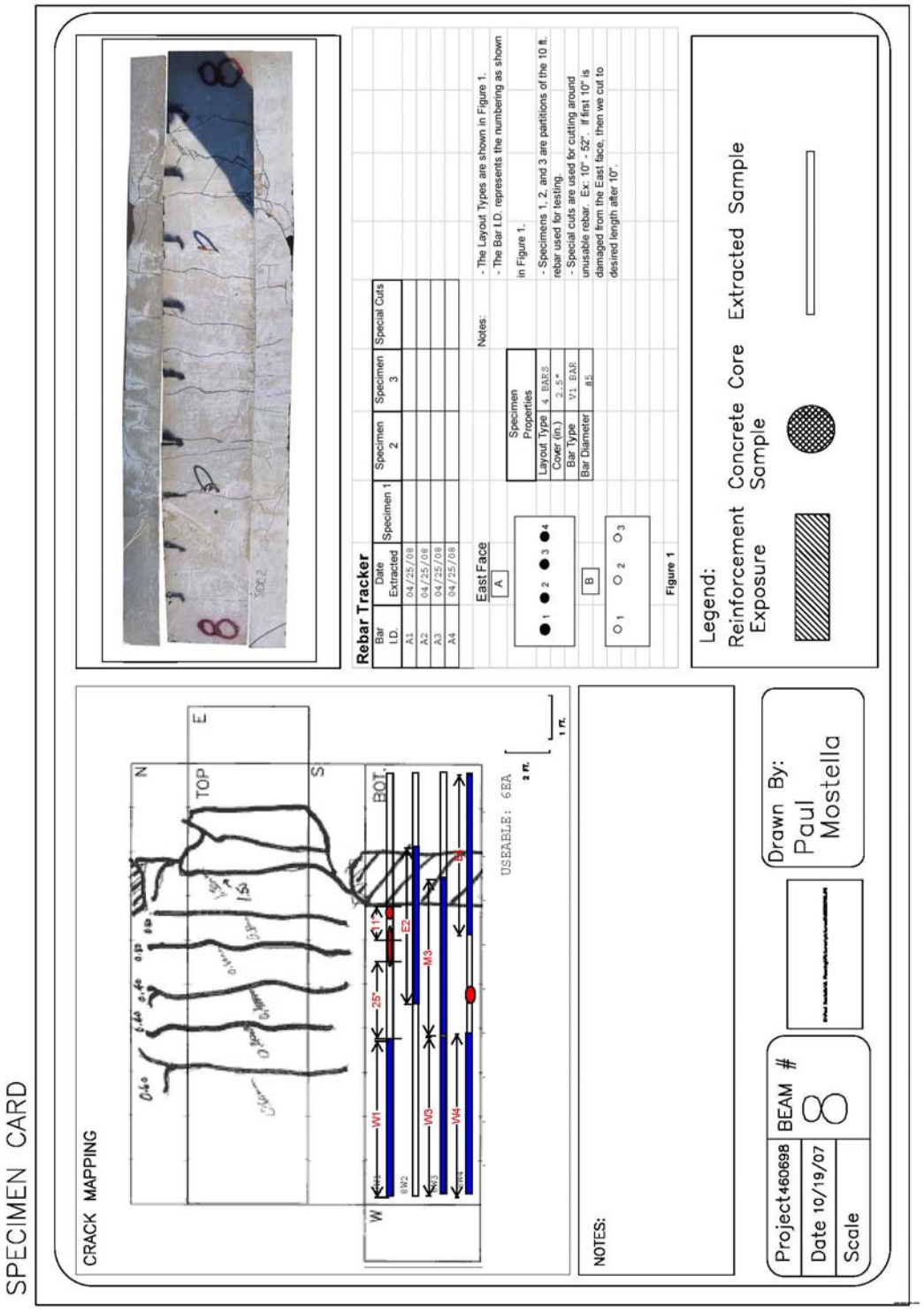

Figure B-8 Beam Card #8

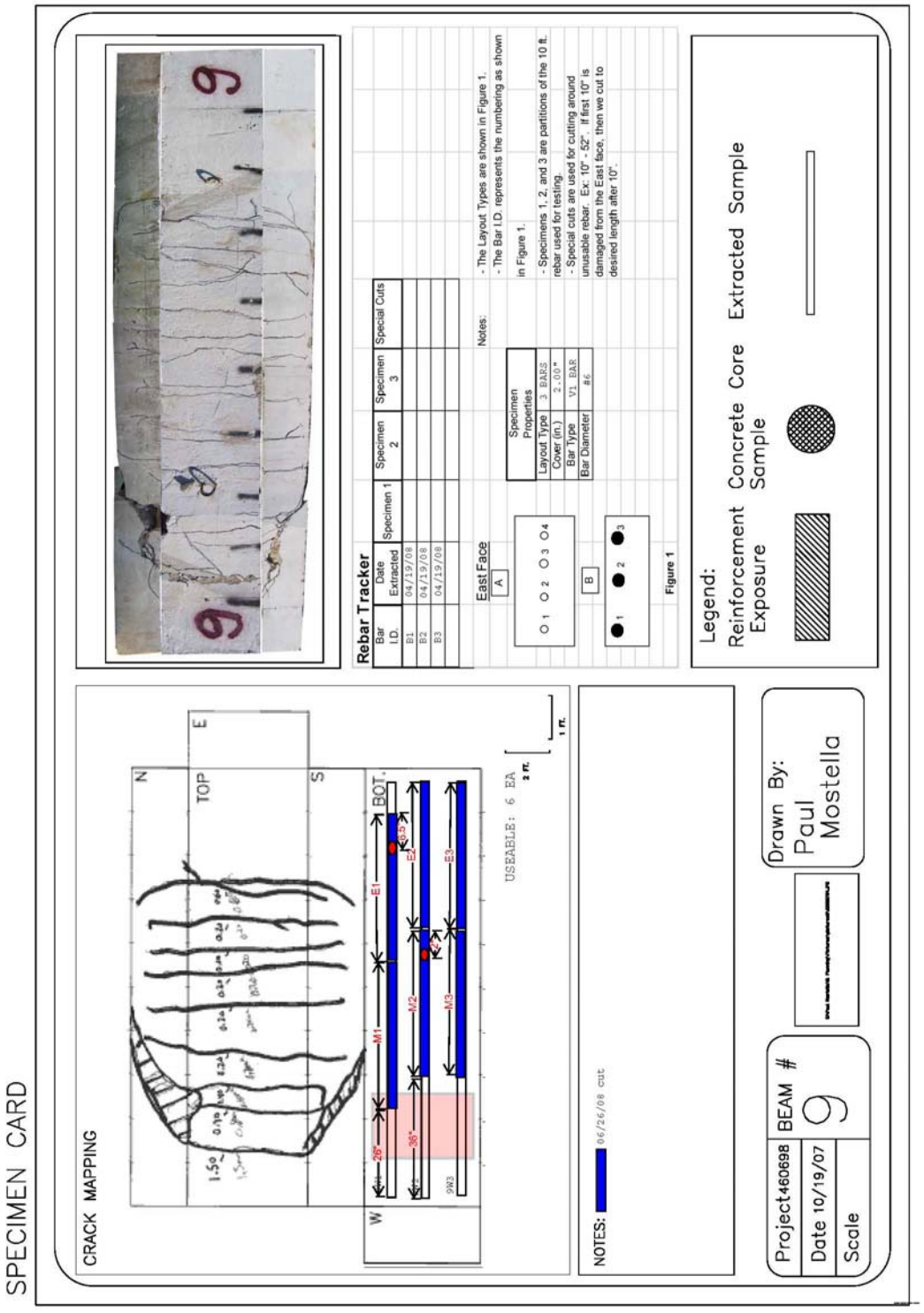

Figure B-9 Beam Card #9

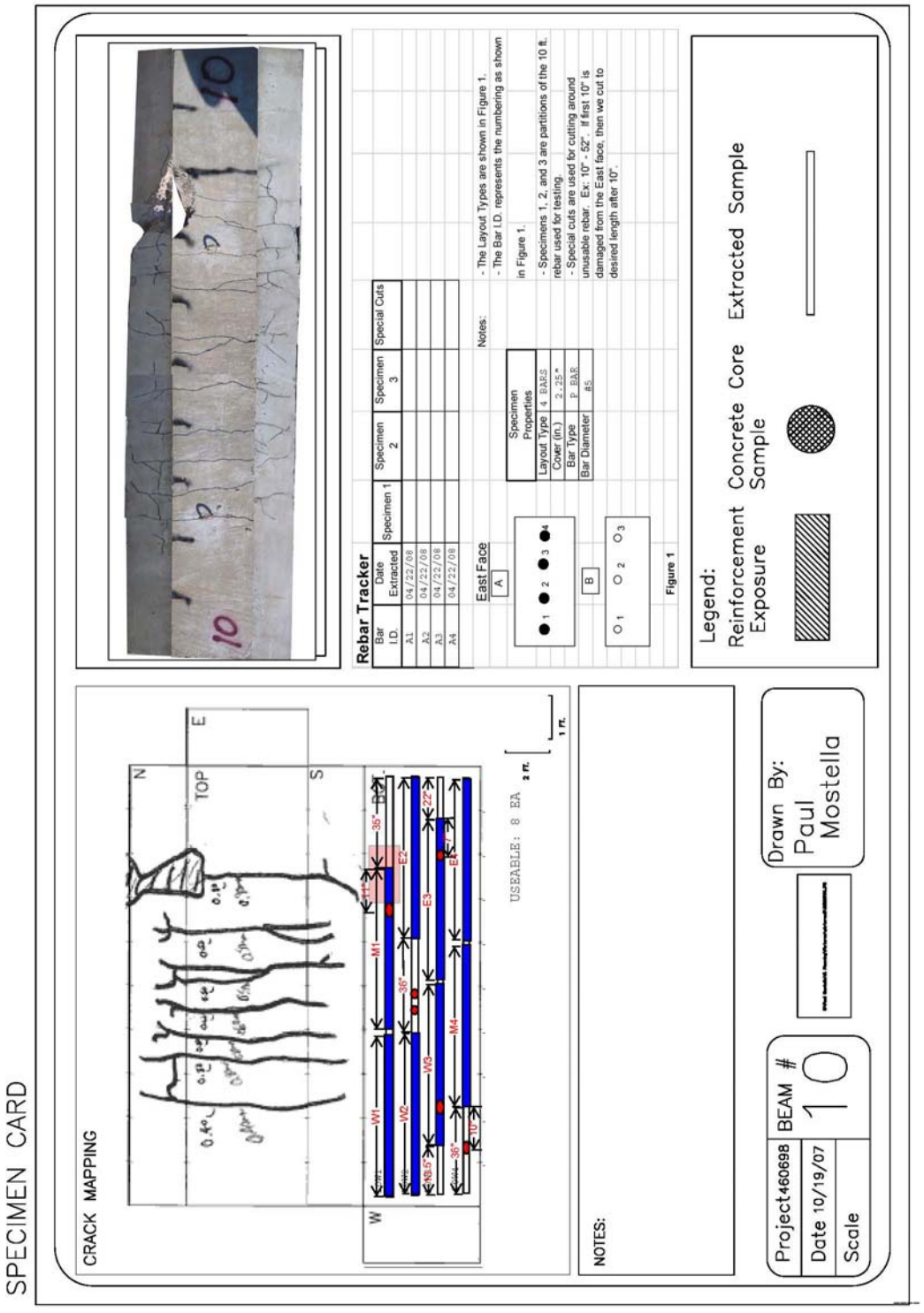

Figure B-10 Beam Card #10

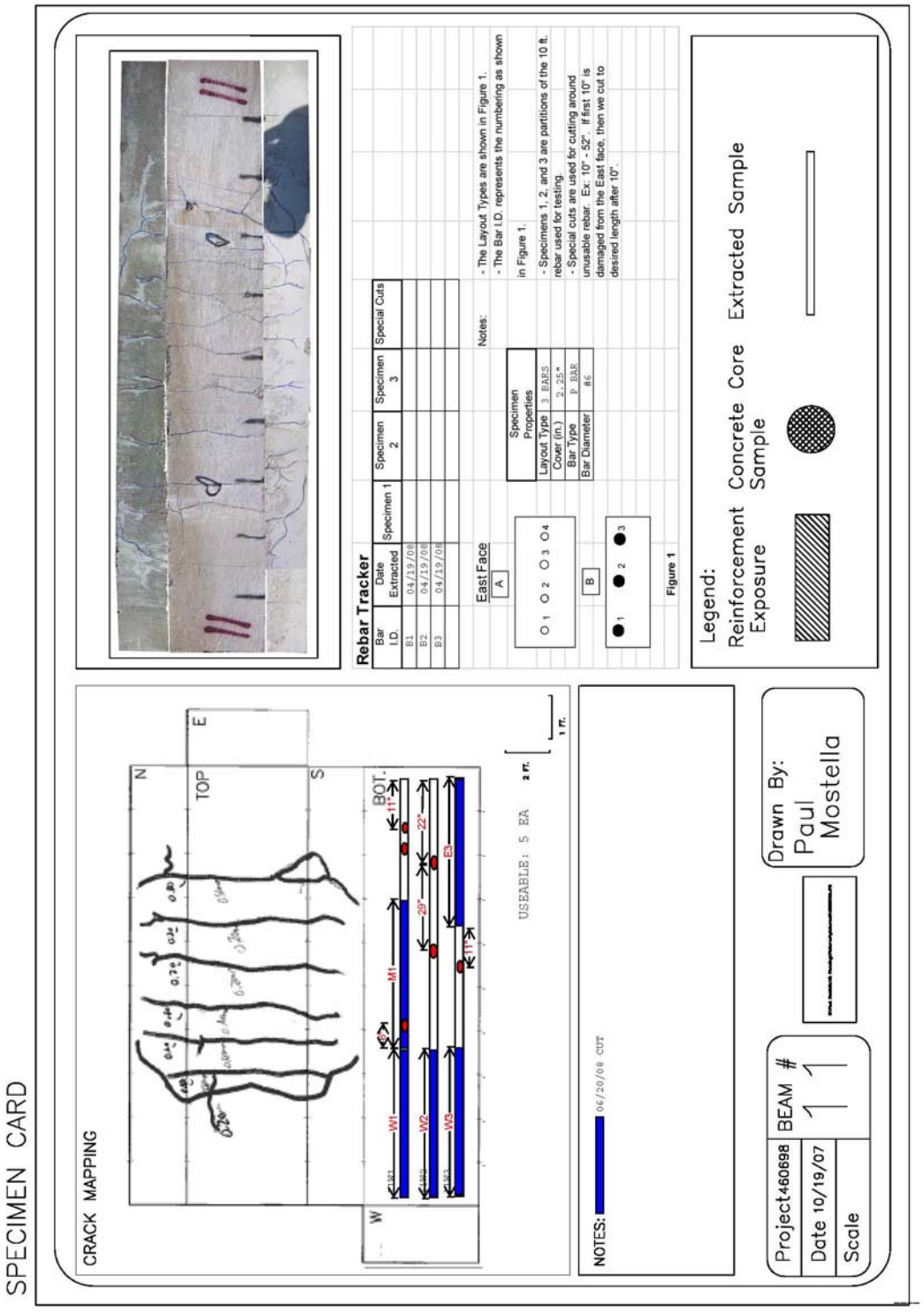

Figure B-11 Beam Card #11

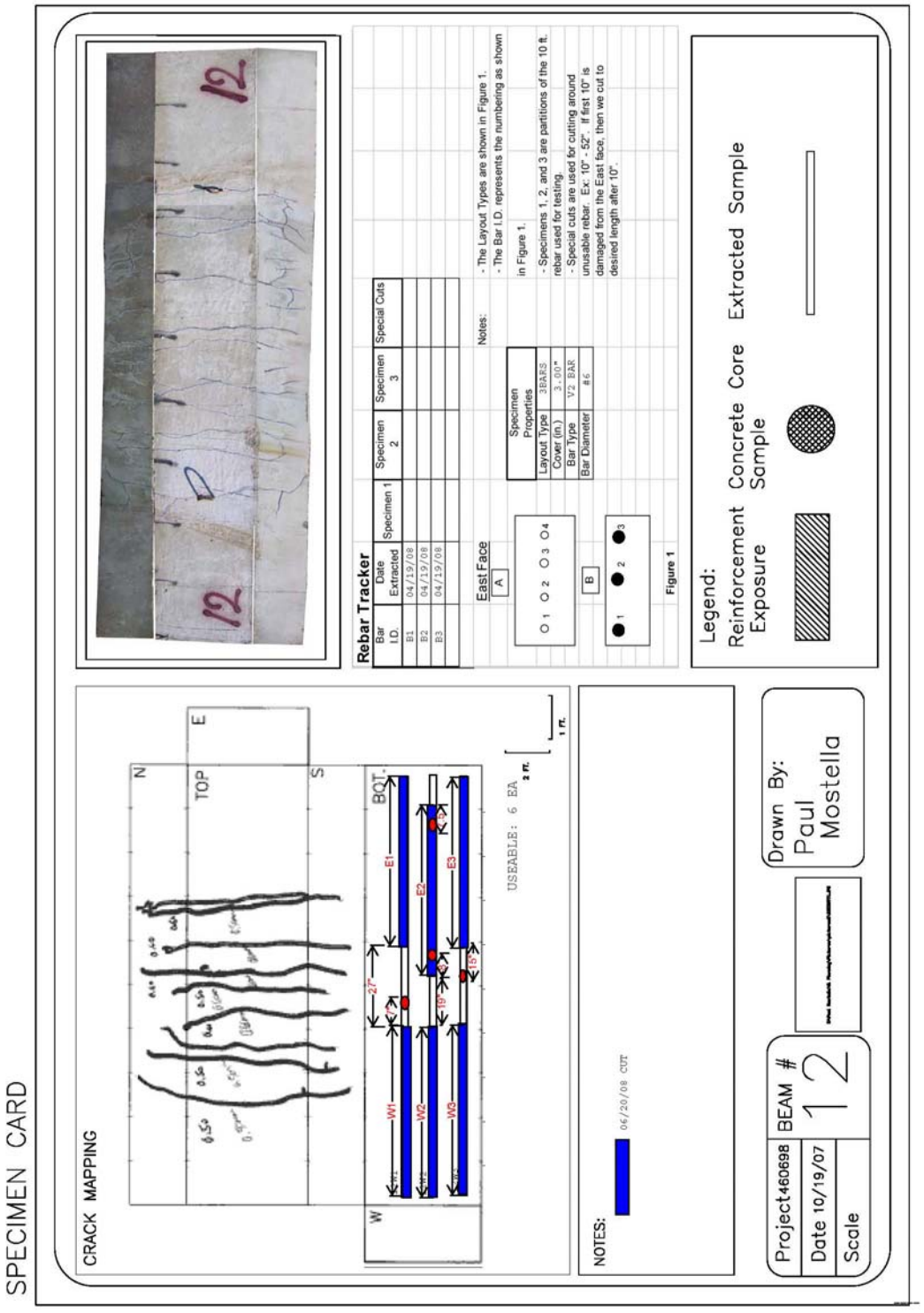

Figure B-12 Beam Card #12

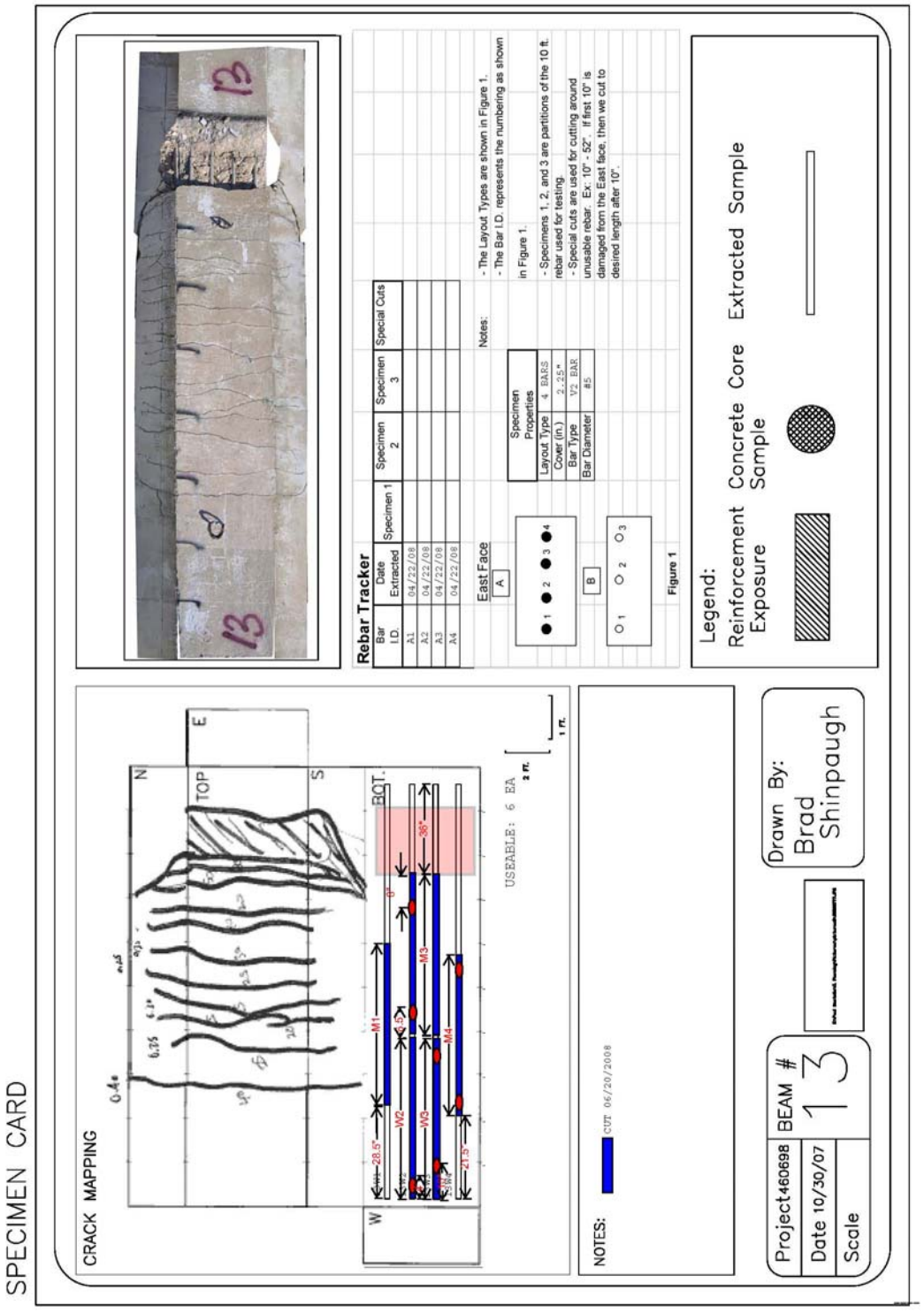

Figure B-13 Beam Card #13

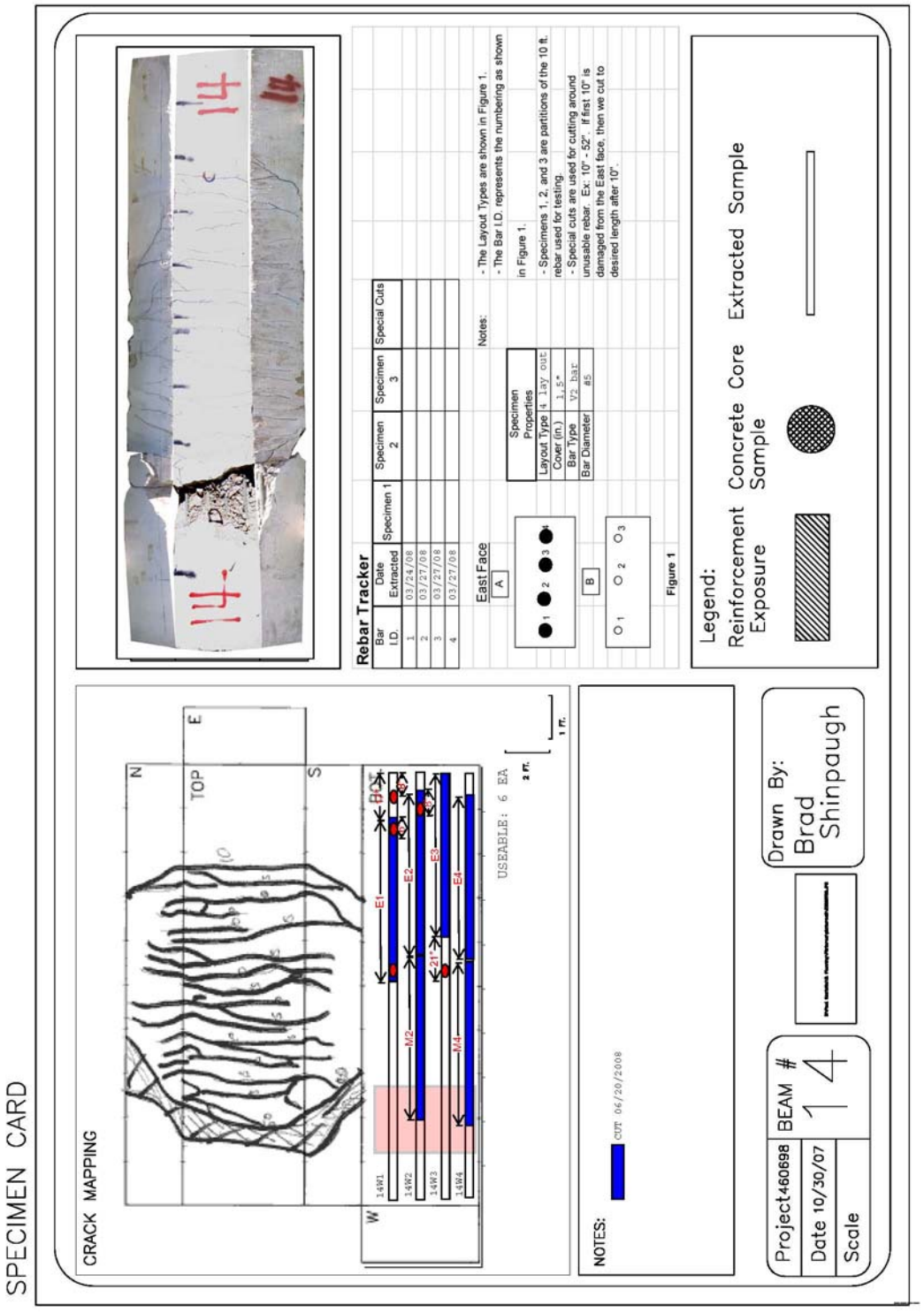

Figure B-14 Beam Card #14

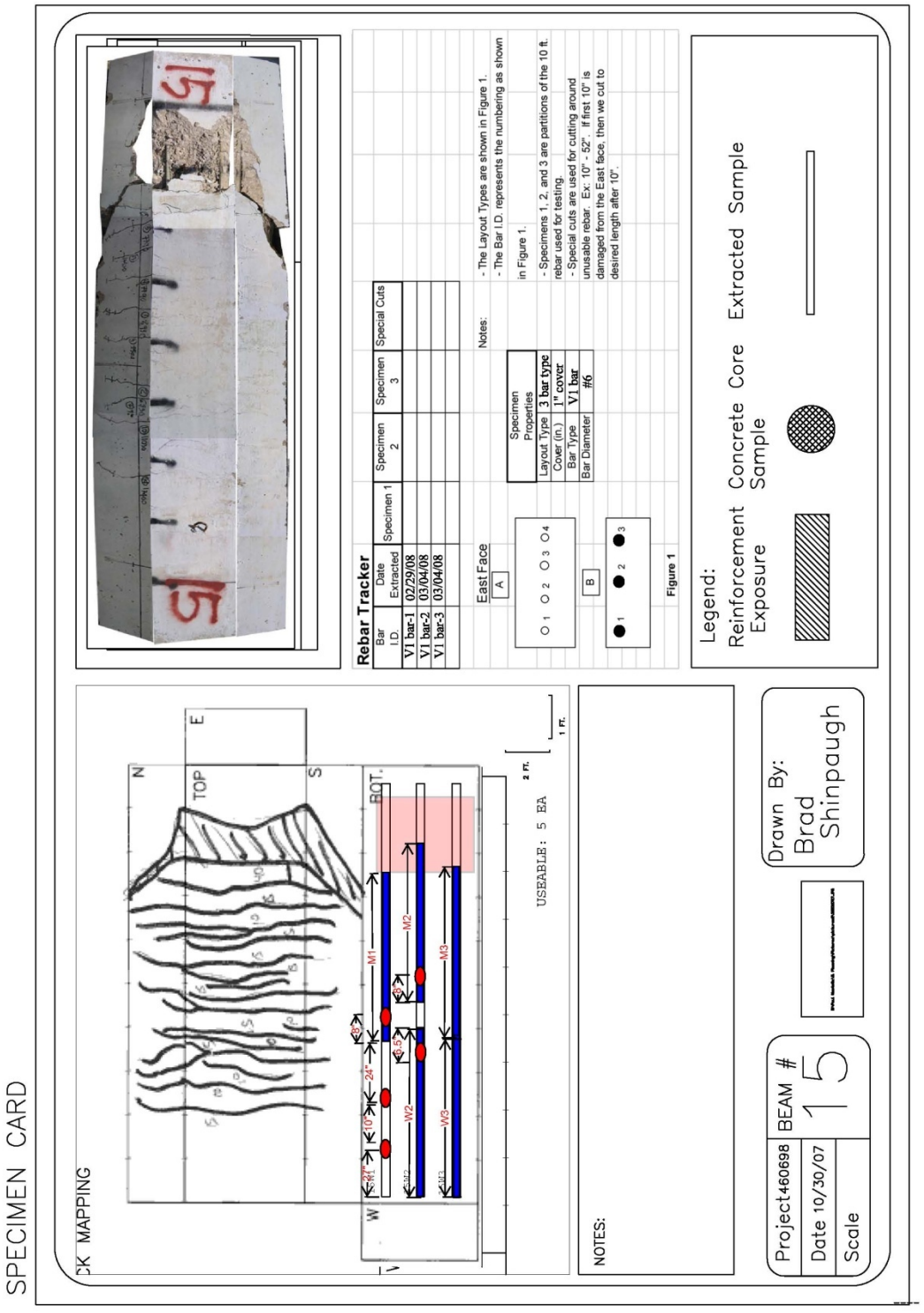

Figure B-15 Beam Card #15

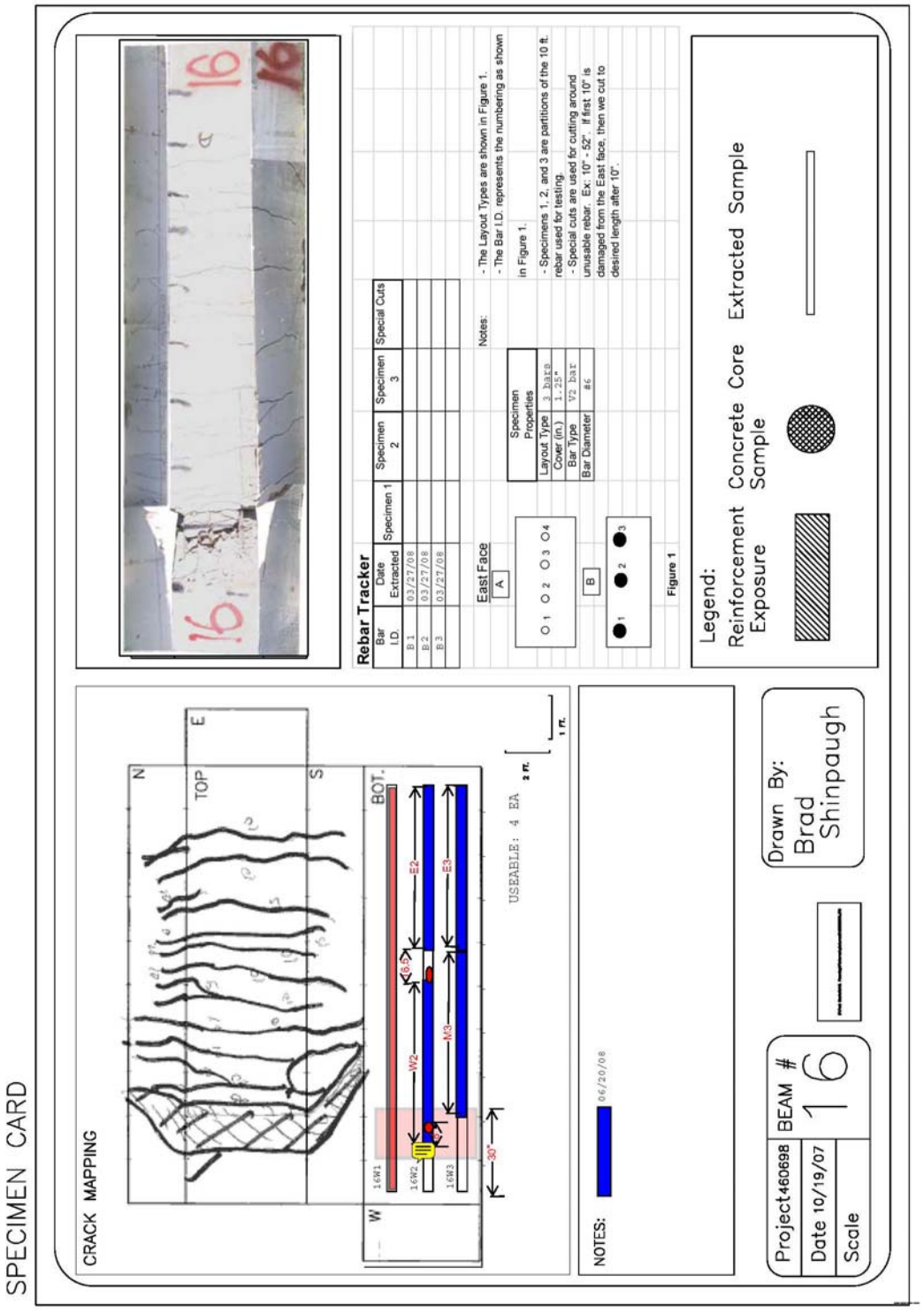

Figure B-16 Beam Card #16

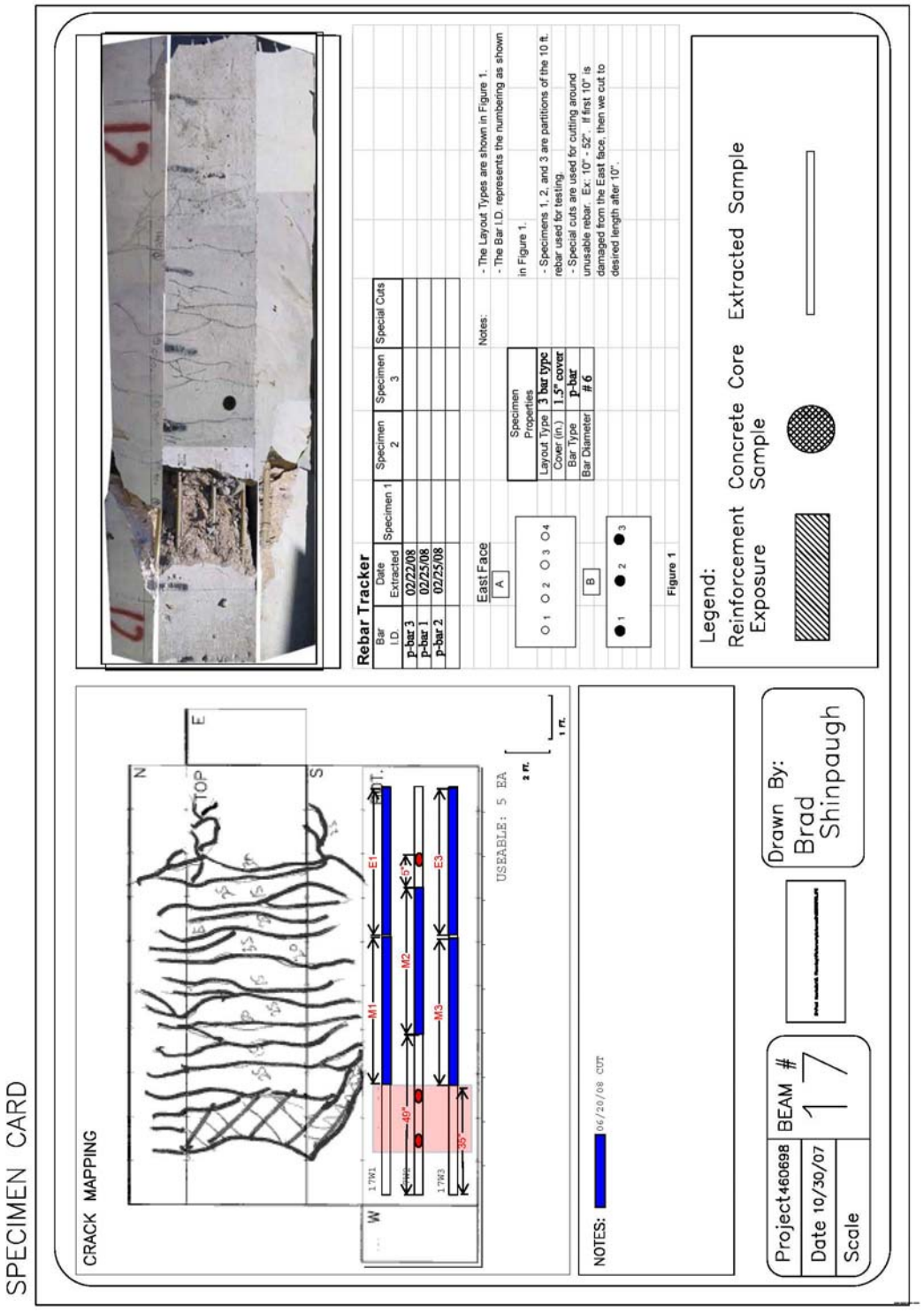

Figure B-17 Beam Card #17

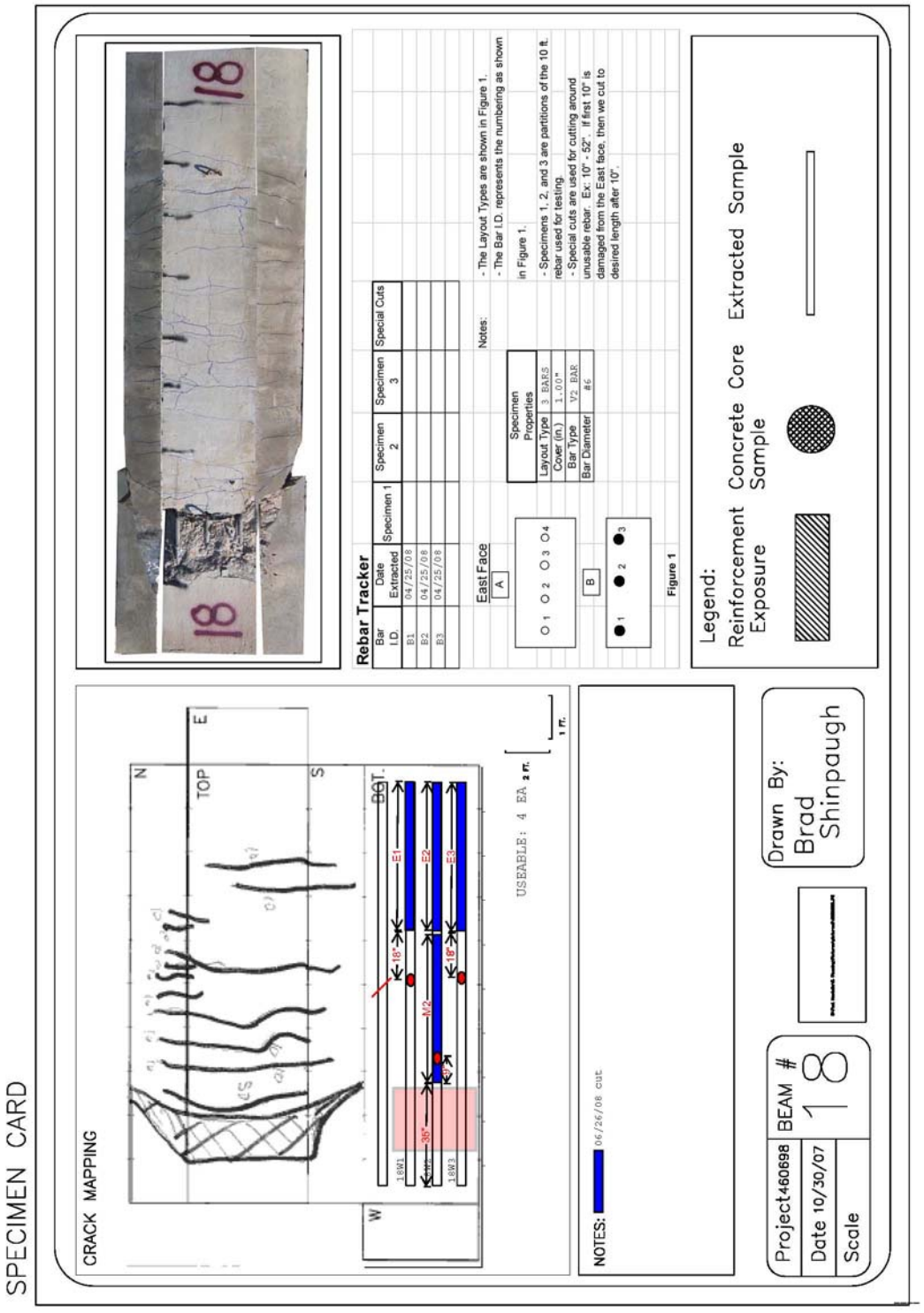

Figure B-18 Beam Card #18

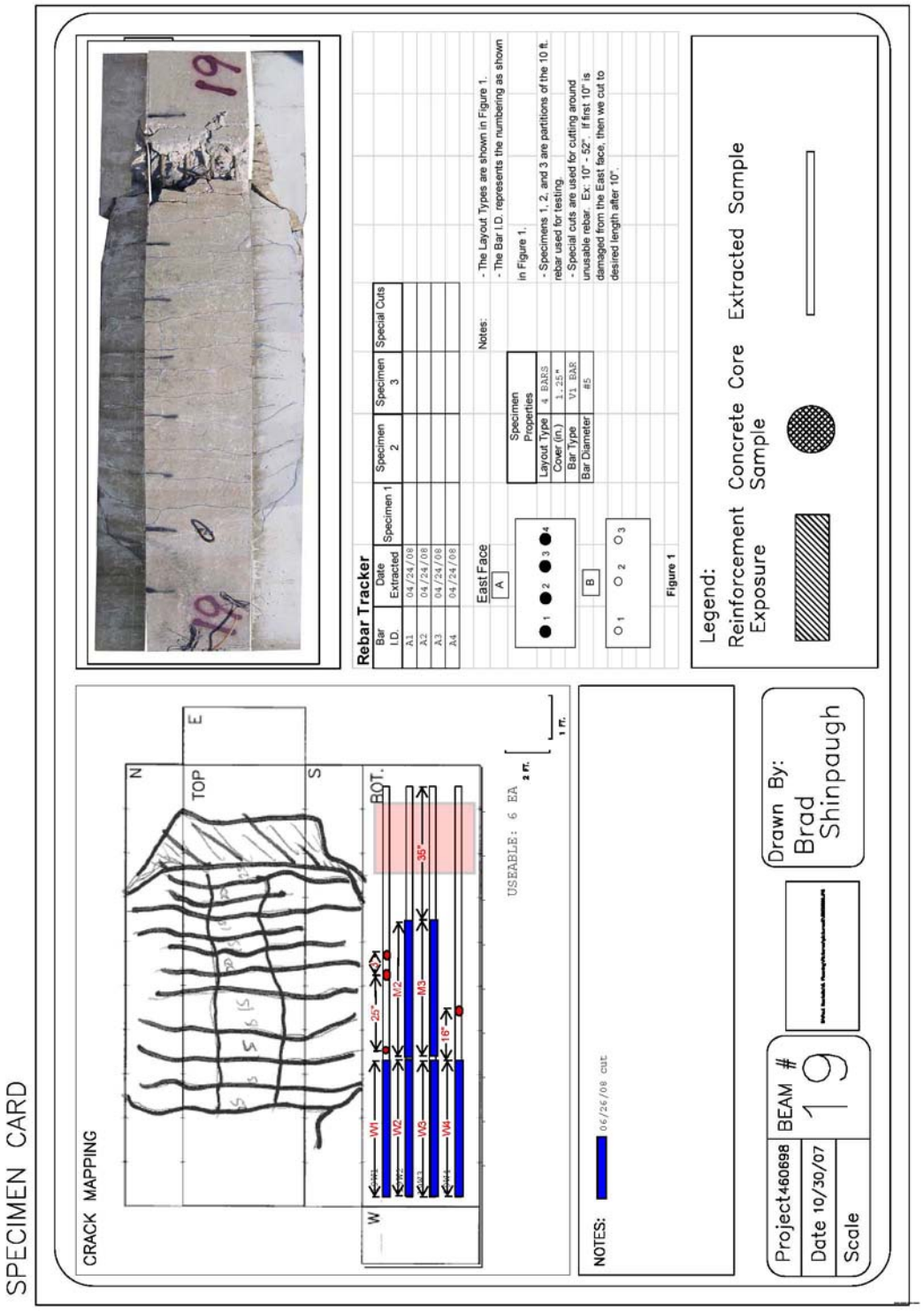

Figure B-19 Beam Card #19

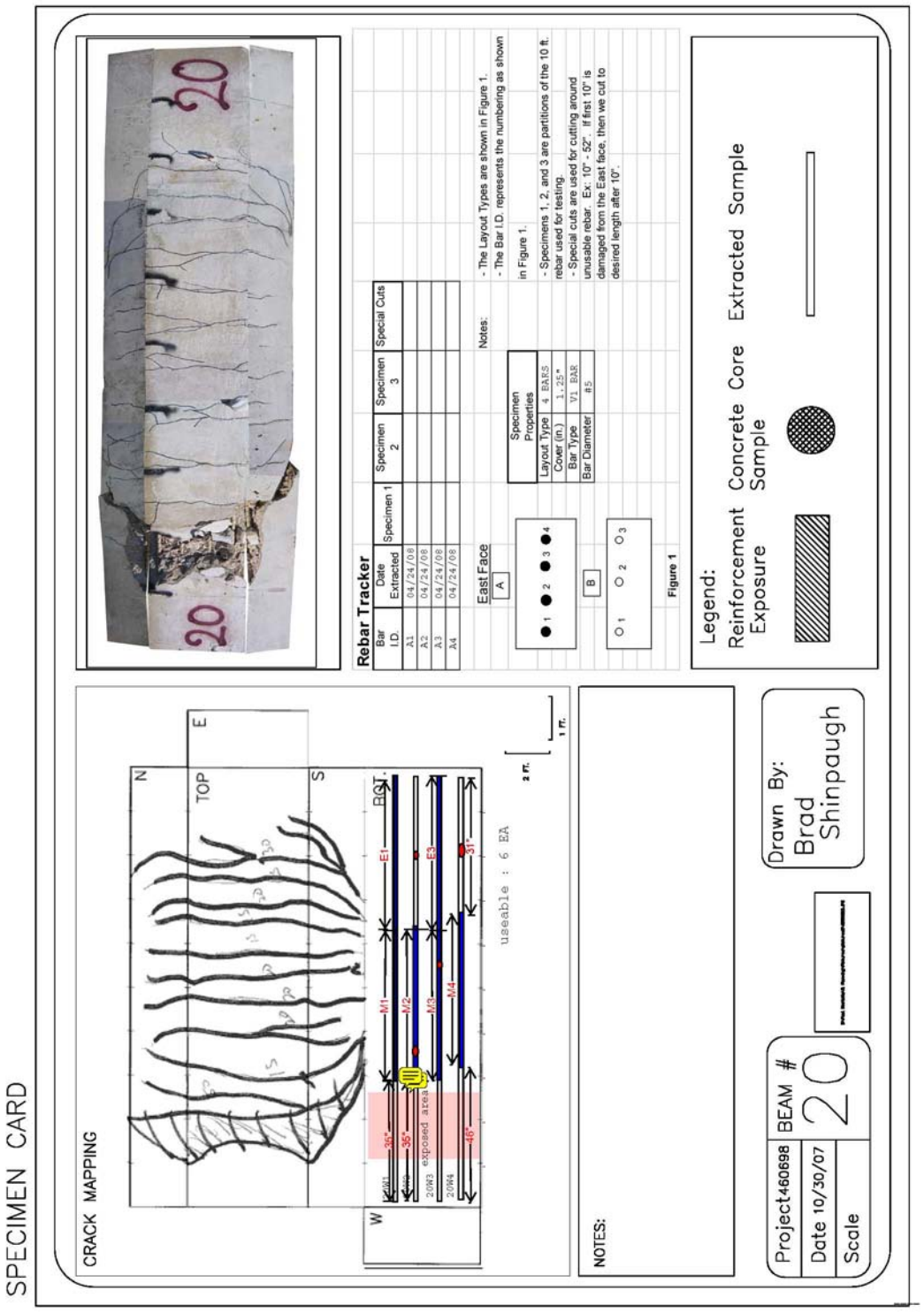

Figure B-20 Beam Card #20

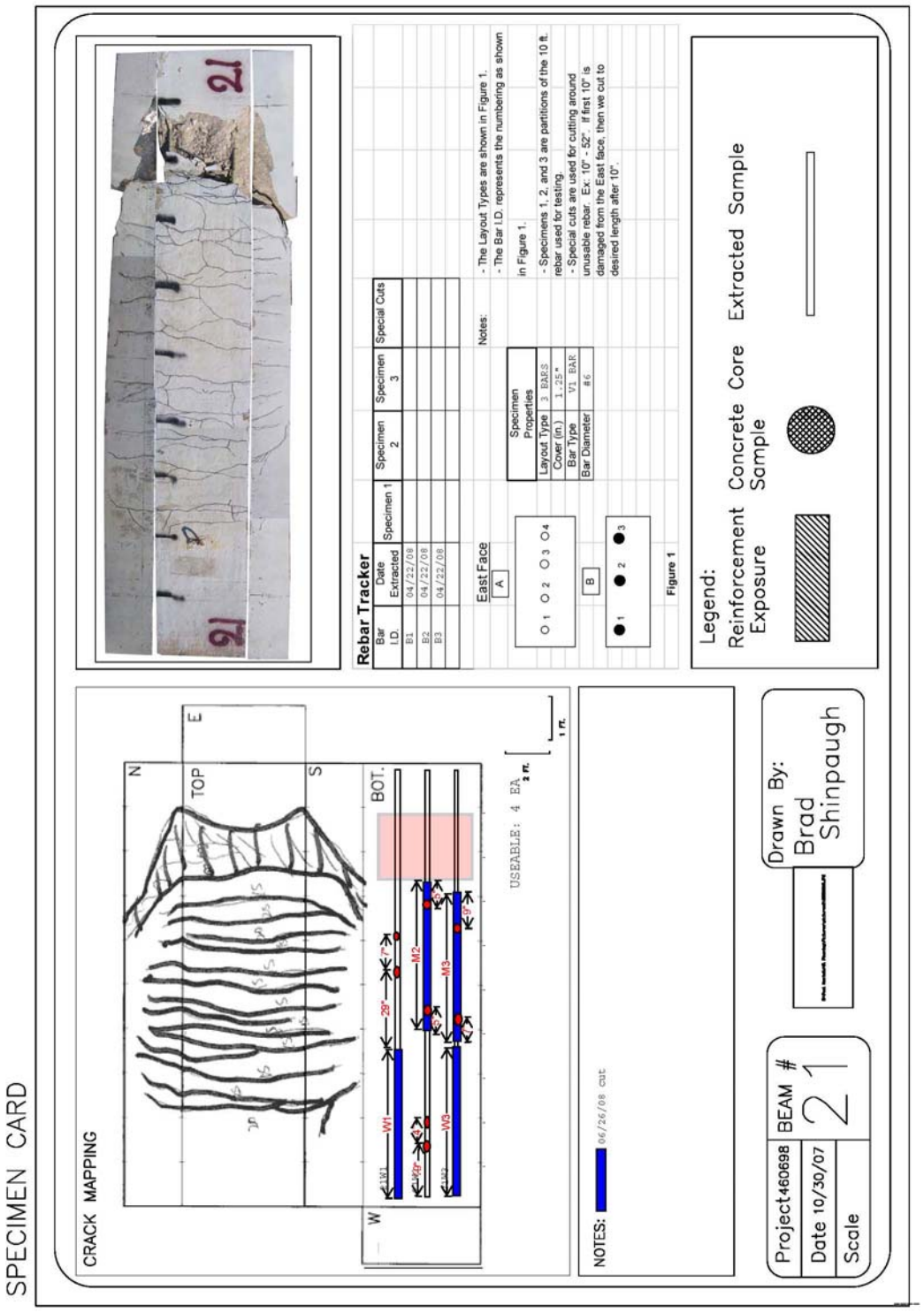

Figure B-21 Beam Card #21

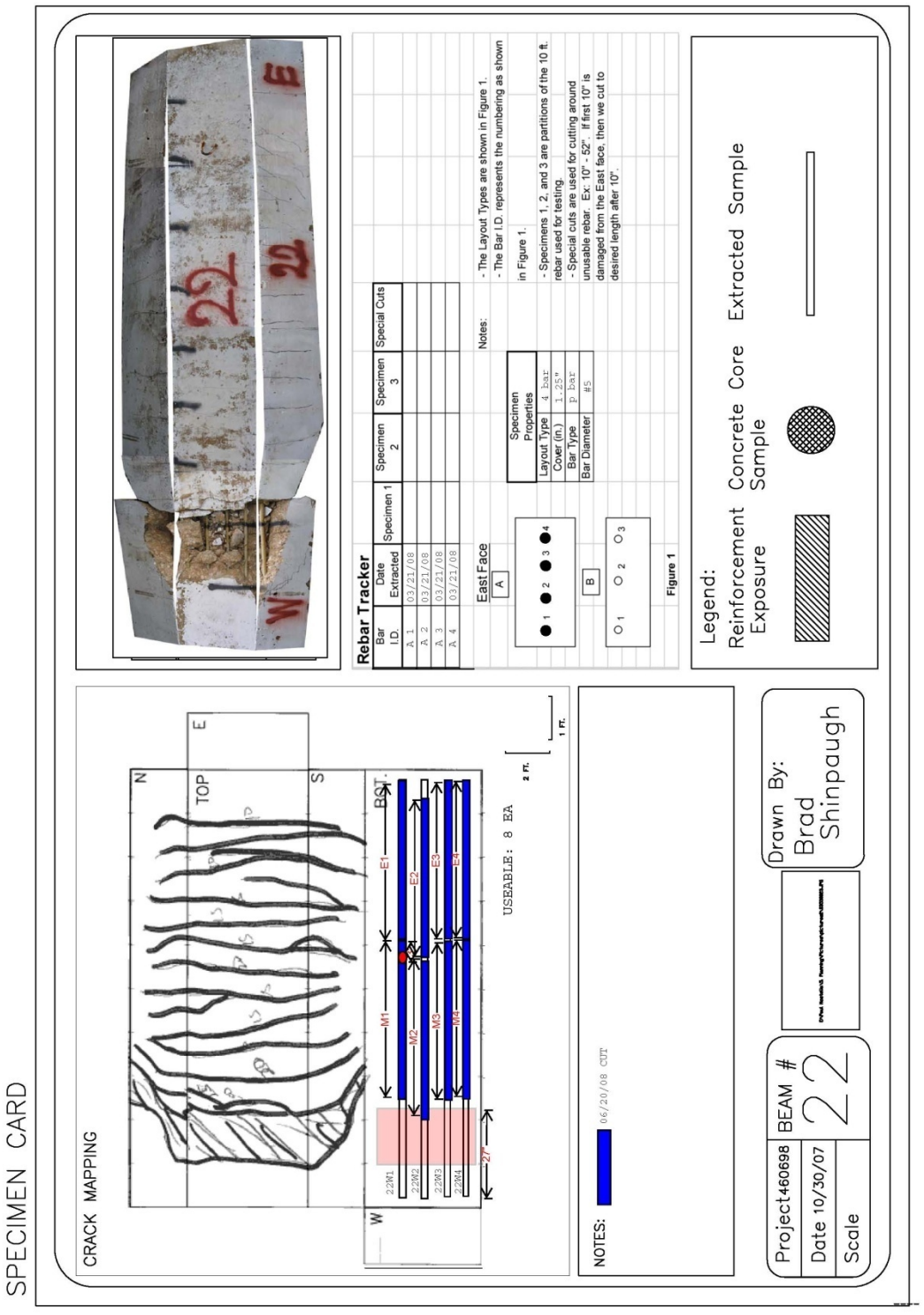

Figure B-22 Beam Card #22

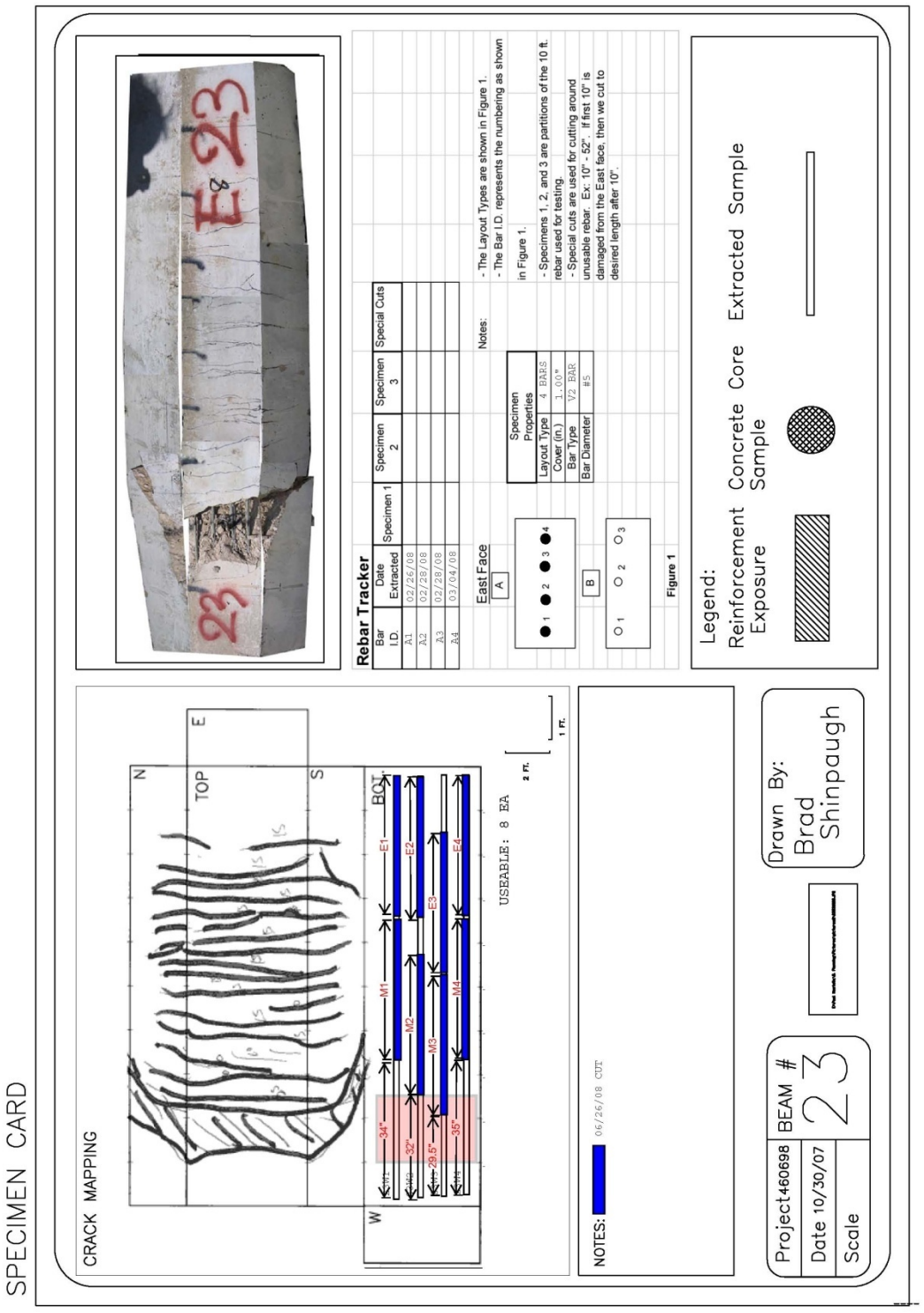

Figure B-23 Beam Card #23

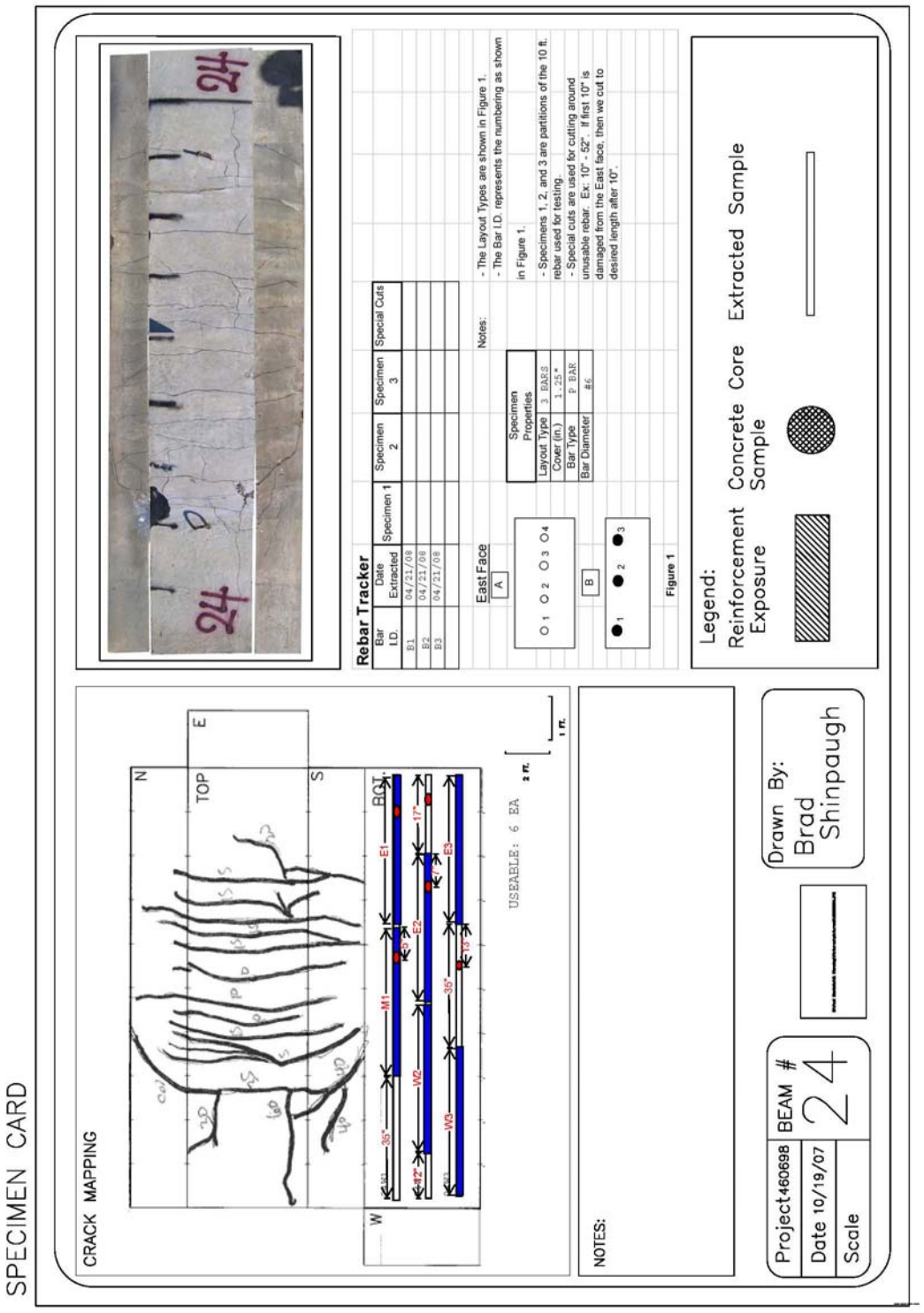

Figure B-24 Beam Card #24

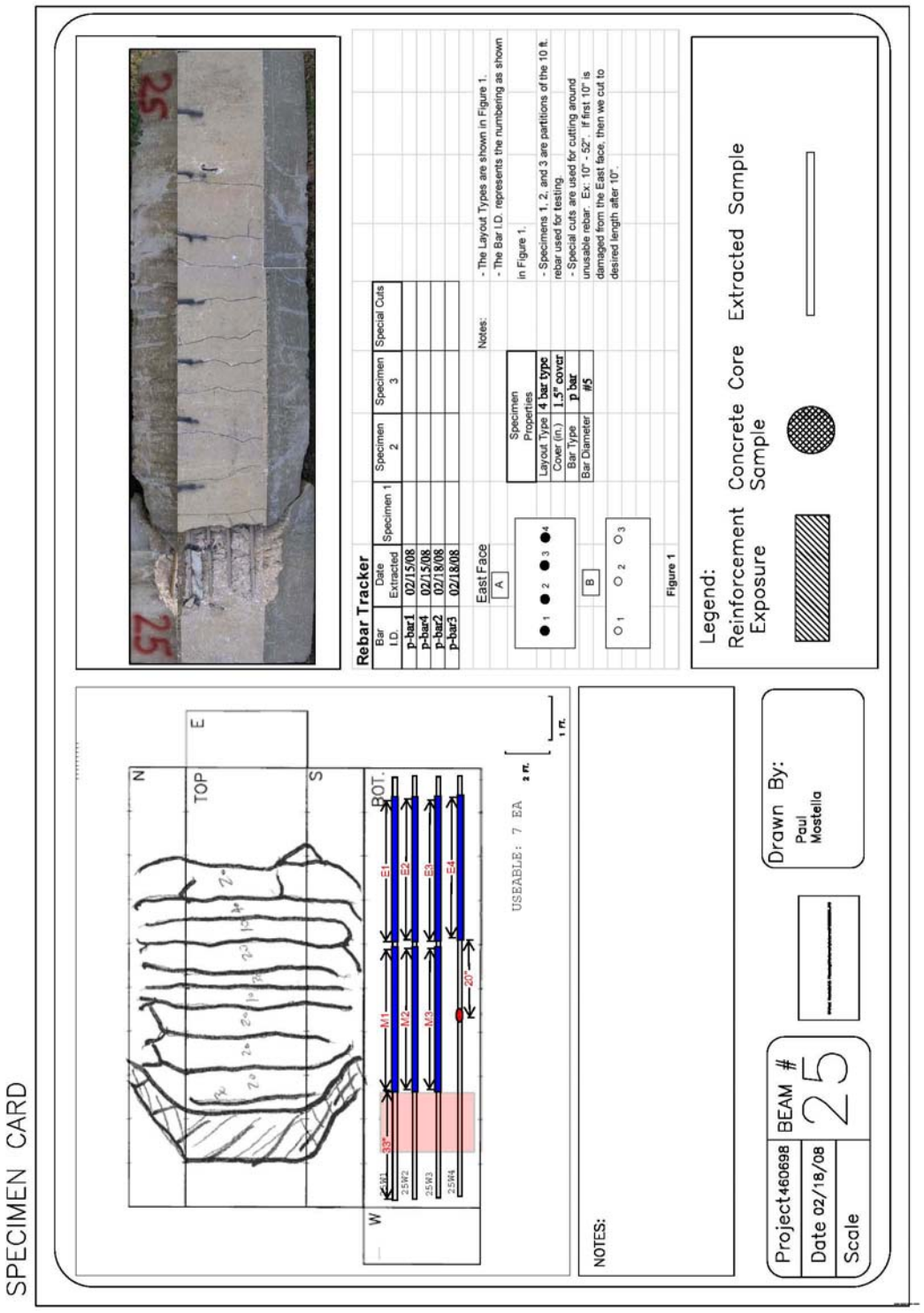

Figure B-25 Beam Card #25

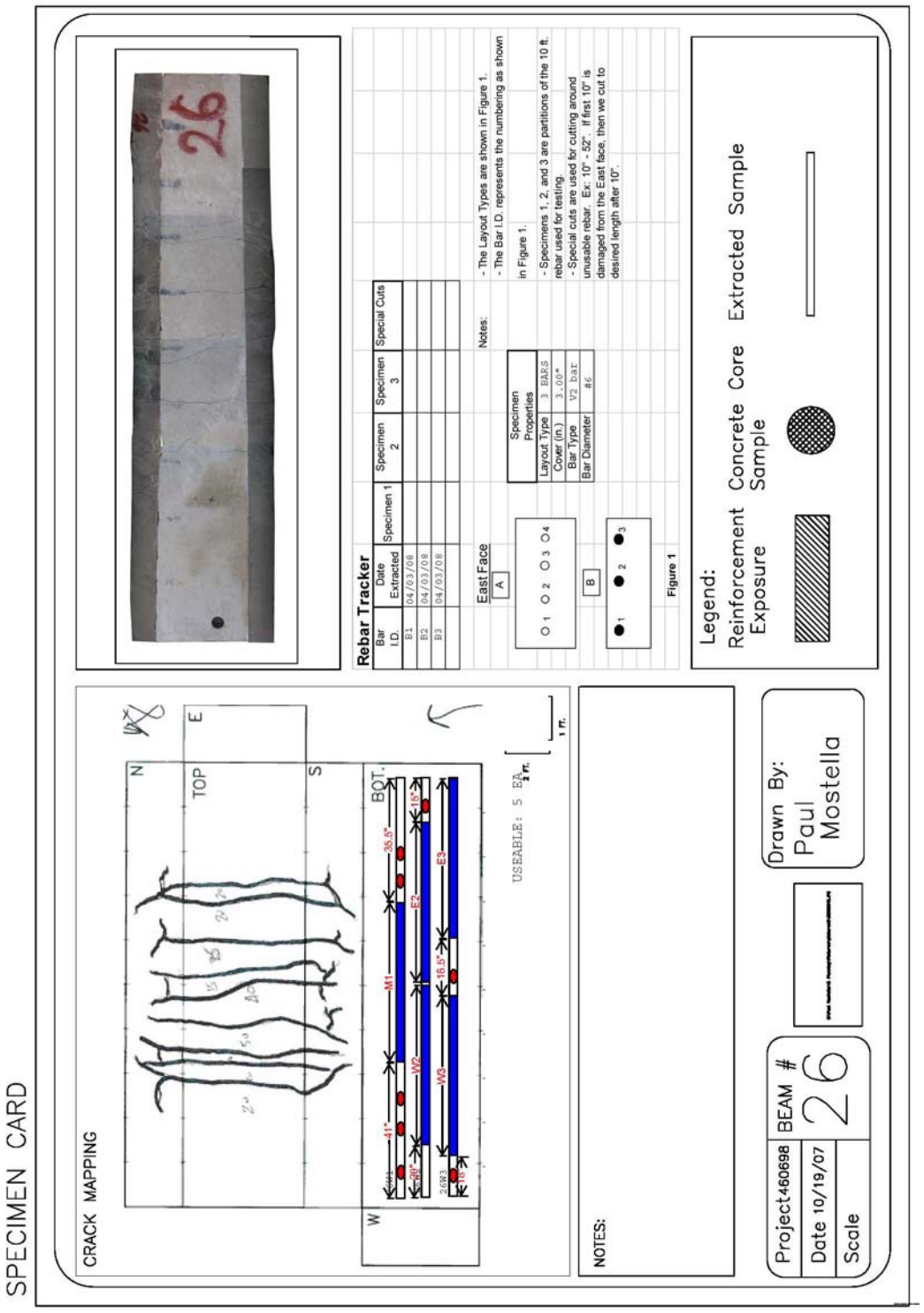

Figure B-26 Beam Card #26

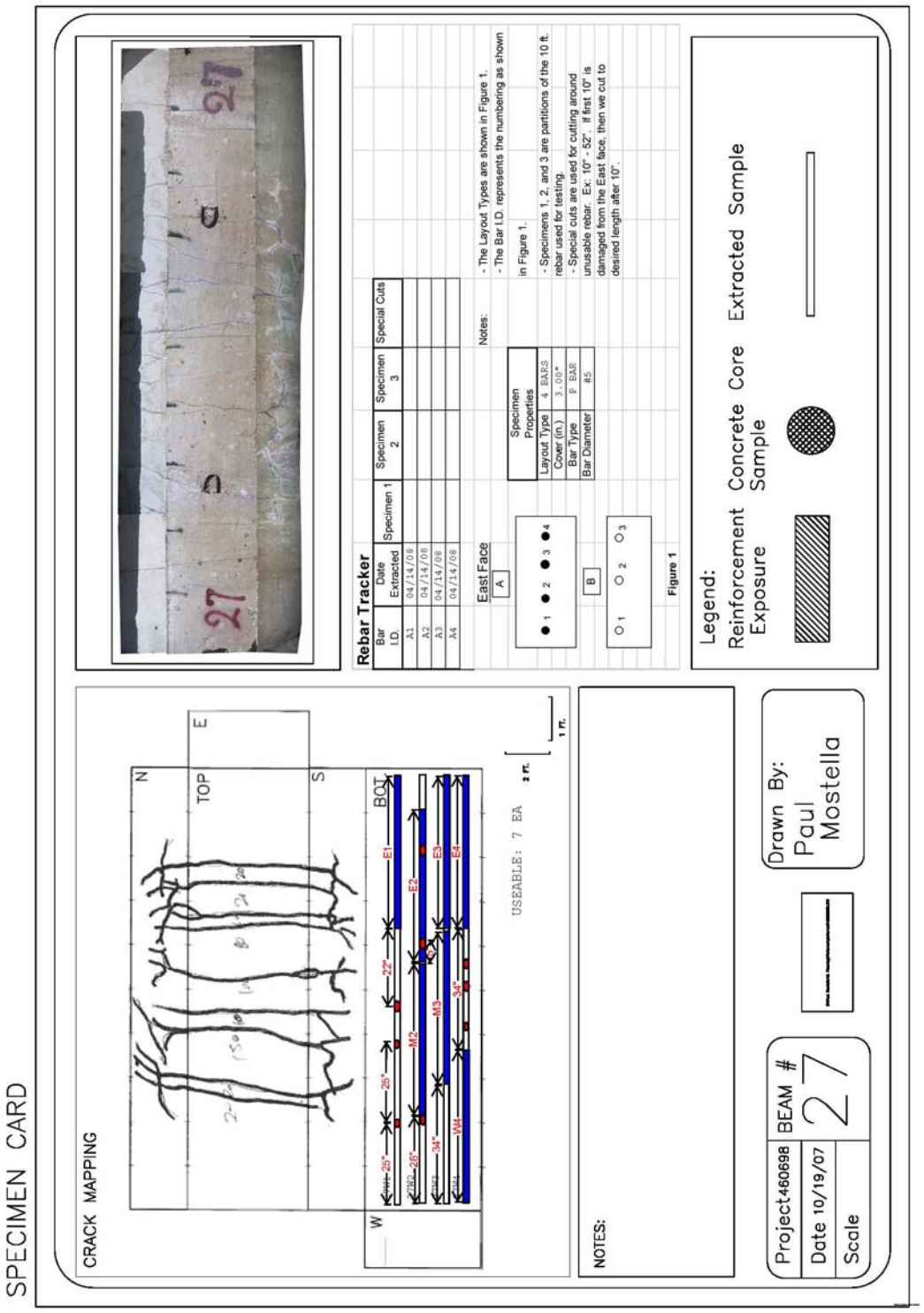

Figure B-27 Beam Card #27

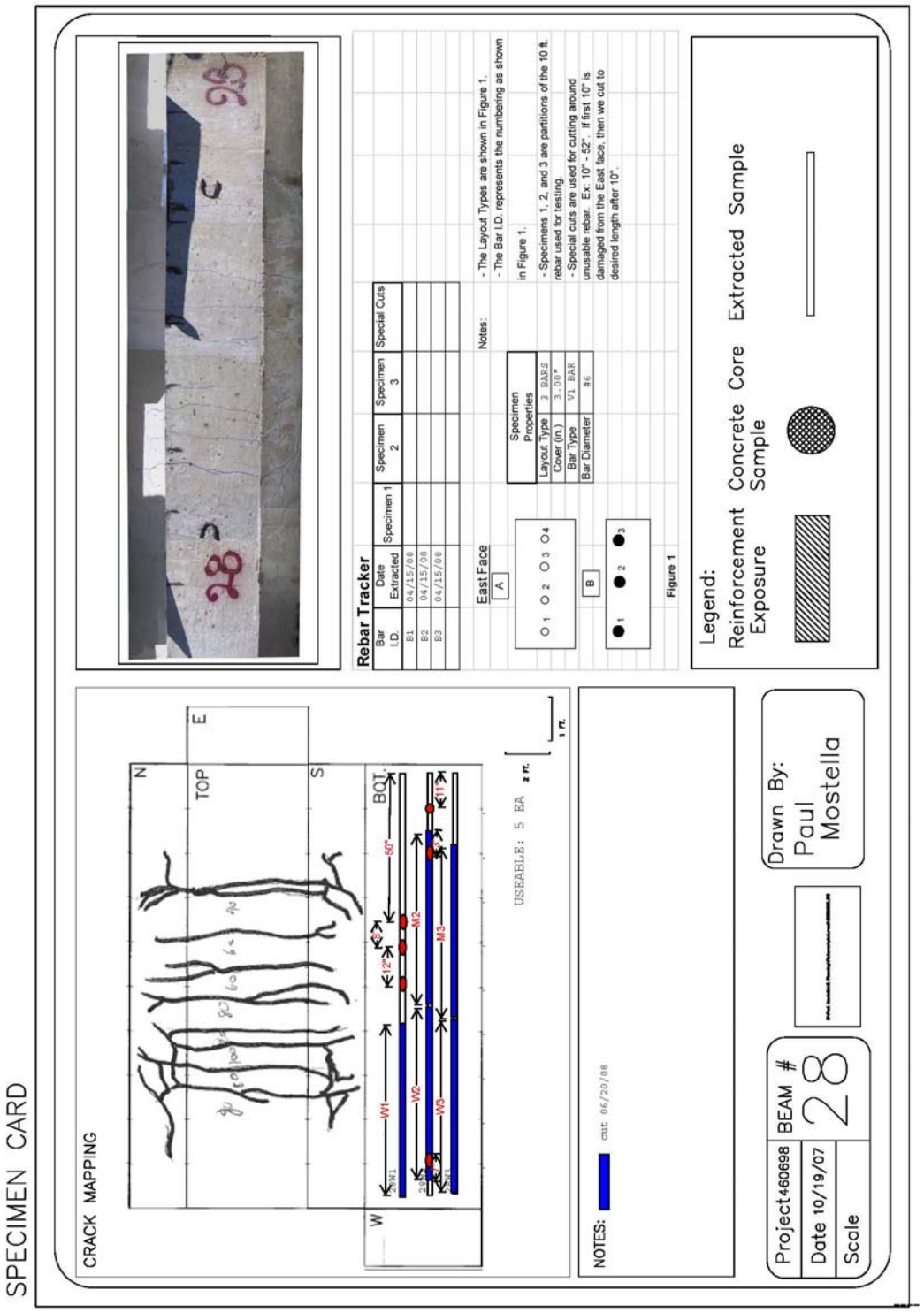

Figure B-28 Beam Card #28

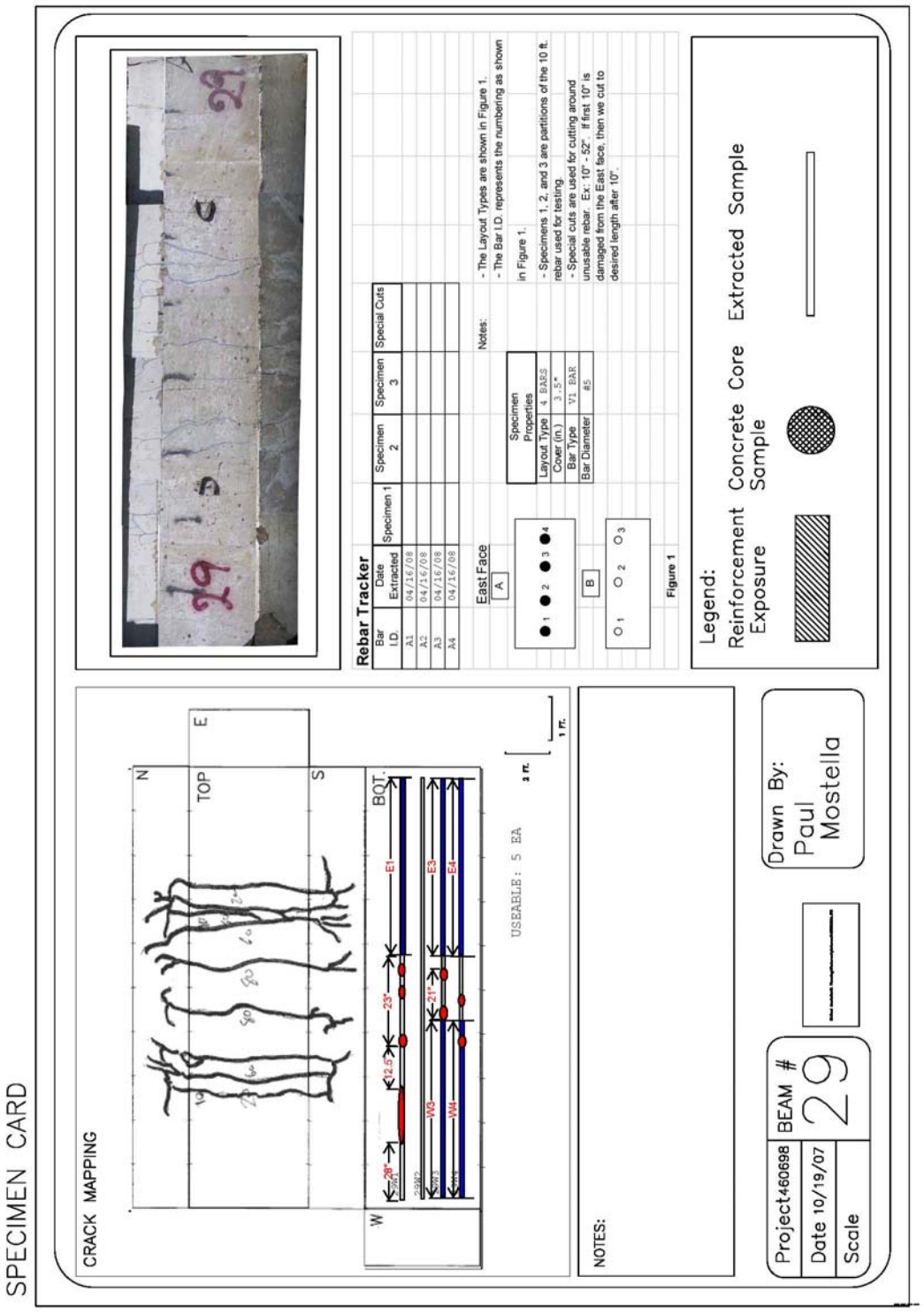

Figure B-29 Beam Card #29

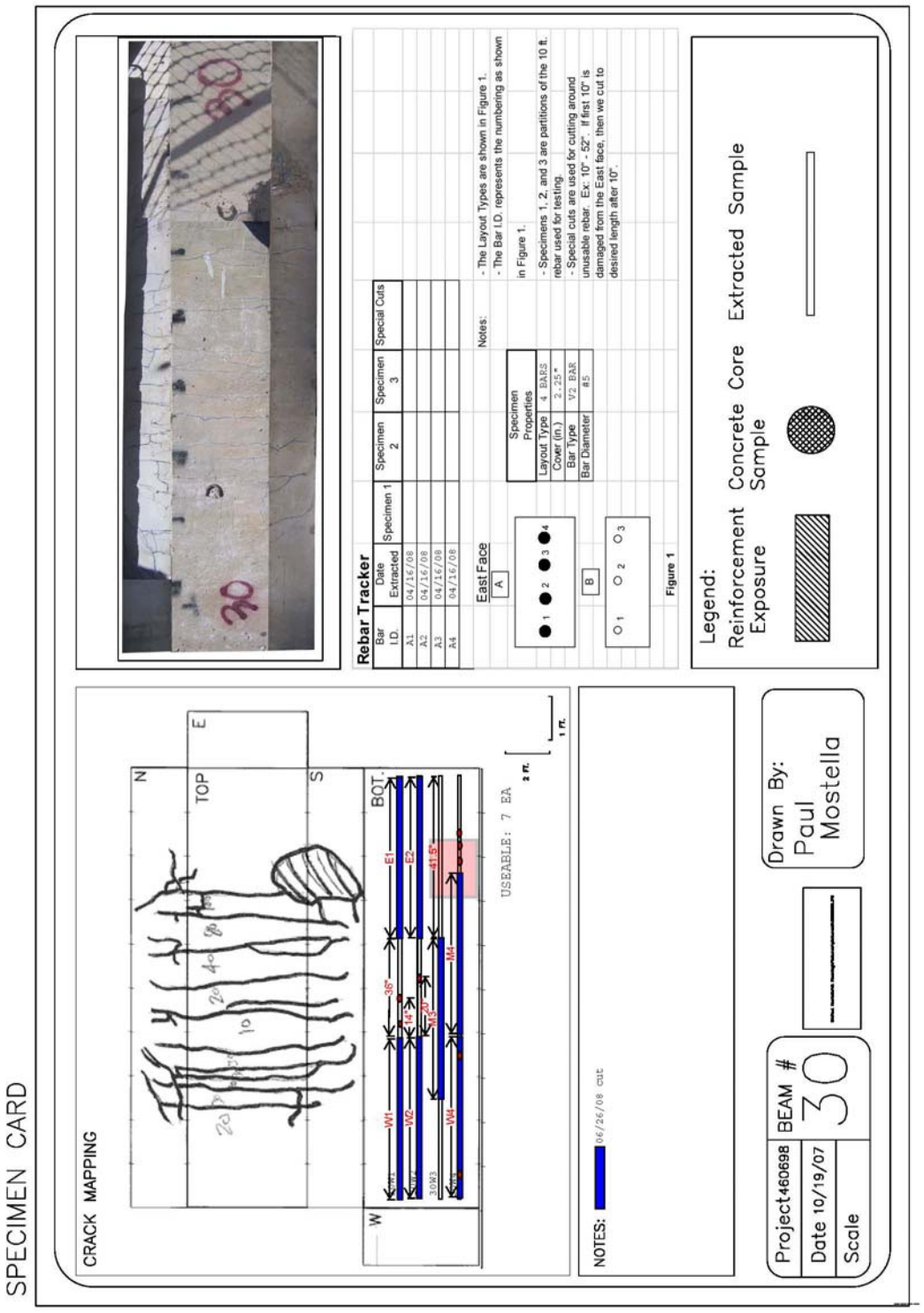

Figure B-30 Beam Card #30

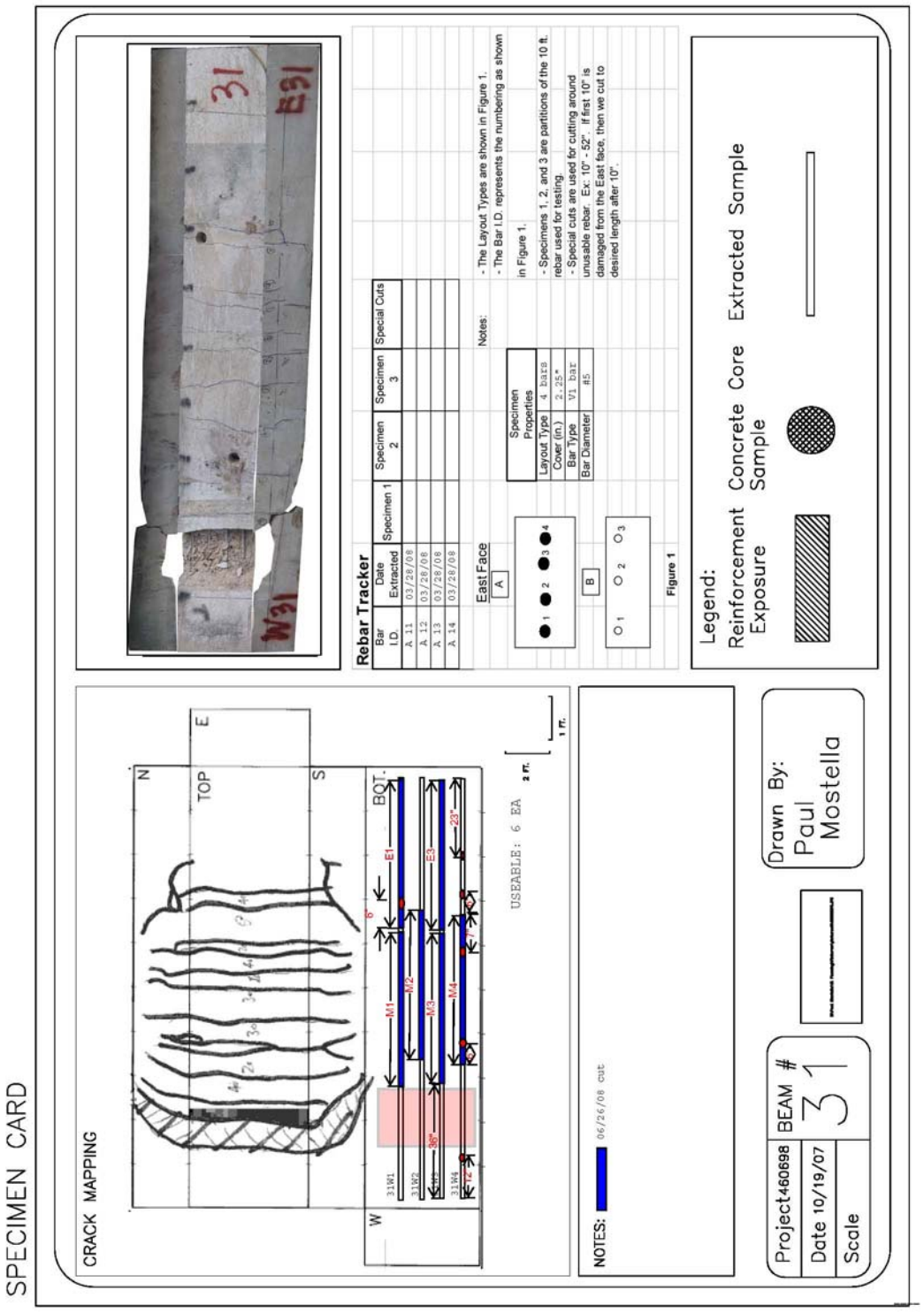

Figure B-31 Beam Card #31

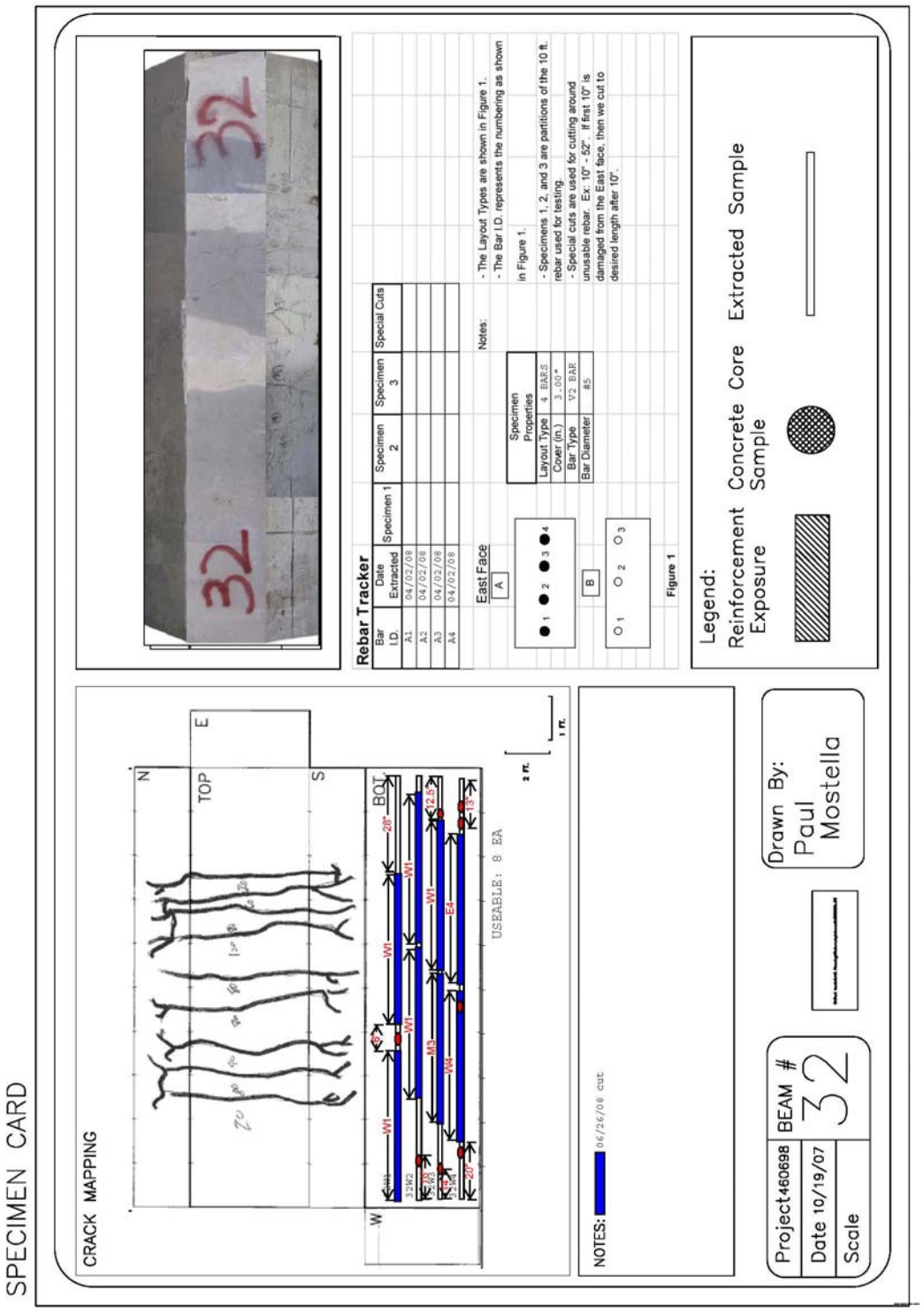

Figure B-32 Beam Card #32

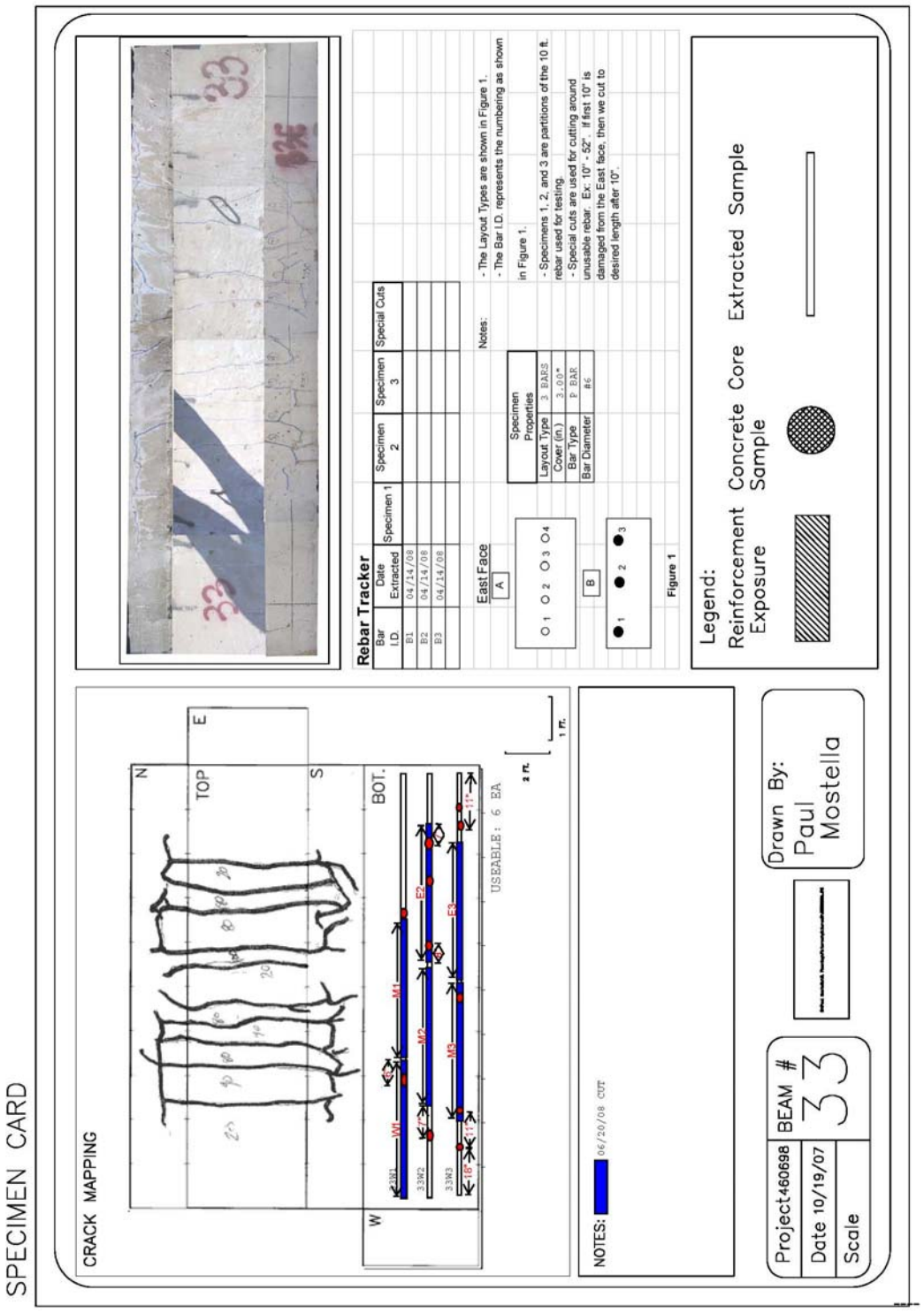

Figure B-33 Beam Card #33

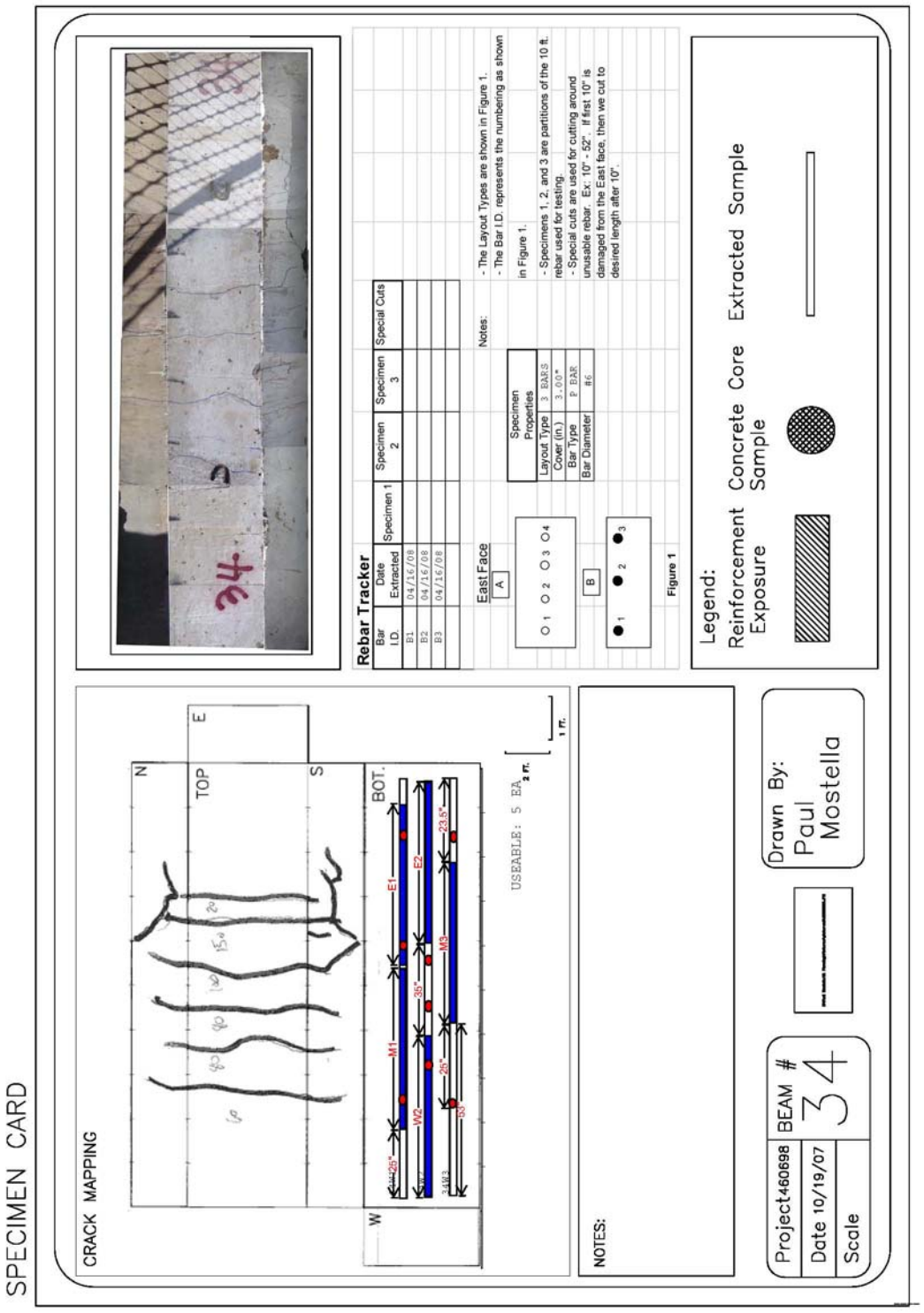

Figure B-34 Beam Card #34

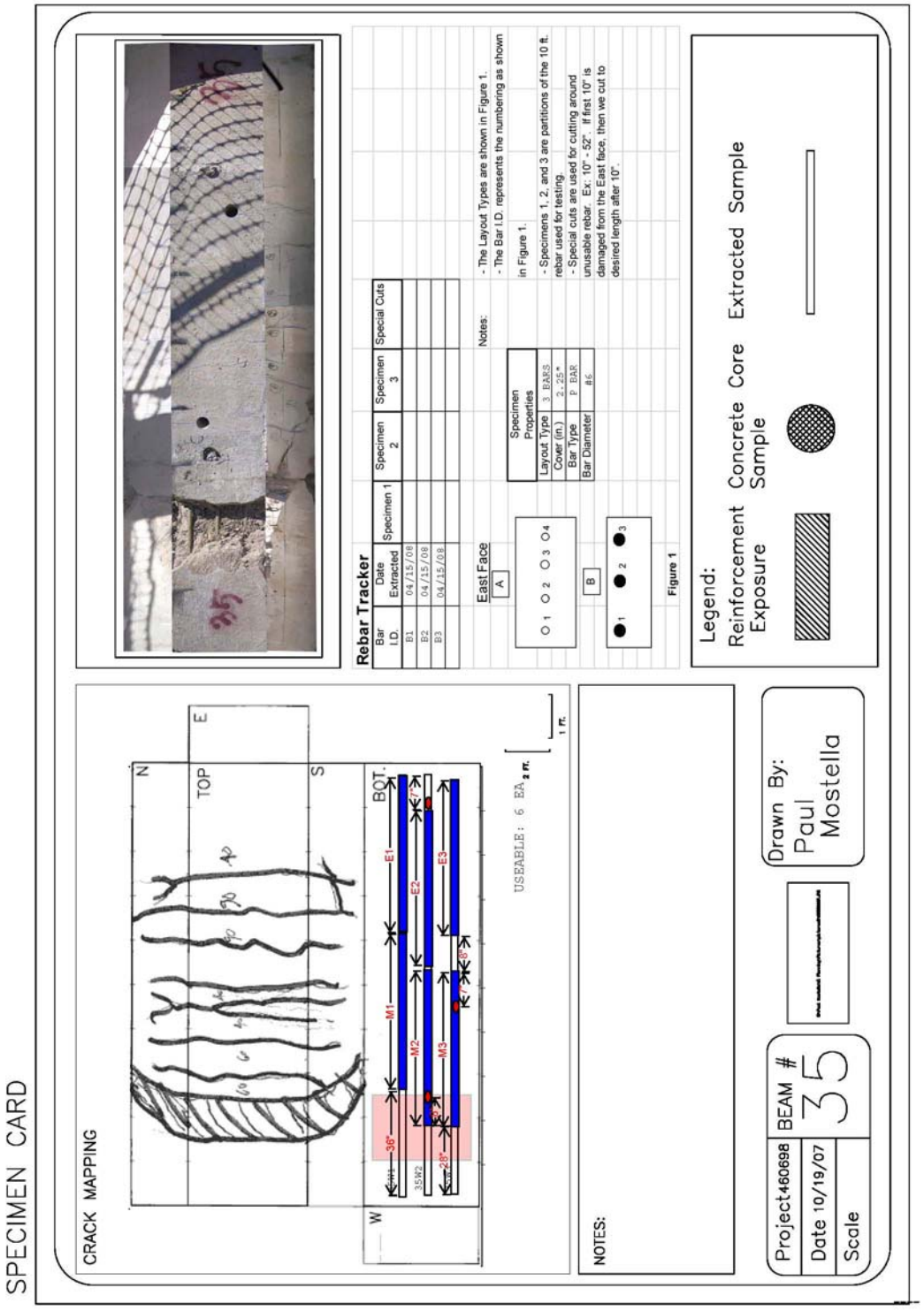

Figure B-35 Beam Card #35

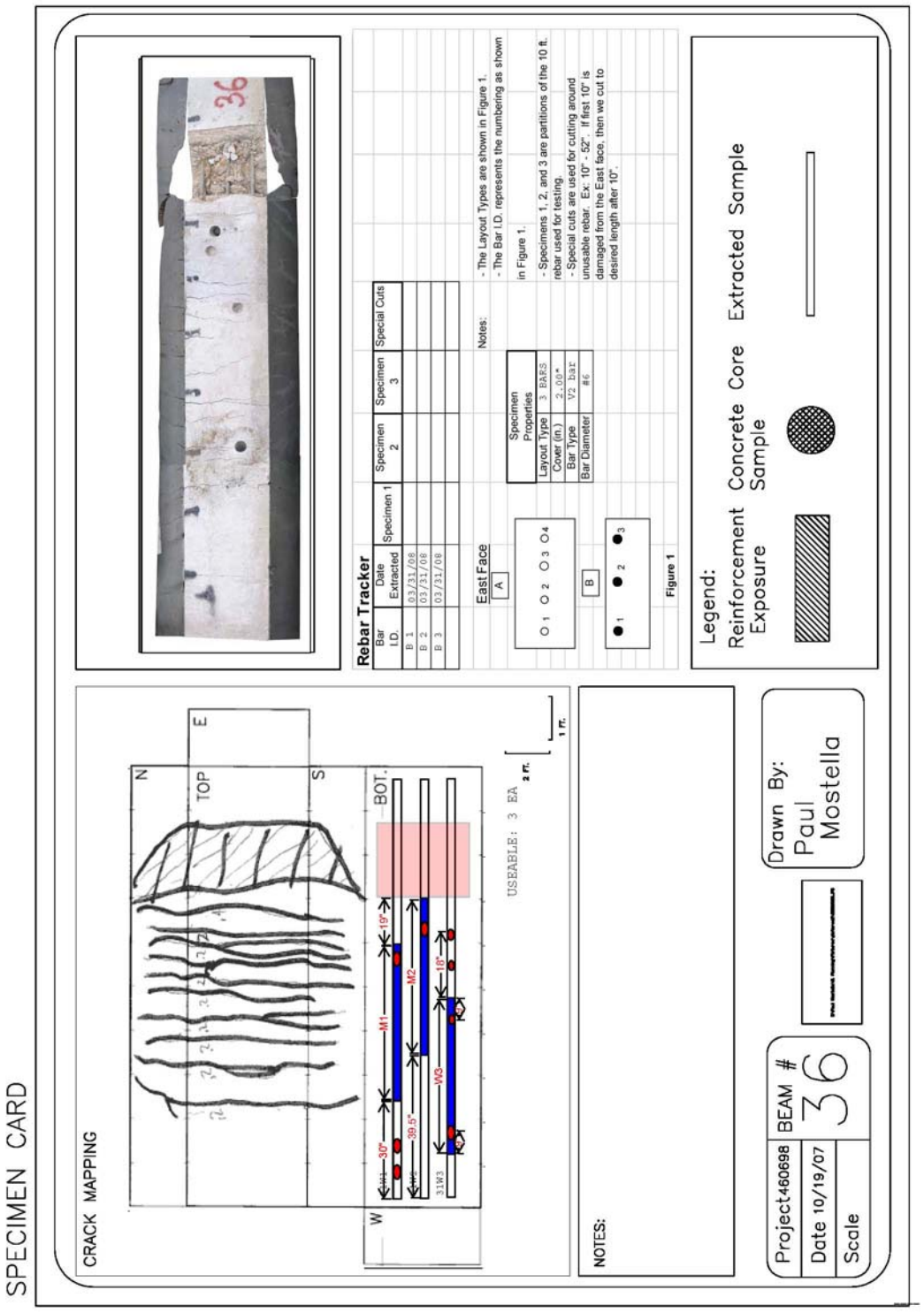

Figure B-36 Beam Card #36

APPENDIX C – MODULUS OF ELASTICITY (MOE) TEST RESULTS

Table C-7 MOE test results for V1 #5 bars

Bar Type	MOE - No exposure ksi (MPa)	MOE after 7 years of Embedment in Concrete ksi (MPa)
V1 #5	6952(47932)	5617(38726)
	5922(40831)	5689(39222)
	6459(44533)	5489(37843)
	5864(40431)	5759(39705)
	6212(42830)	2151(14829)
		5823(40149)
		5271(36340)
		5327(36726)
		5696(39272)
		5505(37956)
		5397(37213)
		5855(40370)
		6133(42283)
		5978(41215)
		5830(40199)
		5894(40640)
		5346(36857)
		5319(36674)
		5913(40771)
		5415(37332)
		5718(39422)
		5092(35108)
		5829(40193)
		5698(39288)
		5728(39491)
		4325(29822)
		6056(41755)
		5780(39854)
		5919(40812)
		5860(40401)
		5487(37830)
		6026(41550)
		5605(38646)
Mean	6282(43311)	5531(38136)
Standard Deviation	444(3063)	697(4809)

Table C-8 MOE test results for V2 #5 bars

Bar Type	MOE - No exposure ksi (MPa)	MOE after 7 years of Embedment in Concrete ksi (MPa)
V2 #5	6923(47732)	5394(37188)
	6880(47436)	5394(37191)
	6328(43630)	5382(37106)
	6110(42127)	5376(37066)
	5660(39024)	5604(38639)
		5040(34748)
		5309(36602)
		5947(41001)
		5607(38656)
		5511(37995)
		5628(38802)
		5564(38361)
		5419(37361)
		5602(38628)
		5103(35186)
		5679(39157)
		5634(38845)
		5964(41122)
		5310(36609)
		5495(37887)
		5418(37359)
		5605(38644)
		5953(41041)
		5496(37893)
		5316(36653)
		5276(36377)
		3540(24407)
		5551(38273)
		5626(38793)
Mean	6380(43990)	5439(37503)
Standard Deviation	534(3679)	426(2937)

Table C-9 MOE test results for P #5 bars

Bar Type	MOE - No exposure ksi (MPa)	MOE after 7 years of Embedment in Concrete ksi (MPa)
P #5	6241(43030)	3501(24138)
	4862(33522)	5051(34823)
	5849(40327)	5336(36788)
	5196(35825)	5591(38549)
		5654(38982)
		5379(37089)
		6547(45139)
		5693(39253)
		5671(39101)
		5498(37906)
		5861(40412)
		5323(36699)
		5757(39694)
		5404(37261)
		5789(39912)
Mean	5537(38176)	5470(37716)
Standard Deviation	623(4296)	640(4415)

Table C-10 MOE test results for V1 #6 bars

Bar Type	MOE - No exposure ksi (MPa)	MOE after 7 years of Embedment in Concrete ksi (MPa)
V1#6	6256(43131)	4290(29577)
	6032(41587)	5915(40783)
	6441(44412)	5866(40442)
	6557(45211)	5820(40124)
	6265(43193)	6746(46512)
	6304(43466)	6012(41451)
	6414(44221)	5990(41302)
	6525(44991)	5393(37181)
	6940(47848)	6450(44474)
		6277(43276)
		6461(44548)
		5840(40268)
		6419(44254)
		6207(42795)
		6116(42169)
		6666(45962)
		5536(38167)
		5975(41193)
		5945(40988)
		5964(41120)
		5838(40252)
		6026(41547)
		5830(40195)
		6379(43985)
		6280(43296)
		5470(37713)
		6684(46083)
		5134(35399)
		6439(44396)
Mean	6415(44229)	5999(41360)
Standard Deviation	254(1751)	510(3518)

Table C-11 MOE test results for V2 #6 bars

Bar Type	MOE - No exposure ksi (MPa)	MOE after 7 years of Embedment in Concrete ksi (MPa)
V2 #6	5810(40059)	5866(40443)
	5724(39463)	5764(39740)
	5827(40174)	3814(26299)
	5850(40333)	5622(38759)
	5674(39124)	6051(41717)
	5511(38000)	6032(41586)
	5609(38674)	5779(39845)
	5743(39594)	5977(41212)
	5730(39509)	5909(40743)
	5532(38142)	5605(38642)
		5940(40953)
		5542(38210)
		5752(39658)
		6087(41969)
		5901(40685)
		5749(39641)
		5837(40244)
Mean	5701(39307)	5719(39432)
Standard Deviation	119(818)	516(3555)

Table C-12 MOE test results for P #6 bars

Bar Type	MOE - No exposure ksi (MPa)	MOE after 7 years of Embedment in Concrete ksi (MPa)
P#6	5893(40628)	4666(32172)
	5686(39202)	5580(38474)
	6086(41960)	5416(37344)
	6525(44991)	5955(41056)
	6940(47848)	5709(39365)
	5657(39005)	5337(36795)
	5750(39646)	5601(38619)
	5852(40347)	5572(38415)
	6557(45211)	5662(39041)
	6265(43193)	5427(37416)
		5574(38428)
		5820(40126)
		5892(40622)
		5492(37866)
		5885(40576)
		5666(39066)
		5417(37348)
		5444(37535)
		5400(37233)
		5454(37603)
		5515(38025)
		5316(36653)
		5737(39558)
		5807(40040)
		5651(38961)
		5757(39696)
		5553(38290)
		5596(38584)
		5913(40767)
		5607(38659)
		5819(40122)
		5760(39711)
Mean	6121(42203)	5594(38568)
Standard Deviation	436(3008)	244(1683)